ANTENNA MUTUAL IMPEDANCE COMPUTATION USING MEASURED OR COMPUTED ELEMENT FIELDS

A THESIS SUBMITTED TO
THE GRADUATE SCHOOL OF NATURAL AND APPLIED SCIENCES
OF
MIDDLE EAST TECHNICAL UNIVERSITY

BY

MEHMET ALİ ÖZTÜRK

IN PARTIAL FULFILLMENT OF THE REQUIREMENTS
FOR
THE DEGREE OF DOCTOR OF PHILOSOPHY
IN
ELECTRICAL AND ELECTRONICS ENGINEERING

SEPTEMBER 2023

Approval of the thesis:

ANTENNA MUTUAL IMPEDANCE COMPUTATION USING MEASURED OR COMPUTED ELEMENT FIELDS

submitted by **MEHMET ALİ ÖZTÜRK** in partial fulfillment of the requirements for the degree of **Doctor of Philosophy in Electrical and Electronics Engineering Department, Middle East Technical University** by,

Prof. Dr. Halil Kalıpçılar
Dean, Graduate School of **Natural and Applied Sciences** _____

Prof. Dr. İlkay Ulusoy
Head of Department, **Electrical and Electronics Engineering** _____

Prof. Dr. Seyit Sencer Koç
Supervisor, **Electrical and Electronics Engineering, METU** _____

Examining Committee Members:

Prof. Dr. Özlem Aydın Çivi
Electrical and Electronics Engineering, METU _____

Prof. Dr. Seyit Sencer Koç
Electrical and Electronics Engineering, METU _____

Prof. Dr. Vakur Ertürk
Electrical and Electronics, Bilkent University _____

Prof. Dr. Gülbin Dural
Electrical and Electronics Engineering, METU _____

Prof. Dr. Özlem Özgün
Electrical and Electronics Engineering, Hacettepe University _____

Date:06.09.2023

I hereby declare that all information in this document has been obtained and presented in accordance with academic rules and ethical conduct. I also declare that, as required by these rules and conduct, I have fully cited and referenced all material and results that are not original to this work.

Name, Surname: MEHMET ALİ ÖZTÜRK

Signature :

ABSTRACT

ANTENNA MUTUAL IMPEDANCE COMPUTATION USING MEASURED OR COMPUTED ELEMENT FIELDS

ÖZTÜRK, MEHMET ALİ
Ph.D., Department of Electrical and Electronics Engineering
Supervisor: Prof. Dr. Seyit Sencer Koç

September 2023, 116 pages

This thesis presents a comprehensive study of mutual coupling between two identical radiators in cases of small element spacing. To calculate the mutual coupling, we utilize spherical harmonics and the reaction theorem. However, for closely spaced antennas, a challenge arises when the minimum spheres enclosing the antennas overlap, leading to issues with the convergence of spherical wave expansions on the surface separating the antennas.

To overcome this problem, our proposed method relies on addition theorems to translate the spherical wave expansions to a different center, effectively redefining the minimum spheres and convergence regions. We validate our method by analyzing the coupling of two half-wave dipoles in a side-by-side configuration. The results show excellent agreement with those obtained from the induced EMF method. Additionally, we conduct experimental tests using a printed dipole antenna, obtaining its spherical harmonic coefficients through spherical near-field measurement, and calculate the mutual impedance of two such dipoles using our method. The computed results for different element spacings in a side-by-side configuration are compared to those obtained from s-parameter measurements and full-wave simulations.

To address the mutual impedance of two infinitely thin half-wave dipoles, we employ the plane wave spectrum and the reaction theorem. Through asymptotic evaluation, we establish a relationship between the spectrum and the far-field pattern function of an infinitely thin dipole. This relationship and the analiticity of the spectrum enable to compute the near fields of the dipole using its known far-field pattern function. By utilizing the computed near fields, we determine the mutual impedance of dipoles in a side-by-side configuration and compare the calculated results for different separation distances with those obtained from the induced EMF method.

Keywords: Mutual coupling, Vector spherical harmonic expansion, Rotation and translation of spherical waves, Addition theorem, Reaction theorem

ÖZ

ÖLÇÜLEN VEYA HESAPLANAN ELEMAN ALANLARI KULLANILARAK ANTEN KARŞILIKLI EMPEDANSININ HESAPLANMASI

ÖZTÜRK, MEHMET ALİ
Doktora, Elektrik ve Elektronik Mühendisliği Bölümü
Tez Yöneticisi: Prof. Dr. Seyit Sencer Koç

Eylül 2023 , 116 sayfa

Bu tez, küçük eleman aralığı durumlarında iki özdeş ışıyıcı arasındaki karşılıklı bağlaşımın kapsamlı bir çalışmasını sunmaktadır. Karşılıklı bağlaşımı hesaplamak için küresel harmoniklerden ve reaksiyon teoreminden yararlanıyoruz. Fakat, yakın aralıklı antenler için, antenleri kapsayan minimum küreler üst üste geldiğinde, antenleri ayıran yüzeydeki küresel dalga açılımlarının yakınsaması ile ilgili sorunlara yol açan bir zorluk ortaya çıkmaktadır.

Bu sorunun üstesinden gelmek için, önerdiğimiz yöntem küresel dalga açılımlarını farklı bir merkeze ötelemek için toplama teoremlerine dayanır, minimum küreleri ve yakınsama bölgelerini etkili bir şekilde yeniden tanımlar. Yöntemimizi, yan yana konfigürasyonda iki yarım dalga dipolün bağlaşımını analiz ederek doğruluyoruz. Sonuçlar, indüklenmiş EMF yönteminden elde edilenlerle mükemmel bir uyum göstermektedir. Buna ek olarak, baskılı bir dipol anten kullanarak deneysel testler yapıyor, küresel yakın alan ölçümü yoluyla küresel harmonik katsayılarını elde ediyor ve yöntemimizi kullanarak bu tür iki dipolün karşılıklı empedansını hesaplıyoruz. Yan yana konfigürasyonda farklı eleman aralıkları için hesaplanan sonuçlar, s-parametre

ölçümlerinden ve tam dalga simülasyonlarından elde edilenlerle karşılaştırılmıştır.

İki sonsuz ince yarım dalga dipolün karşılıklı empedansını ele almak için düzlem dalga spektrumunu ve reaksiyon teoremini kullanıyoruz. Asimptotik değerlendirme yoluyla, spektrum ve sonsuz ince bir dipolün uzak alan örüntü fonksiyonu arasında bir ilişki kuruyoruz. Bu ilişki ve spektrumun analitikliği, bilinen uzak alan örüntü fonksiyonunu kullanarak dipolün yakın alanlarını hesaplamayı sağlar. Hesaplanan yakın alanları kullanarak, yan yana konfigürasyondaki dipollerin karşılıklı empedansını belirliyor ve farklı ayırma mesafeleri için hesaplanan sonuçları indüklenmiş EMF yönteminden elde edilenlerle karşılaştırıyoruz.

Anahtar Kelimeler: Karşılıklı bağlaşım, Vektör küresel harmonik açılımı, Küresel dalgaların döndürülmesi ve ötelenmesi, Reaksiyon teoremi, Toplama teoremi

To my family

ACKNOWLEDGMENTS

I am using this opportunity to express my gratitude to everyone who supported me throughout the course of this thesis. Firstly, I would like to thank Prof. Dr. Sencer Koç for his invaluable guidance and support. I am fortunate to have an advisor who gave me the freedom to explore my own approach, without his guidance and support, this work would not have been accomplished. I would like to extend my heartfelt gratitude to ASELSAN for providing me with the necessary facilities and test conditions for my thesis. Without ASELSAN's support, I would not have finished these tasks. Lastly, I would like to express my heartfelt gratitude to my family whose love, support and encouragement have always helped me to find right path. None of this would have been possible without love and patience of my family.

TABLE OF CONTENTS

LIST OF TABLES

TABLES

LIST OF FIGURES

FIGURES

LIST OF ABBREVIATIONS

2D	2 Dimensional
3D	3 Dimensional
SWE	Spherical wave expansion
HFSS	High frequency structure simulator
MIMO	Multiple input multiple output
TE	Transverse electric
TM	Transverse magnetic
UWB	Ultra wideband

CHAPTER 1

INTRODUCTION

1.1 Problem Definition

A fundamental issue that arises in the design of antenna arrays is the dependence of the reflection from an individual element's port on the excitations of all other elements. This dependency is caused by the interaction between array elements through electromagnetic fields, known as mutual coupling. When an element is embedded in an array with all elements excited, the properties of the elements, such as radiation pattern and input reflection coefficient, differ from the isolated case due to mutual coupling. This leads to a deterioration in the desired radiation pattern and variations in the input impedance of the antenna elements. For example, in phased arrays, the input impedance of an individual element changes with the magnitude and phase of the element excitations due to mutual coupling [1]. This variation can result in excessive reflections from the element ports, leading to scan blindness at certain scan angles and potential damage to the power amplifier unit of an individual element.

Multiple antennas are used in MIMO systems to enhance channel capacity. In collocated MIMO systems, antennas are typically placed close to each other to create a compact system. However, this proximity increases mutual coupling between the elements, which can reduce the diversity performance of the MIMO system [2]. It has also been noted in the literature that antenna coupling can significantly impact the performance of adaptive arrays, even when large element spacings are used [3]. Therefore, accurately computing the mutual coupling is essential for the successful design of an antenna array. The mutual impedance serves as one of the qualitative measures to describe mutual coupling. It is the ratio of the induced voltage at the

open circuit terminal of one element to the current applied to another element while all other elements are terminated in an open circuit.

The mutual impedance between two radiators can be determined using the reaction theorem, which uses the known fields associated with both radiators and the port currents, as mentioned in [4].

Consider two antennas positioned in their respective coordinate systems as illustrated in Figure 1.1.

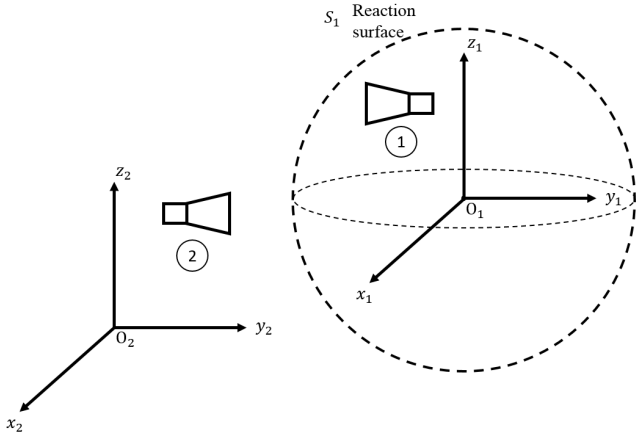

Figure 1.1: Two antennas in their own coordinate systems.

The mutual impedance, z_{12}, can be calculated as follows:

$$z_{12} = -\frac{1}{I_1 I_2} \oint_{S_1} (\bar{E}_1 \times \bar{H}_2 - \bar{E}_2 \times \bar{H}_1) \cdot d\bar{S}_1 \tag{1.1}$$

where S_1 is an arbitrary surface separating the two antennas, which is called the "reaction surface". In this expression, $\bar{E}_1$, $\bar{H}_1$ denote the fields of antenna 1, and $\bar{E}_2$, $\bar{H}_2$ denote the fields of antenna 2 when both antennas are radiating in the presence of each other. Typically, the reaction surface S_1 lies in the near-field region of antennas, requiring the evaluation of the near fields of the antennas to calculate the mutual impedance. One approach to express these fields is to utilize the spherical harmonic expansion technique. The fields radiated by each antenna can be written as:

$$\bar{E}(r,\theta,\phi) = k\sqrt{\eta} \sum_{s=1}^{2} \sum_{n=1}^{\infty} \sum_{m=-n}^{n} Q_{smn}^{(c)} \bar{F}_{smn}^{(c)}(r,\theta,\phi) \tag{1.2}$$

$$\bar{H}(r,\theta,\phi) = \frac{jk}{\sqrt{\eta}} \sum_{s=1}^{2} \sum_{n=1}^{\infty} \sum_{m=-n}^{n} Q_{smn}^{(c)} \bar{F}_{3-s,m,n}^{(c)}(r,\theta,\phi) \tag{1.3}$$

where $k = w\sqrt{\mu\epsilon}$ is the wavenumber, and η is the instrinsic impedance of the medium. The upper index (c) defines the radial dependencies of the spherical wave function. $c = 3$ corresponds to spherical Hankel functions of the first kind, representing an incoming wave, while $c = 4$ corresponds to spherical Hankel functions of the second kind, representing an outward propagating wave. The incoming wave expansion converges inside any sphere that excludes all sources, while outgoing wave expansion converges outside any sphere that includes all sources. A sphere with a minimum radius enclosing an antenna is called the minimum sphere. Figure 1.2 illustrates the convergence region of the vector wave expansion representing the outgoing waves, and minimum sphere for an arbitrary antenna.

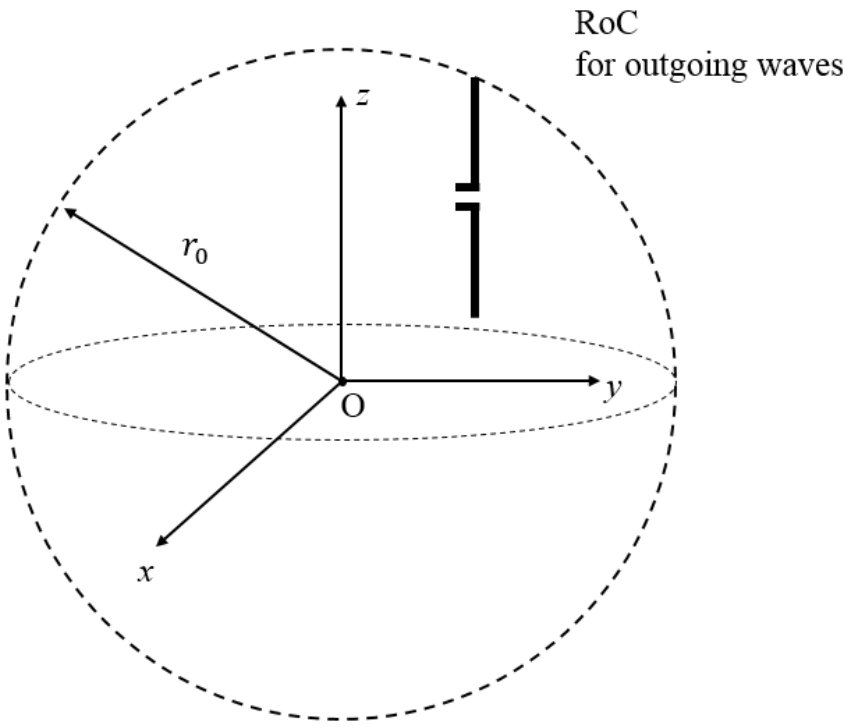

Figure 1.2: Convergence region of outgoing spherical waves.

When two antennas are positioned close to each other, the minimum spheres that enclose both antennas overlap, as depicted in Figure 1.3. Consequently, establishing a "proper" reaction surface within the region where both spherical harmonic expansions

representing the radiated fields from the antennas converge becomes impossible. The primary issue addressed in this thesis is to expand the fields of the antennas in new coordinate frames in order to find a "proper" reaction surface. This is imperative for computing the mutual impedance between two closely spaced antennas.

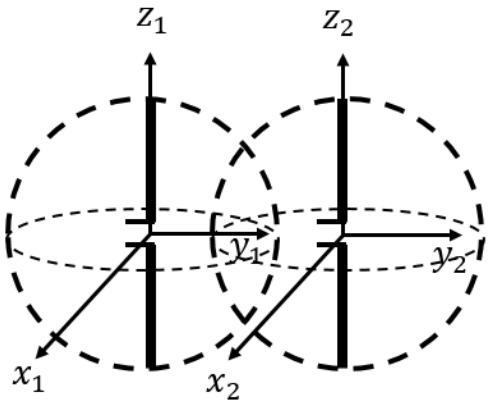

Figure 1.3: Overlapping of minimum spheres.

1.2 Literature Survey

This section primarily focuses on conducting a literature survey regarding the use of spherical harmonics in solving antenna problems and explores various techniques proposed to analyze the issue of mutual coupling in antenna arrays.

The calculation of mutual impedance between antenna elements can be achieved by utilizing Richmond's reaction theorem [4]. This theorem expresses the mutual impedance as an integral over a closed surface that fully surrounds only one of the antennas, known as the reaction surface. As stated in [4], having knowledge of the port currents, and the fields radiated by the antennas on the reaction surface will be sufficient for calculating the mutual impedance.

In [5], a reaction surface is introduced as an infinitely large plane that separates two antennas and is closed by a hemisphere on one side. The plane wave spectrum technique is used to express the fields of both antennas, and the coupling coefficient is computed through an integral over S. However, the effects of the evanescent spec-

trum are disregarded, and errors may arise when two antennas are very close, as stated in the same study.

The work presented in [6] establishes the mutual admittance formulation between two identical planar radiators by employing the reaction theorem and the plane wave spectrum technique. This method allows the mutual admittance to be expressed as a bidimensional Fourier transform of the inner products of the plane wave spectra associated with the fields radiated by two rectangular slots. To obtain the plane wave spectrum of the second slot, the propagation direction of the plane waves is reversed relative to that of the first slot. The dimensions of the slots are considered small in comparison to the wavelength, and it is assumed that the fields radiated by the first slot do not affect the aperture field distribution of the second slot. It is asserted that when the separation distance is significantly large, the expression can be evaluated asymptotically. The method is utilized to compute the mutual admittances between two rectangular slots in various configurations.

In [7], a novel approach is introduced for estimating the mutual impedance between radiators. This method uses the radiation pattern of a single isolated antenna to calculate the mutual impedance between two identical elements. By utilizing the radiation pattern of an antenna and the array factor, the real part of the surface integral of the Poynting vector on an infinitely distant sphere is determined. The total radiated power is also expressed in terms of the input port currents and voltages, and the real part of the mutual impedance is represented as the surface integral of the Poynting vector. The imaginary part is computed using Kramer-Kronig relations applied to the real part. The validity of this technique is demonstrated by computing the mutual impedance between half-wave dipoles and microstrip antennas, showing good agreement with results obtained from other methods.

An analytical method for calculating the mutual impedance between two arbitrary antennas using vector spherical harmonics and the reaction integral is proposed in [8]. The fields of the two antennas are expanded into vector spherical harmonics in their respective coordinate systems, and the fields of the first antenna are translated to the coordinate system of the second antenna using the addition theorem. This allows the integrations to be evaluated in closed form over a spherical surface that encloses

the second antenna. As a result, the mutual impedance is expressed as a sum of the products of the expansion coefficients. The details of the technique is explained in Appendix A, since the method is the starting point of the approach proposed in this study. The final result is given below for convenience which expresses the mutual impedance as the sum of products of spherical harmonic coefficients of the antennas.

$$z_{12} = z_{21} = \frac{1}{i_1 i_2} \frac{1}{k^2} \sqrt{\frac{\epsilon}{\mu}} \sum_{n=1}^{\infty} \sum_{m=-n}^{n} (-1)^m ({}_1b_{n,-m}^{TE} \, {}_2b_{n,m}^{TE} + {}_2b_{n,m}^{TM} \, {}_1b_{n,-m}^{TM}) \qquad (1.4)$$

where ${}_2b_{n,m}^{TE}$ and ${}_2b_{n,m}^{TM}$ are spherical harmonic coefficients of antenna 2. ${}_1b_{n,-m}^{TE}$ and ${}_1b_{n,-m}^{TM}$ denote spherical harmonic coefficients of antenna 1 in the translated coordinate frame (coordinate frame of the second antenna). The units of the spherical harmonic coefficients are volts/m and the port currents of the antennas i_1 and i_2 have units of amperes. The mutual impedance given in (1.4) is expressed as a sum of the products of spherical harmonic coefficients with known currents. However, this analytical method is not applicable for all separation distances. The outgoing waves represented by spherical harmonics converge within the region outside of the minimum sphere that encloses the antenna. A "proper" reaction surface should be defined in the region where the expansions of both antennas converge. However, when the antennas are placed very close to each other, the minimum spheres that enclose these antennas overlap and the proposed method in [8] does not work for mutual impedance computation.

The work described in [12] eliminates the need for the translation step by directly utilizing the spherical harmonic expansion to evaluate the fields on the reaction surface, which is a sphere surrounding one of the antennas. To accomplish this, an FFT/Interpolation method over an eccentric sphere is proposed. The adoption of the FFT/Interpolation approach allows for rapid computation of the fields on the reaction surface.

The outgoing vector spherical harmonic expansions converge outside the minimum sphere of an antenna. If the two antennas are positioned close to each other, their minimum spheres will overlap, making it impossible to define a reaction surface that lies entirely within the convergence regions of both antennas. As a result, the methods described in [8] and [12] are not applicable. The problem of overlapping minimum

spheres has also been addressed in the literature [13], [14].

In [13], a finite-size antenna is modeled using infinitesimal dipoles to ensure that the minimum spheres of individual dipoles do not overlap. This allows for the application of spherical harmonic methods. However, the drawback of this approach is the challenge of accurately modeling the antenna.

In [14], transformation properties of spherical and plane vector waves are employed to overcome the problem of overlapping minimum spheres. The spherical modes of antenna 1 are expressed as plane waves in the coordinate system of antenna 1, then translated into the coordinate system of antenna 2, and finally expanded in terms of incoming spherical modes for antenna 2. This approach is similar to applying the addition theorem. Although it is less efficient, it provides a solution to overcome the overlapping minimum spheres problem.

The problem of overlapping spheres is also encountered in T-matrix formulation of multiple obstacles. The method presented in [15] addresses this problem for two obstacles close to each other, where their enclosing spheres overlap. The idea is based on shifting the coordinate origin of the spherical harmonic expansion of the obstacles away from each other. This translation also moves the enclosing spheres so that they do not overlap.

The following studies emphasize the characteristics, benefits, and practical applications of employing spherical harmonic expansion in antenna-related problems. The work in [16], a spherical mode expansion (SME) with cartesian vector coefficients is utilized to analyze the radiation pattern of arbitrary wire antennas. In order to find the spherical harmonic coefficients, the proposed method uses a spherical harmonic series for the free space Green's function in conjuction with the current distribution computed with the method of moments. This expansion offers a compact and accurate representation of the radiation patterns of arbitrary shape wire antennas. For spherical mode expansion, $N = kR$ is chosen as a truncation number to compute the radiation patterns for several typical wire antennas. R denotes the radius of the minimum sphere that encloses the antenna, while k is the wavenumber. To investigate the convergence of spherical expansion with this truncation number, several wire antennas are also computed directly from method of moments. The results of trun-

cated SME method are compared to that obtained from method of moments using a root mean square (rms) error criterion. It is shown that the radiation patterns of arbitrary shape wire antennas are represented using spherical mode expansions and its accuracy is certainly adequate when arbitrary shape wire antennas are concerned.

The radiation pattern of any antenna can be expressed in a concise manner by employing spherical harmonic expansion, as suggested in [17]. Instead of utilizing vector spherical wave functions, this study proposes the use of scalar spherical harmonics with vector coefficients to represent the vector-valued transverse electric far-field. The complex vector-valued expansion coefficients are derived using a linear least squares approach. The convergence of the expansion is assessed by examining the relative error between the measured and reconstructed fields, employing a semi-spherical dual-polarized antenna array. This error is evaluated in relation to the maximum expansion level, which decreases as the expansion level increases, as mentioned in the study. Additionally, it is claimed that this expansion method offers a convenient way to rotate and interpolate radiation patterns, which is quite useful for various signal processing algorithms involving sensor arrays, such as beamforming and direction of arrival estimation.

In [18], vector spherical harmonics are employed to reduce the data required for representing the radiation pattern of antennas in UWB channel simulations. These simulations demand the description of the antenna radiation pattern across the entire frequency band over 4π steradians. However, this necessity leads to challenges such as a large volume of data and long computation times. These problems become even more pronounced when working with Ray tracing-based propagation simulators, making signal extraction a highly challenging task.

To address these issues, a solution is proposed using vector spherical harmonic (VSH) expansion. This approach allows for the compact representation of the vector radiation function $F(\theta, \phi)$, where (θ, ϕ) are the spherical coordinate angles. By employing VSH expansion, the storage, processing, and analysis of the radiation patterns can be simplified.

Vector radiation function is expanded in terms of VSH which seems to be efficient solution for data access and compression. These functions are divided into real and

imaginary parts, and secondly expressed in terms of VSH coefficients. In order to reconstruct $F(\theta, \phi)$ for each frequency and for a given (θ, ϕ), these coefficients are utilized. ϕ and θ components of vector radiation functions is defined as:

$$F_\theta(\theta,\phi) \cong \sum_{n=0}^{N}\sum_{m=0}^{n}[V_m^n(br_{m,n}\cos m\phi - bi_{m,n}sinm\phi) + W_n^m(-ci_{m,n}\cos m\phi - cr_{m,n}sinm\phi)] \quad (1.5)$$

$$F_\phi(\theta,\phi) \cong \sum_{n=0}^{N}\sum_{m=0}^{n}[W_n^m(bi_{m,n}\cos m\phi - br_{m,n}sinm\phi) + V_n^m(cr_{m,n}\cos m\phi - ci_{m,n}sinm\phi)] \quad (1.6)$$

This usage of vector spherical harmonics brings about one of the key benefits in these simulations: a significant reduction in data requirements when describing the antenna radiation pattern. Additionally, the evaluation of vector radiation functions can be performed quickly in the desired directions of interest.

The work in [19] is related to finding SWE coefficients of a $\lambda/10$ Hertzian dipole that is shifted by λ distance from the origin. These coefficients are computed by utilizing orthogonality relations with the known $\bar{E}$ field of $\lambda/10$ dipole. FEKO is a numerical EM solver which directly gives the spherical harmonic coefficients of an arbitrary antenna as a simulation output. The same dipole configuration is analyzed with this solver to obtain these coefficients. The magnitude and phase of the SWE coefficients are compared to that obtained from this numerical EM solver, and the results show good agreement with $\%5$ maximum error in terms of magnitude. Additionally, the power distribution of n modes is also compared to the results from the numerical solver in order to validate computations of spherical harmonic coefficients.

1.3 Proposed Method

Consider two antennas positioned in their respective coordinate systems, as illustrated in Figure 1.4. The feed points of each antenna coincide with the origins of their unprimed coordinate systems. When the two antennas are very close to each other, their

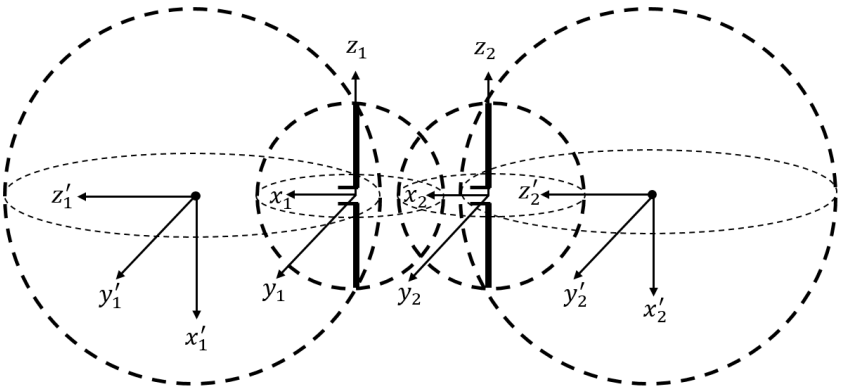

Figure 1.4: Overlapping of minimum spheres.

minimum spheres may overlap, as shown in Figure 1.4. The case of overlapping minimum spheres makes it difficult to directly apply the spherical harmonic expansion technique for calculating the mutual coupling between elements, since defining a reaction surface for computing the mutual impedance becomes problematic in such cases. However, it is possible to address this issue by altering the center of the expansion sphere for each antenna, effectively finding a "proper" reaction surface.

By employing new (primed) coordinate systems, where the minimum spheres no longer overlap, it becomes feasible to define a "proper" reaction surface within the region where the spherical harmonics representing the fields of both antennas converge. Consequently, the mutual impedance can be determined either through numerical integration over the reaction surface by directly evaluating the fields on this surface or through analytical integration by transforming the SWE coefficients to the same coordinate frame. The addition theorem for SWE functions can be used to expand the fields of an antenna in a different coordinate frame.

Translational addition theorem is quite complex in arbitrary directions, but rotation and translation along the z-axis are simpler. Therefore, a general translation is achieved by first rotating the z-axis of the coordinate frame in the translation direction. The rotation and translation formulas are available in the literature [10], and the coefficients for z translation can be easily generated by the recursive formulas given in [20].

To illustrate the idea, consider a half-wave dipole antenna positioned in the unprimed coordinate system, as shown in Figure 1.5. Suppose that the fields of the dipole

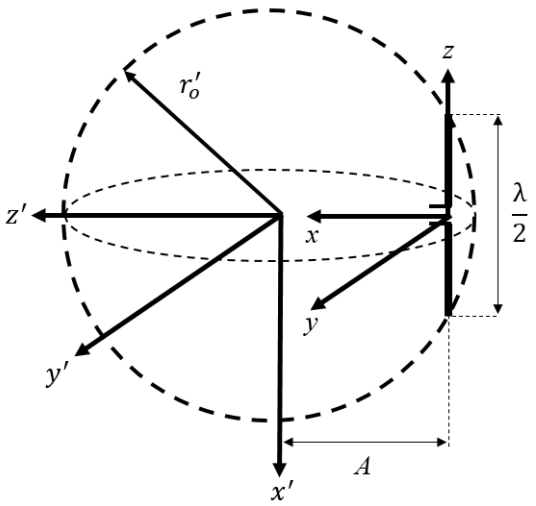

Figure 1.5: Rotation and translation of spherical waves.

are expanded in the unprimed coordinate frame, with the origin referenced to its feed point. This original coordinate frame is first rotated about its y-axis by 90 degrees (through θ), and then translated along the (rotated) z-axis is by a distance A to obtain the primed coordinate system. The radius of the minimum sphere in the new (primed) coordinate system is given by

$$r'_o = \sqrt{A^2 + \left(\frac{\lambda}{4}\right)^2} \tag{1.7}$$

Since the radius of the minimum sphere is larger, the truncation number N' for SWE in the new coordinate system is also larger approximately by the same factor. If the minimum sphere of the second antenna does not include the sources of the first antenna, translation of a single antenna would be sufficient to find a "proper" reaction surface as shown in Figure 1.4. However, if we shift both antennas in opposite directions, the required translation distance will be smaller. This approach has two advantages:

- The radii of the minimum spheres are smaller resulting smaller value of N'
- It is easier to find a "proper" reaction surface that is sufficiently away from the minimum spheres of both antennas.

In any case, the number of SWE coefficients is higher in the new coordinate system,

which means that the computational requirements are higher. This is the trade-off we make to solve the problem.

The proposed method can be utilized to calculate mutual coupling between two antennas using the measured or computed near fields of any antenna. The novelty of this approach lies in the utilization of a technique that involves relocating the expansion centers of spherical harmonics for individual antennas to compute mutual impedance. Spherical near-field measurement systems can easily provide the spherical harmonic coefficients of the antenna being tested, which can then be directly used by the proposed method for mutual impedance computation.

1.4 The Outline of the Thesis

This section briefly summarizes the general structure of this thesis.

Chapter 2 provides theoretical background necessary for the subsequent chapters by discussing the reaction theorem and its application to mutual impedance computations. It offers a comprehensive treatment of vector spherical wave expansions, including their definitions and properties. Spherical harmonic expansion constitutes a complete orthogonal set defined on the surface of a sphere. The chapter highlights the orthogonality property of spherical harmonic expansion, which allows for the computation of spherical harmonic coefficients from known fields. This property is briefly summarized in this chapter.

The addition theorem for spherical harmonics states that a spherical harmonic function referenced to one coordinate system can be expressed as a summation of spherical waves referenced to another coordinate system, which is a translated version of the first one. The chapter also presents the translational addition theorem in the general case. The formulas describing translation in arbitrary directions are quite complex. However, translation along the z- axis can be combined with the rotational addition theorem to achieve general translation in arbitrary directions. The necessary theoretical background for rotation and translation along z-axis is detailed in this chapter.

Chapter 3 briefly discusses the convergence problem of spherical wave expansion

when dealing with overlapping minimum spheres. To address this problem, the proposed technique utilizes spherical wave rotation and translation to redefine the region where the outgoing waves radiated by an antenna converge. While this technique is applicable to all types of antennas, an infinitely thin half-wave dipole is specifically chosen as an illustrative example for explaining the concept. To apply the proposed technique for mutual impedance computation, it is necessary to calculate the spherical harmonic coefficients of these dipoles either analytically or numerically. Since well-defined analytical expressions for the near fields of an infinitely thin dipole are available in the literature, the spherical harmonic coefficients are obtained using these near-field expressions and the orthogonality relation. The proposed technique allows for the numerical computation of mutual impedance between two closely spaced dipoles using spherical harmonics. Additionally, an analytical expression for the mutual impedance is derived using this technique, spherical harmonic expansion, and the reaction theorem. The derived analytical formula expresses the mutual impedance as a sum of the products of the spherical harmonic coefficients of both antennas in the same coordinate frame. The numerical and analytical implementation of the proposed method provides a general solution for an array using the known fields of a single element. It is important to note that the fields of the dipoles in free space are used in the application of the proposed method, assuming that the presence of the second antenna does not significantly affect the fields of the first antenna.

Chapter 4 focuses on the application of the proposed technique to the computation of mutual impedance between two infinitely thin half-wave dipoles, and printed dipole antennas. The proposed method is validated numerically and analytically by analyzing the coupling between two half-wave dipoles in a side-by-side configuration. The results show excellent agreement with those obtained from the induced EMF method. The theory is also tested experimentally by designing a printed dipole antenna, and obtaining its spherical harmonic coefficients through spherical near-field measurement. The mutual impedance of two such dipoles is computed using the proposed method, and the results for different element spacings are compared to those obtained from s-parameter measurements. Furthermore, s- parameters are measured for a printed dipole array consisting of four elements. Based on the s-parameter measurements, the active return losses of each port are computed. The active return losses

calculated using the proposed method are then compared to those obtained from the s-parameter measurements.

Chapter 5 focuses on the computation of mutual impedance between two infinitely thin dipoles using the plane wave spectrum technique and reaction theorem. The chapter briefly introduces the plane wave spectrum technique and demonstrates that the plane wave spectrum is an analytical function of its arguments in a certain complex domain. It also discusses the analytical continuation of the spectrum. By using analytical continuation of the spectrum and asymptotic evaluation of radiated fields, the near fields of an infinitely thin half-wave dipole are determined from far-field function for mutual impedance computation. The magnitude and phase distribution of the integrand of the reaction integral are investigated to explore the effective size of the reaction surface. The mutual impedance of two dipoles is computed for different separation distances on a truncated reaction surface, and the results are compared to those obtained from the induced EMF method.

Chapter 6 serves as the conclusion and future work section of this thesis. In the conclusion, we provide a comprehensive summary of our main findings. We analyze both the computational and experimental outcomes and discuss the limitations of the proposed method. Additionally, we examine the effects of disregarding multiple reflections between elements and compare the active return loss results obtained through the proposed method with s-parameter measurements.

In the future work section, we discuss potential extensions of the proposed method, specifically by incorporating multiple reflections between elements, which were not addressed in this thesis.

CHAPTER 2

THEORY

2.1 Reaction theorem and mutual impedance

The concept of reaction, first introduced by Rumsey in [21], describes the interaction between electromagnetic sources through the fields they radiate. This concept is closely related to the Lorentz reciprocity principle [22],[23],[24], and it is a good idea to discuss the reciprocity principle first in order to better understand the reaction concept.

Consider two sets of electric and magnetic current sources, ($\bar{J}_1$,$\bar{M}_1$) and ($\bar{J}_2$,$\bar{M}_2$), that exist in the same simple (linear and isotropic) medium as shown in Figure 2.1. These currents simultaneously radiate at the same frequency and generate ($\bar{E}_1$, $\bar{H}_1$),

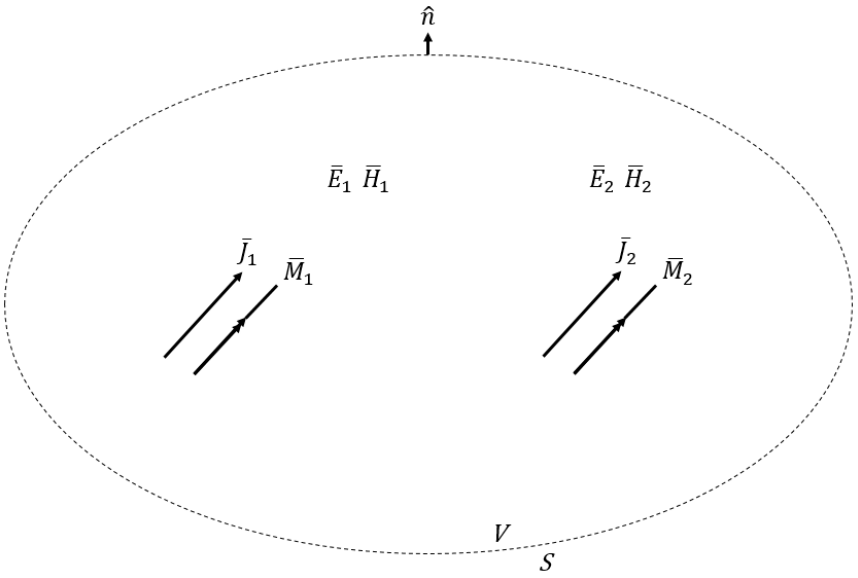

Figure 2.1: Two pair of current sources in the same medium.

and ($\bar{E}_2$, $\bar{H}_2$), respectively. These sources and fields satisfy the differential form of the Lorentz Reciprocity theorem,[23], [25], which can be written as:

$$\nabla \cdot (\bar{E}_1 \times \bar{H}_2 - \bar{E}_2 \times \bar{H}_1) = \bar{E}_2 \cdot \bar{J}_1 - \bar{E}_1 \cdot \bar{J}_2 + \bar{H}_1 \cdot \bar{M}_2 - \bar{H}_2 \cdot \bar{M}_1 \tag{2.1}$$

This equation can be integrated over a volume V which encloses all the sources to obtain:

$$\begin{aligned} \int_V \nabla \cdot (\bar{E}_1 \times \bar{H}_2 - \bar{E}_2 \times \bar{H}_1) dV &= \oint_S (\bar{E}_1 \times \bar{H}_2 - \bar{E}_2 \times \bar{H}_1) \cdot d\bar{S} \\ &= \int_V (\bar{E}_2 \cdot \bar{J}_1 - \bar{E}_1 \cdot \bar{J}_2 + \bar{H}_1 \cdot \bar{M}_2 - \bar{H}_2 \cdot \bar{M}_1) dV \end{aligned} \tag{2.2}$$

where S is the surface that encloses the volume V, and $\hat{n}$ is the outward normal to the surface S. Equation (2.2) is the integral form of the Lorentz Reciprocity theorem. The surface integral in (2.2) becomes zero if the currents are confined in a finite region so that the surface S can be chosen to be a sphere whose radius tends to infinity. Then, (2.2) simplifies to:

$$\int_V (\bar{E}_2 \cdot \bar{J}_1 - \bar{E}_1 \cdot \bar{J}_2 + \bar{H}_1 \cdot \bar{M}_2 - \bar{H}_2 \cdot \bar{M}_1) dV = 0 \tag{2.3}$$

This volume integral can be split into two parts if each set of currents are positioned in separate locations and these sets are included in non-intersecting finite volumes V_1 and V_2 as illustrated in Figure 2.2, yielding:

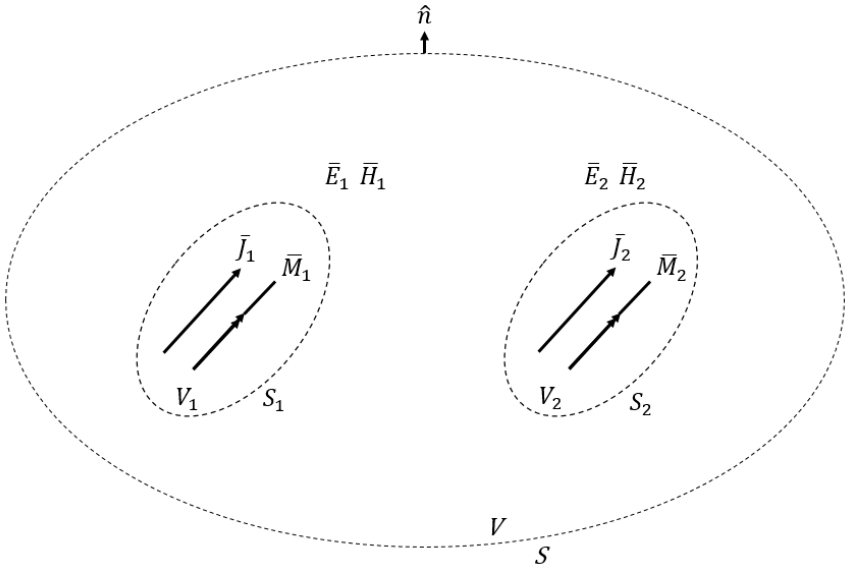

Figure 2.2: Current pairs defined in V_1 and V_2 volumes.

$$\int_V (\bar{E}_2 \cdot \bar{J}_1 - \bar{E}_1 \cdot \bar{J}_2 + \bar{H}_1 \cdot \bar{M}_2 - \bar{H}_2 \cdot \bar{M}_1) dV = \int_{V_1} (\bar{E}_2 \cdot \bar{J}_1 - \bar{H}_2 \cdot \bar{M}_1) dV_1 - \int_{V_2} (\bar{E}_1 \cdot \bar{J}_2 - \bar{H}_1 \cdot \bar{M}_2) dV_2 \tag{2.4}$$

V_1 contains only ($\bar{J}_1$,$\bar{M}_1$) and V_2 contains only ($\bar{J}_2$,$\bar{M}_2$). Then, (2.4) becomes:

$$\int_{V_1} (\bar{E}_2 \cdot \bar{J}_1 - \bar{H}_2 \cdot \bar{M}_1) dV_1 = \int_{V_2} (\bar{E}_1 \cdot \bar{J}_2 - \bar{H}_1 \cdot \bar{M}_2) dV_2 \tag{2.5}$$

Another useful form is obtained by considering that the integration is evaluated on the source free volume as illustrated in Figure 2.3, then the volume integral on the right hand side of (2.2) can be decomposed into three surface integrals as:

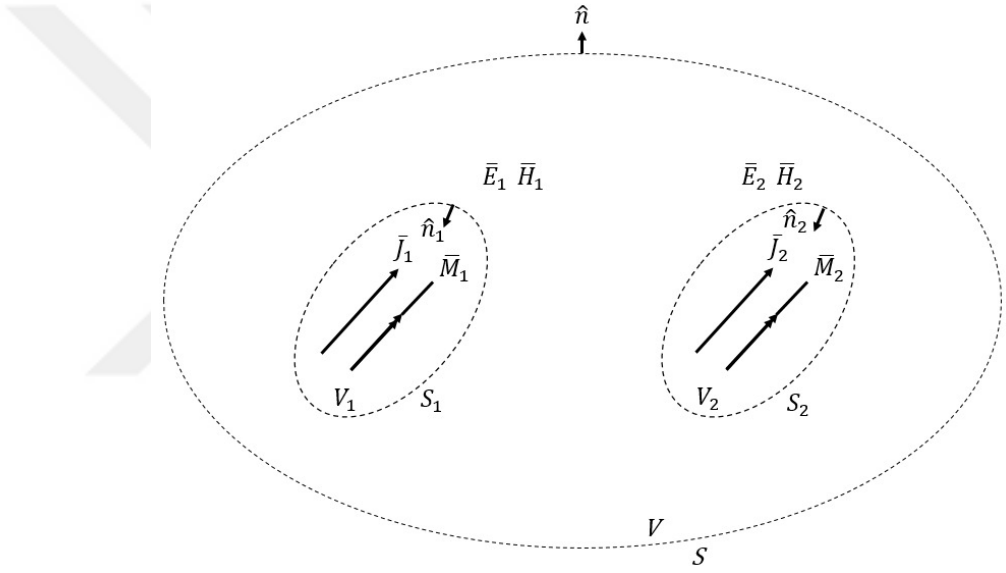

Figure 2.3: Surfaces enclosing source free volume.

$$\oint_S (\bar{E}_1 \times \bar{H}_2 - \bar{E}_2 \times \bar{H}_1) \cdot d\bar{S} + \oint_{S_1} (\bar{E}_1 \times \bar{H}_2 - \bar{E}_2 \times \bar{H}_1) \cdot d\bar{S}_1 + \oint_{S_2} (\bar{E}_1 \times \bar{H}_2 - \bar{E}_2 \times \bar{H}_1) \cdot d\bar{S}_2 \tag{2.6}$$

where S encloses the volume V, S_1 and S_2 are the surfaces of volumes V_1 and V_2, respectively. The direction of $d\bar{S}$ is taken outward from surface enclosing source free region as shown in Figure 2.3. This implies that normal vectors in the integrals over S_1 and S_2 are directed towards the volume including currents. The volume integral in the right hand side of (2.2) will be zero because the volume does not include any sources. The integral over S vanishes when the surface expands to infinity. As a

result, (2.2) simplifies to:

$$\oint_{S_1} (\bar{E}_1 \times \bar{H}_2 - \bar{E}_2 \times \bar{H}_1) \cdot d\bar{S}_1 + \oint_{S_2} (\bar{E}_1 \times \bar{H}_2 - \bar{E}_2 \times \bar{H}_1) \cdot d\bar{S}_2 = 0 \qquad (2.7)$$

If the volume of the integration in (2.2) includes only ($\bar{J}_1$,$\bar{M}_1$), the integral form of Lorentz Reciprocity can be written as:

$$\oint_{S_1} (\bar{E}_1 \times \bar{H}_2 - \bar{E}_2 \times \bar{H}_1) \cdot d\bar{S}_1 = \int_{V_1} (\bar{E}_2 \cdot \bar{J}_1 - \bar{H}_2 \cdot \bar{M}_1) dV_1 \qquad (2.8)$$

A similar expression for ($\bar{J}_2$,$\bar{M}_2$) current pair can be obtained.

$$\oint_{S_2} (\bar{E}_1 \times \bar{H}_2 - \bar{E}_2 \times \bar{H}_1) \cdot d\bar{S}_2 = -\int_{V_2} (\bar{E}_1 \cdot \bar{J}_2 - \bar{H}_1 \cdot \bar{M}_2) dV_2 \qquad (2.9)$$

The right hand sides of equations (2.8) and (2.9) consist of volume integrals that represent the interaction or coupling between a set of fields and a set of currents. This interaction is referred to as "Reaction" in [21], and the volume integrals are denoted as:

$$< 1, 2 >= \int_{V_1} (\bar{E}_2 \cdot \bar{J}_1 - \bar{H}_2 \cdot \bar{M}_1) dV_1 \qquad (2.10)$$

$$< 2, 1 >= \int_{V_2} (\bar{E}_1 \cdot \bar{J}_2 - \bar{H}_1 \cdot \bar{M}_2) dV_2 \qquad (2.11)$$

In this notation, the first index refers to the currents within the volume of integration, while the second index represents the fields produced by the other set of currents that lie outside of the volume. With the help of equations (2.10) and (2.11), the reaction can also represented as surface integrals of the fields, as given in equations (2.12), and (2.13).

$$< 1, 2 >= \oint_{S_1} (\bar{E}_1 \times \bar{H}_2 - \bar{E}_2 \times \bar{H}_1) \cdot d\bar{S}_1 \qquad (2.12)$$

$$< 2, 1 >= \oint_{S_2} (\bar{E}_2 \times \bar{H}_1 - \bar{E}_1 \times \bar{H}_2) \cdot d\bar{S}_2 \qquad (2.13)$$

Consider two sources j and k embeded in the same medium, and excited with terminal currents i_j, and i_k. Richmond [4] indicates that the reaction can also be expressed in terms of network quantities as given in (2.14).

$$v_{jk} i_j = - < j, k > \qquad (2.14)$$

where v_{jk} is the induced voltage at the open terminals of source j in the existence of the fields generated by applied current i_k to the terminal k. In a multiport network

with N terminals, voltage at each terminal may be defined in terms of Z matrix and input currents as

$$\begin{bmatrix} v_1 \\ v_2 \\ : \\ v_n \end{bmatrix} = \begin{bmatrix} z_{11} & ... & z_{1n} \\ z_{21} & ... & z_{2n} \\ : & ... & : \\ z_{n1} & ... & z_{nn} \end{bmatrix} \begin{bmatrix} i_1 \\ i_2 \\ : \\ i_n \end{bmatrix} \tag{2.15}$$

Using (2.12), (2.14), and (2.15), the mutual impedance can be expressed as

$$z_{jk} = \frac{v_j}{i_k}\bigg|_{i_m=0, m\neq k} = \frac{v_{jk}}{i_k} = \frac{-<j,k>}{i_j i_k} = -\frac{1}{i_j i_k}\oint_{S_j}(\bar{E}_j \times \bar{H}_k - \bar{E}_k \times \bar{H}_j)\cdot d\bar{S}_j \tag{2.16}$$

where v_{jk} is the induced voltage at the open terminals of source j in the existence of $(\bar{E}_k, \bar{H}_k)$ fields generated by applied current i_k to the terminal k. $(\bar{E}_j, \bar{H}_j)$ denotes the generated fields by terminal current i_j.

The mutual impedance between two antennas can be calculated from (2.16) when the fields produced by each antenna are measured or computed on a surface S_j that encloses one of the antennas, given the known terminal currents i_j and i_k. This formula only requires knowledge of the port currents and radiated fields, without the need to determine the current distribution.

The expression for mutual impedance given in (2.16) implies that the fields radiated by each source should be known in the presence of the other. Nevertheless, as explained by Richmond [4], knowing the radiated fields of antenna 1 in the presence of antenna 2, along with the fields of antenna 2 in isolation, will be adequate for computing the mutual impedance. In order to understand this situation, consider two arbitrary antennas are placed in the same medium as shown in Figure 2.4. The an-

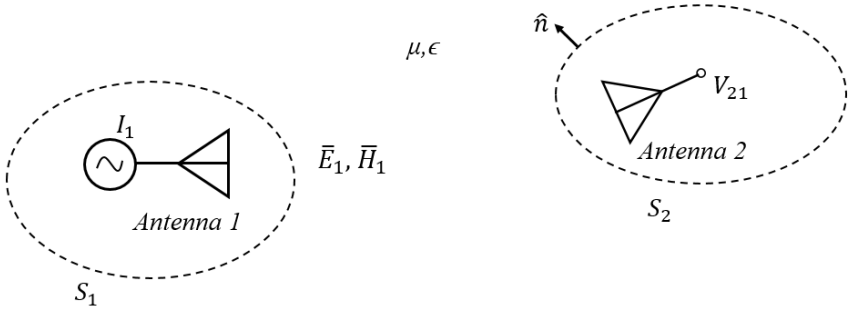

Figure 2.4: Two antennas are embedded in the same medium.

tennas are surrounded by the medium whose electrical properties defined by complex permeability μ, and permittivity ϵ. The medium is assumed to be linear, and time invariant. There is no requirement for the medium to be homogeneous. S_1 and S_2 denote the arbitrary surfaces enclosing antenna 1 and antenna 2, respectively. $\hat{n}$ is the unit normal vector whose direction is taken outward from S_2. When the antenna 1 is excited with current I_1, it radiates in the presence of antenna 2, and generates the fields ($\bar{E}_1$,$\bar{H}_1$). This radiation induces a voltage V_{21} at the open circuited terminals of antenna 2.

In the conventional reciprocity derivations, the roles of antennas are interchanged. This time antenna 2 radiates in the presence of antenna 1, while antenna 1 is terminated with open circuit in the same medium. On the other hand, as claimed in [4], antenna 2 is considered to radiate in a new medium (μ',ϵ') as shown in Figure 2.5. This medium does not include antenna 1, and ($\bar{E}_2'$,$\bar{H}_2'$) denote the fields generated

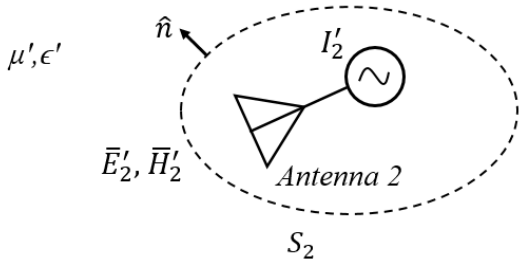

Figure 2.5: Antenna 2 radiates in a new medium.

by antenna 2. Nevertheless, μ' and ϵ' are considered to be the same as unprimed permittivity and permeability, respectively.

As given in [4], the following equation represents the general formula for the reaction theorem.

$$V_{21}I_2' = -\int_{S_2} (\bar{E}_2' \times \bar{H}_1 - \bar{E}_1 \times \bar{H}_2') \cdot dS \tag{2.17}$$

The medium given in Figure 2.4 need not to be isotropic, while antenna 2 is embedded in an isotropic medium. I_2' denotes the current applied to antenna 2. When the induced voltage V_{21} is computed using (2.17), terminal voltages for different load impedances may be found using Thevenin's theorem.

It is important to note that V_{21} denotes the induced voltage in the original case as

given in Figure 2.4. When the constant current source is utilized to feed antenna 2, the current I_2' will remain unchanged even if antenna 2 is embedded in a different medium. Consequently, the left hand side of (2.17) is invariant with respect to the variations in the medium depicted in Figure 2.5. Similarly, this condition applies to the integral on the right-hand side, even though $\bar{E}_2'$ and $\bar{H}_2'$ depend on the medium. As a result, the electrical parameters of the medium (μ', ϵ') can be adjust to represent free space or the same medium in which the antenna 1 radiates. This means that the fields ($\bar{E}_1$,$\bar{H}_1$) of antenna 1 in the presence of the antenna 2, and the fields ($\bar{E}_2'$,$\bar{H}_2'$) of antenna 2 in isolated case will be sufficient to compute the mutual impedance.

In the literature, the induced EMF is a well-known method for calculating the mutual impedance between antennas [26], [27], [28]. This method relies on the free space fields of the antennas while disregarding the effects of multiple reflections between elements. When the antennas are positioned close proximity, the multiple reflections become significant and cannot be ignored. Nevertheless, there is a range of antenna separations where the multiple reflections become negligible, and the mutual impedance can be adequately computed using the free space fields of both antennas. This range is significant in practice since the most antenna arrays employs such distances. Thus, the multiple reflections between elements are disregarded in this study, and the free space fields radiated by antennas are used in the calculation of mutual impedance between antennas.

The subsequent section concentrates on expressing the electromagnetic fields using vector spherical harmonic functions.

2.2 Spherical wave expansion

Spherical wave expansion is a well-known technique in the literature which provides particular solutions to Maxwell's equations [10],[29]. This expansion is well-defined and enables to express the electromagnetic fields as a sum of infinite series of discrete spherical waves. This series expansion constitudes a complete set of orthogonal functions defined on the surface of the sphere. These waves can be widely used in many different applications of electromagnetism, such as antenna theory, electromagnetic

scattering, spherical near-field measurements etc. The formulations of spherical harmonics were first introduced in [30], and the detailed derivation and formulation are performed by Stratton in [31]. A more recent form was derived in [10] for spherical near-field antenna measurements. These expansions are also treated in several books in the literature [9], [25], [32], [33], [34].

In a simple (linear, homogeneous and isotropic) medium, Maxwell's equations can be written as:

$$\bar{\nabla} \times \bar{E} = -j\omega\mu\bar{H} - \bar{M} \tag{2.18}$$

$$\bar{\nabla} \times \bar{H} = \bar{J} + j\omega\epsilon\bar{E} \tag{2.19}$$

where ϵ and μ are permittivity and permeability of the medium. ω is the angular frequency of EM waves. $\bar{E}$ and $\bar{H}$ denote the electric and magnetic fields, respectively and these fields are assumed to be time harmonic with $e^{j\omega t}$ dependence. The electrical and magnetic current sources generating these fields are $\bar{J}$ and $\bar{M}$, respectively. Vector wave equation can be easily derived from Maxwell's equations. This wave equation given in (2.20) is valid for both $\bar{E}$ and $\bar{H}$ fields in a source free region.

$$\bar{\nabla} \times (\bar{\nabla} \times \bar{C}) - k^2\bar{C} = 0 \tag{2.20}$$

where $k = \omega\sqrt{\mu\epsilon}$ is the wavenumber. By choosing k as a complex value, loss in the medium can be taken into account. Nevertheless, in our formulations, the medium is assumed to be lossless.

Consider scalar wave equation is given in a source free region as:

$$(\bar{\nabla}^2 + k^2)f = 0 \tag{2.21}$$

where f is the generating function and this function can be found by solving (2.21). The spherical harmonics are described in the spherical coordinates (r,θ,ϕ) with unit vectors ($\hat{a}_r$, $\hat{a}_\theta$, $\hat{a}_\phi$) as shown in Figure 2.6, and spherical coordinates (r,θ,ϕ) are defined in a usual manner with respect to rectangular coordinates (x,y,z).

Vector functions $\bar{m}$ and $\bar{n}$ can be described as:

$$\bar{m} = \bar{\nabla} f \times \bar{r} \tag{2.22}$$

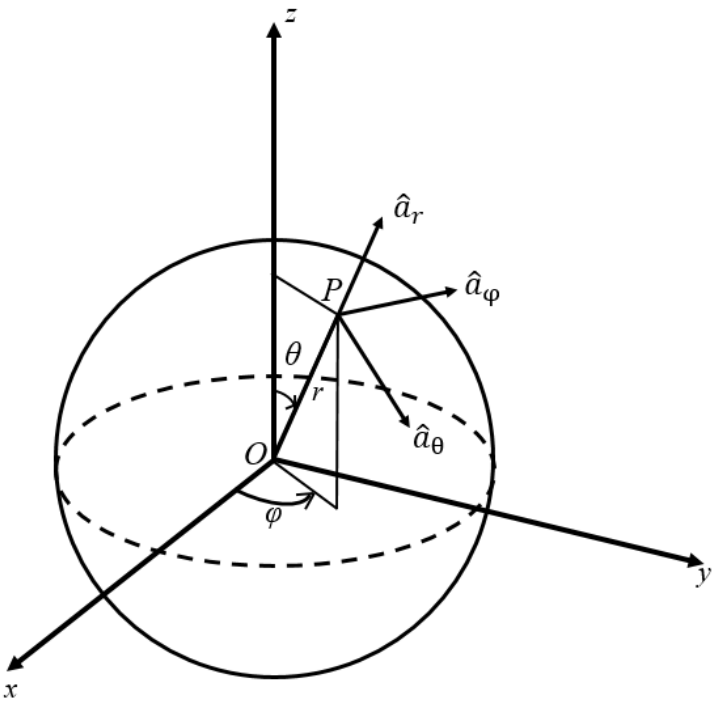

Figure 2.6: Rectangular coordinate system (x,y,z) and spherical coordinate system (r,θ,ϕ).

$$\bar{n} = k^{-1}\bar{\nabla} \times \bar{m} \tag{2.23}$$

where $\bar{r} = r\hat{a}_r$. $\bar{m}$ and $\bar{n}$ functions also satisfy vector wave equation given in (2.20). Using (2.20) and (2.23), we can derive (2.24) as:

$$\bar{m} = k^{-2}\bar{\nabla} \times (\bar{\nabla} \times \bar{m}) = k^{-1}\bar{\nabla} \times \bar{n} \tag{2.24}$$

$\bar{m}$ can be obtained in terms of k and curl of $\bar{n}$ as given in (2.24). Since the similar relation exists between $\bar{E}$ and $\bar{H}$ fields in a homogeneous and source free medium, $\bar{m}$ and $\bar{n}$ may be used to represent $\bar{E}$ and $\bar{H}$ fields.

By using the method of separation variables given in [31], the power normalized generating function can be written as:

$$F_{mn}^{(c)}(r,\theta,\phi) = \frac{1}{\sqrt{2\pi}} \frac{1}{\sqrt{n(n+1)}} \left(- \frac{m}{|m|} \right)^m z_n^{(c)}(kr) \bar{P}_n^{|m|}(\cos\theta) e^{jm\phi} \tag{2.25}$$

By substituting the generating function in (2.25) into (2.22) and (2.23), then we can obtain spherical harmonic functions $\bar{m} = \bar{F}_{1mn}^{(c)}$, and $\bar{n} = \bar{F}_{2mn}^{(c)}$. The mathematical

expressions of these functions are provided in Appendix B.1 and B.2. This notation for vector spherical harmonic functions are used throughout this thesis.

2.2.1 Spherical wave expansion of EM fields

A monochromatic electromagnetic wave can be represented as a combination of spherical waves in a source free region of space. The electric and magnetic fields emitted by an arbitrary antenna can be expressed using these wave functions, as described in equations (2.26) and (2.27), respectively.

$$\bar{E}(r,\theta,\phi) = k\sqrt{\eta}\sum_{s=1}^{2}\sum_{n=1}^{\infty}\sum_{m=-n}^{n} Q_{smn}^{(c)}\bar{F}_{smn}^{(c)}(r,\theta,\phi) \tag{2.26}$$

$$\bar{H}(r,\theta,\phi) = \frac{jk}{\sqrt{\eta}}\sum_{s=1}^{2}\sum_{n=1}^{\infty}\sum_{m=-n}^{n} Q_{smn}^{(c)}\bar{F}_{3-s,m,n}^{(c)}(r,\theta,\phi) \tag{2.27}$$

where $k = w\sqrt{\mu\epsilon}$ is the wave number and η is the instrinsic impedance of the medium. The notation is similar to that used in [10] apart from time dependence which is taken $e^{j\omega t}$. The upper index (c) defines the radial dependencies of the spherical wave function. $c = 3$ corresponds to spherical Hankel functions of the first kind, representing an incoming wave, while $c = 4$ corresponds to spherical Hankel functions of the second kind, representing an outward propagating wave. The electric and magnetic fields expanded using outgoing spherical waves are only valid within the region outside of the minimum sphere enloses the antenna. The incoming wave expansion converges inside any sphere that excludes all sources, while outgoing wave expansion converges outside any sphere that includes all sources. Figure 2.7 illustrates convergence region of spherical harmonic functions representing outgoing waves, and the minimum sphere for an arbitrary antenna. When the array elements are placed very close to each other, the minimum spheres may overlap, making it difficult to directly utilize the spherical harmonic expansion technique to compute the mutual coupling between elements.

The index s in the spherical wave functions as given in (2.26) and (2.27) represents two different functions, $\bar{F}_{1mn}^{(c)}$ and $\bar{F}_{2mn}^{(c)}$, which are power-normalized spherical vector wave functions. The function $\bar{F}_{1mn}^{(c)}$ has no radial component, meaning it describes the transverse part of an electric or magnetic field with respect to the radial coordinate r.

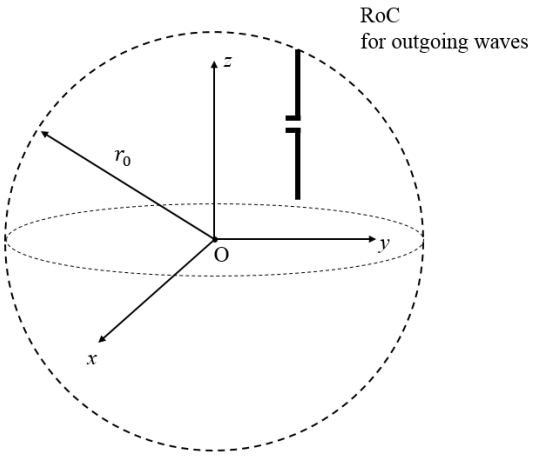

Figure 2.7: Convergence region of outgoing spherical waves.

The electric field of a transverse magnetic (TM) wave is represented by $\bar{F}_{2mn}^{(c)}$, while its magnetic field is represented by $\bar{F}_{1mn}^{(c)}$. For transverse electric (TE) waves, the electric field is represented by $\bar{F}_{1mn}^{(c)}$ and the magnetic field is proportional to $\bar{F}_{2mn}^{(c)}$. The index s has a slightly different meaning in the definition of Q_{smn}. Q_{1mn} defines the strength of the transverse electric (TE) part of an electromagnetic field, while Q_{2mn} describes the strength of the transverse magnetic (TM) part. The sum of the index s in the expansion functions as given in (2.26) or (2.27) is always 3.

The spherical wave functions $\bar{F}_{1mn}^{(c)}$ and $\bar{F}_{2mn}^{(c)}$ are dimensionless, while the wave coefficients have the dimension of $\sqrt{W}$.

The variation over the spherical angle θ is represented by the index n, while the index m describes the variation over the spherical angle ϕ. The index n takes positive integer values, while the index m ranges from $-n$ to n. For numerical purposes, the infinite sum in (2.26) and (2.27) must be truncated at some N. Although there are many different formulas proposed for the truncation number N, in this work $N \simeq kr_o + 3\sqrt[3]{kr_o}$ is used as proposed in [8] and [10], where r_o is the radius of the minimum sphere enclosing the antenna. However, it should be noted that for points very close to the boundary of convergence region, a higher truncation number must be chosen. Even then numerical errors may prevent convergence of the spherical wave expansion (SWE).

2.3 Orthogonality relation for spherical harmonic functions

The spherical harmonic functions constitute a complete set of orthogonal functions defined on the surface of a sphere. The general form of orthogonality relation for spherical harmonics given in [10] is expressed as:

$$\int_{\phi=0}^{2\pi}\int_{\theta=0}^{\pi} \bar{F}^{(c)}_{smn}(r,\theta,\phi)\cdot\bar{F}^{(\gamma)*}_{\sigma\mu v}(r,\theta,\phi)\sin\theta d\theta d\phi =$$

$$\delta_{s,\sigma}\delta_{m,\mu}\delta_{n,v}(-1)^m\left\{R^{(c)}_{sn}(kr)R^{(\gamma)*}_{sn}(kr)+\delta_{s,2}n(n+1)\frac{z^{(c)}_n(kr)}{kr}\frac{z^{(\gamma)*}_n(kr)}{kr}\right\} \quad (2.28)$$

The following subsection introduces computation of SWE coefficients of a field using orthogonality relation.

2.3.1 The computation of SWE coefficients of a field using orthogonality

The orthogonality of spherical harmonics can be utilized to determine SWE coefficients of a field by taking the inner product of $\bar{F}^*_{smn}$ and the $\bar{E}$ field expansion given in (2.26). Using this inner product with orthogonality integral in (2.28), the spherical wave coefficients can be found as:

$$Q_{1mn} = \frac{\int_{\phi=0}^{2\pi}\int_{\theta=0}^{\pi}\bar{E}\cdot\bar{F}^*_{1mn}\sin\theta d\theta d\phi}{k\sqrt{\eta}\Delta_1(kr)}, \quad (2.29)$$

$$Q_{2mn} = \frac{\int_{\phi=0}^{2\pi}\int_{\theta=0}^{\pi}\bar{E}\cdot\bar{F}^*_{2mn}\sin\theta d\theta d\phi}{k\sqrt{\eta}\left[\frac{n(n+1)}{(kr)^2}\Delta_1(kr)+\Delta_2(kr)\right]} \quad (2.30)$$

where $\Delta_1(kr)=R_{1n}(kr)R^*_{1n}(kr)$, $\Delta_2(kr)=R_{2n}(kr)R^*_{2n}(kr)$, $R_{1n}(kr)=h^{(2)}_n(kr)$, and $R_{2n}(kr)=\frac{1}{kr}\frac{d(krh^{(2)}_n(kr))}{d(kr)}$. The sign $*$ denotes complex conjugate operator. If we have knowledge of the $\bar{E}$ field radiated by an antenna, obtained through computation or measurement on a surface surrounding the antenna, we can then calculate the SWE coefficients of the antenna using equations (2.29), and (2.30).

2.4 Addition theorems for vector spherical harmonics

The translational addition theorem for spherical harmonic functions states that a spherical vector wave function defined in one coordinate system can be expressed as a

linear combination of spherical harmonic functions in another coordinate system obtained by translating the former, as depicted in Figure 2.8. The primed coordinate

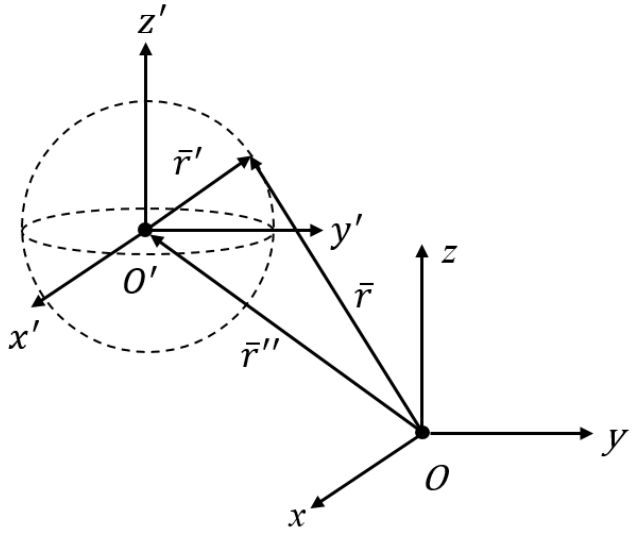

Figure 2.8: Addition theorem for spherical waves.

system is translated version of unprimed one in an arbitrary direction. The derivation of formulas for translation in an arbitrary direction is outlined well by [35]. However, the notation used in [8] is utilized here to briefly summarize translational addition theorem in general case. The general addition theorem states that vector spherical harmonic functions $\bar{\mathbf{M}}^{(2)}_{n,m}(\bar{\mathbf{r}})$ and $\bar{\mathbf{N}}^{(2)}_{n,m}(\bar{\mathbf{r}})$ can be expressed as:

$$\bar{\mathbf{M}}^{(2)}_{n,m}(\bar{\mathbf{r}}) = \sum_{n',m'} A_{n',m';n,m}\bar{\mathbf{M}}^{(i)}_{n',m'}(\bar{\mathbf{r}}') + B_{n',m';n,m}\bar{\mathbf{N}}^{(i)}_{n',m'}(\bar{\mathbf{r}}') \tag{2.31}$$

$$\bar{\mathbf{N}}^{(2)}_{n,m}(\bar{\mathbf{r}}) = \sum_{n',m'} A_{n',m';n,m}\bar{\mathbf{N}}^{(i)}_{n',m'}(\bar{\mathbf{r}}') + B_{n',m';n,m}\bar{\mathbf{M}}^{(i)}_{n',m'}(\bar{\mathbf{r}}') \tag{2.32}$$

The mathematical expressions of $A_{n',m';n,m}$ and $B_{n',m';n,m}$ coefficients is given in Appendix (C.3), (C.4). The coefficients $A_{n',m';n,m}$ and $B_{n',m';n,m}$ in equation (2.31) and (2.32), can be very complex for a translation in a general direction. However, if the translation is along the z-axis of the original coordinate frame, these expressions can be greatly simplified, and recursive formulas are available to obtain these coefficients [20].

Similarly, the rotational addition theorem expresses the spherical vector functions in a coordinate frame as a linear combination of spherical wave functions in a rotated

coordinate frame. The coefficients for the rotational addition theorem are relatively simple.

A general coordinate transformation typically involves three successive transformations. Firstly, a rotation of the original coordinate frame is done to align the translation vector along the z-axis, followed by a translation along the z-axis, and finally, a rotation is performed to align the axes in the desired direction.

2.4.1 Rotational addition theorem

Consider two right-handed rectangular coordinate systems initially referenced to the same origin and aligned with each other. The unprimed coordinate system remains unchanged, while the primed coordinate system is rotated around the origin from its initial position to an arbitrary position in space. The final position of the primed coordinate system can be obtained by applying three consecutive rotations, as shown in Figure 2.9 [10]. The (x_1,y_1,z_1) coordinate system shows the coordinate system after the first rotation about the z-axis through an angle of ϕ_o. The rotation about the y_2-axis then moves the (x_1,y_1,z_1) coordinate frame to the (x_2,y_2,z_2) frame through an angle of θ_o. Finally, the primed coordinate system is obtained by a rotation of the (x_2,y_2,z_2) coordinate frame about the z_2-axis through an angle of χ_o. The rotational movement from the unprimed to the primed coordinate system is defined by three Euler angles (χ_o,θ_o,ϕ_o). A spherical vector wave function associated with the unprimed coordinate system $\bar{F}^{(c)}_{smn}(r,\theta,\phi)$ can be written as a summation of spherical vector wave functions referenced to primed coordinate system (r',θ',ϕ'), which is rotated with respect to the unprimed one. This expansion is given as:

$$\bar{F}^{(c)}_{smn}(r,\theta,\phi) = \sum_{\mu=-n}^{n} e^{jm\phi_o} d^n_{\mu m}(\theta_o) e^{j\mu\chi_o} \bar{F}^{(c)}_{s\mu n}(r',\theta',\phi') \tag{2.33}$$

where $d^n_{\mu m}(\theta_o)$ denotes the rotation coefficient and its mathematical expression is given in Appendix D.2.

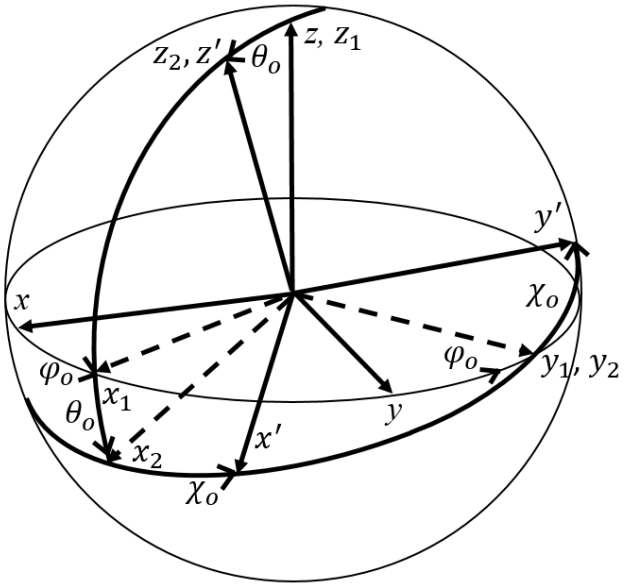

Figure 2.9: Rotation of spherical waves.

2.4.2 Translational addition theorem along z- axis

Consider two rectangular coordinate systems which are initially aligned and referenced to the same origin. The first system, denoted as unprimed system (x,y,z), remains stationary in its initial position. On the other hand, the second system, denoted as primed system (x',y',z'), is shifted by a distance A in the positive z direction, as illustrated in Figure 2.10. A spherical vector wave function, represented as $\bar{F}^{(c)}_{smn}(r,\theta,\phi)$ and referenced to the unprimed coordinate system, may be expressed as a sum of vector spherical wave functions referenced to the primed coordinate system which is translated by distance A. Translation is performed in the z direction by a distance A. The expressions for two cases are given in (2.34) and (2.35).

$$\bar{F}^{(c)}_{s\mu n}(r,\theta,\phi) = \sum_{\sigma=1}^{2}\sum_{\substack{\nu=|\mu|\\ \nu\neq 0}}^{\infty} C^{sn(c)}_{\sigma\mu\nu}(kA)\bar{F}^{(1)}_{\sigma\mu\nu}(r',\theta',\phi') \quad r' < |A| \tag{2.34}$$

$$\bar{F}^{(c)}_{s\mu n}(r,\theta,\phi) = \sum_{\sigma=1}^{2}\sum_{\substack{\nu=|\mu|\\ \nu\neq 0}}^{\infty} C^{sn(1)}_{\sigma\mu\nu}(kA)\bar{F}^{(c)}_{\sigma\mu\nu}(r',\theta',\phi') \quad r' > |A| \tag{2.35}$$

where translation coefficient $C^{sn(c)}_{\sigma\mu\nu}(kA)$ takes the product of wave number k and translation distance A as the input argument. The expression for translation coefficients in the z direction for positive arguments $(kA > 0)$ is given in Appendix D.6.

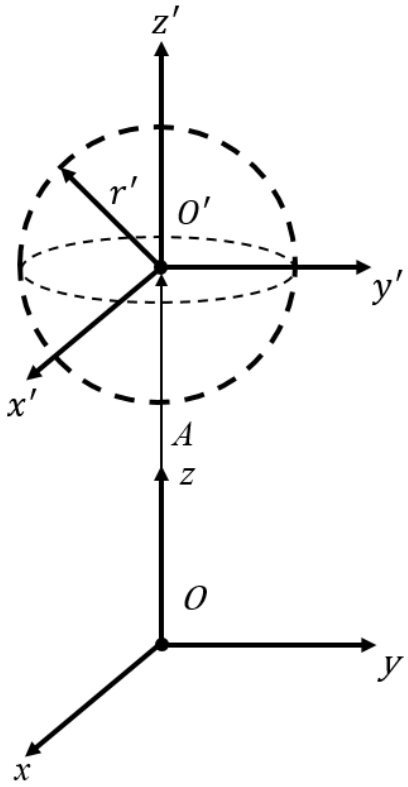

Figure 2.10: Translation of spherical waves.

It is evident that the spherical wave functions on the right hand side of (2.34) or (2.35) include the same azimuthal index μ as the left-hand side. This means that translation in the z direction does not affect the ϕ dependence of spherical wave functions. These formulas describing z-translation should be considered as a special form of general translation in arbitrary direction. However, the translation in arbitrary direction may be achieved by consecutive application of three operations: rotation, axial translation, and inverse rotation.

Translation coefficients for negative arguments may be evaluated by using simple symmetry relation given below.

$$C_{\sigma\mu\nu}^{sn(c)}(-kA) = (-1)^{s+\sigma}(-1)^{n+\nu}C_{\sigma\mu\nu}^{sn(c)}(kA) \tag{2.36}$$

CHAPTER 3

PROPOSED METHOD

3.1 Convergence problem of SWE for overlapping spheres

Consider two dipole antennas positioned in the right hand rectangular coordinate system as shown in Figure 3.1. The unprimed coordinate frames have their origins aligned with the feed points of each antenna. The centers of the smallest spheres that enclose the dipoles are situated at the origins of the unprimed coordinate systems, namely (x_1, y_1, z_1) and (x_2, y_2, z_2), respectively.

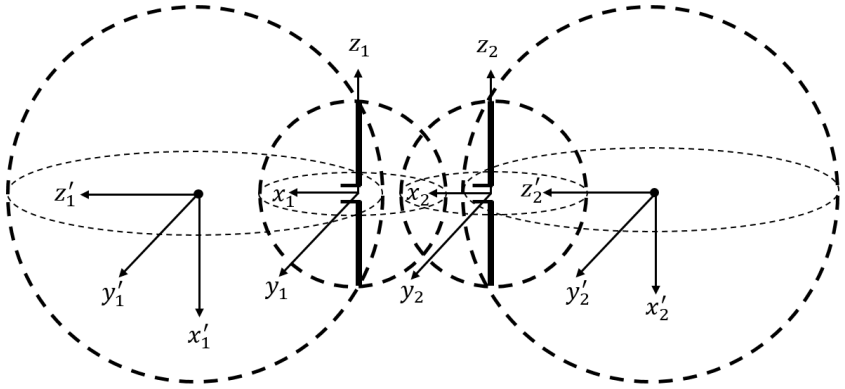

Figure 3.1: Overlapping of minimum spheres.

When the port currents, and the fields of both antennas are known on a "proper" reaction surface that encloses one of the antennas, the mutual impedance can be found using reaction theorem. A "proper" reaction surface should entirely encompass one of the antennas, and lie completely within the region where the spherical harmonics representing the fields of the two dipoles converge. In a general case, spherical wave functions that represent outwardly propagating waves converge in the outer region

of the minimum sphere that surrounds the antenna. However, when two dipoles are closely positioned as depicted in Figure 3.1, the minimum spheres enclosing the antennas overlap. Consequently, it becomes impossible to establish a "proper" reaction surface in the area where the spherical harmonic functions, representing outgoing waves from both antennas, converge. To resolve the problem of overlapping minimum spheres, the proposed technique uses rotation and translation of spherical waves to move the expansion centers of the spherical harmonic functions away from each other, and enables to redefine the new minimum spheres as shown in Figure 3.1.

Spherical harmonic expansions are infinite summations and in practice we must truncate these infinite summations. This raises convergence issues in implementing the proposed algorithm. The translation distance, truncation numbers in the original and the translated coordinate frames are important parameters that affect numerical accuracy of the algorithm. These issues are discussed in the next chapter.

3.2 Rotation and translation of spherical waves

The main objective of this section is to explore the utilization of spherical wave rotation and translation in order to redefine the region where the outgoing waves radiated by an antenna converge. While this technique can be applied to any type of antenna, an infinitely thin half-wave dipole has been specifically chosen as the antenna to serve as an illustrative example for conveying the concept.

Following section describes the rotation and translation along the rotated z-axis to redefine the convergence region of the outgoing waves associated with antenna 1.

3.2.1 Rotation and translation of spherical waves for antenna 1

Consider an infinitely thin half-wave dipole antenna (antenna 1) which is placed in the unprimed right handed rectangular coordinate system as shown in Figure 3.2. The feed point of the dipole is positioned at the origin, and the arms of the dipole extend along z_1 axis. The unprimed coordinate system is first rotated about its y_1 axis by 90 degree (through θ), and then translated along the rotated z_1 axis by a distance A

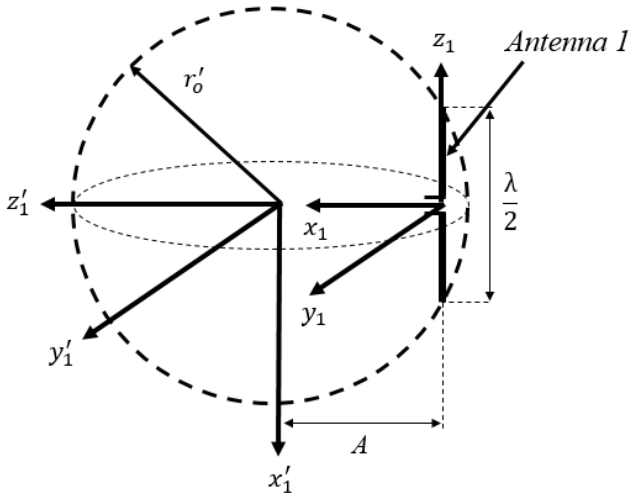

Figure 3.2: Translation of coordinate system for antenna 1.

to obtain primed coordinate system. The region outside the new minimum sphere, which is centered at the origin of the primed coordinate system, and has a radius of r'_o, now serves as the new convergence region for antenna 1. The outgoing waves within this region can be expressed using vector spherical harmonics referenced to the primed coordinate frame. The radius of the minimum sphere in the new (primed) coordinate system is given by

$$r'_o = \sqrt{A^2 + \left(\frac{\lambda}{4}\right)^2} \tag{3.1}$$

Since the radius of the minimum sphere in primed coordinate system r'_o is larger than unprimed case, the truncation number N' for SWE in the primed coordinate system is also larger approximately by the same factor.

The translation from unprimed to primed coordinate system is accomplished through a two-step process. The unprimed coordinate system is first rotated by 90 degrees (through θ) about its y_1-axis, then as a second step, the rotated coordinate frame is translated along its z_1 axis by a distance A.

The process of rotating the system around the y_1-axis by 90 degrees involves expressing the spherical vector wave functions associated with the unprimed coordinate system $\bar{F}^{(c)}_{smn}(r, \theta, \phi)$ in terms of the spherical vector wave functions referenced to the rotated coordinate frame $(r_{R1}, \theta_{R1}, \phi_{R1})$ through the use of the rotational addition

theorem. Given that the rotation occurs only about the y_1-axis with an angle of 90 degrees (i.e., $\theta_o = 90$), this expansion takes on a simplified form, as shown in (3.2).

$$\bar{F}^{(c)}_{smn}(r,\theta,\phi) = \sum_{\mu=-n}^{n} d^n_{\mu m}(\theta_o)\bar{F}^{(c)}_{s\mu n}(r_{R1},\theta_{R1},\phi_{R1}) \tag{3.2}$$

Then, as the second step, the spherical harmonics referenced to the rotated frame, $\bar{F}^{(c)}_{s\mu n}(r_{R1},\theta_{R1},\phi_{R1})$, are expressed in terms of spherical harmonics associated with the primed coordinate frame as:

$$\bar{F}^{(c)}_{s\mu n}(r_{R1},\theta_{R1},\phi_{R1}) = \sum_{\sigma=1}^{2}\sum_{\substack{\nu=|\mu| \\ \nu\neq 0}}^{Nt} C^{sn(1)}_{\sigma\mu\nu}(kA)\bar{F}^{(c)}_{\sigma\mu\nu}(r'_1,\theta'_1,\phi'_1) \quad r'_o > |A| \tag{3.3}$$

where the truncation number N_t for translation is specified as $kr'_o + 3\sqrt[3]{kr'_o}$. It is worth emphasizing that the upper index (c) in the spherical harmonic functions is invariant under rotation, as indicated in (3.2). Furthermore, the upper index (c) remains unchanged when the value of r'_o exceeds that of A as given in (3.3).

3.2.2 Rotation and translation of spherical waves for antenna 2

Suppose that an infinitely thin half-wave dipole (antenna 2) is positioned in the unprimed right handed rectangular coordinate system as illustrated in Figure 3.3. In this case, the unprimed coordinate system for antenna 2 is rotated about its y_2 axis by 90 degree (through θ) as we did for antenna 1. Since the expansion centers of the antennas are shifted away from each other, this time translation in the rotated z_2 axis is done in z_2 direction by a distance $-A$. The new convergence region of antenna 2 is again specified by consecutive application of rotation and translation operations as shown in Figure 3.3. The outwardly propagating waves within this region can be expressed using vector spherical harmonics referenced to (x'_2, y'_2, z'_2) primed coordinate frame. The same expansion in (3.3), along with the symmetry relation for translation coefficients given in (3.4) enables us to obtain the translation from the rotated frame to the (x'_2, y'_2, z'_2) coordinate system.

$$C^{sn(c)}_{\sigma\mu\nu}(-kA) = (-1)^{s+\sigma}(-1)^{n+\nu}C^{sn(c)}_{\sigma\mu\nu}(kA) \tag{3.4}$$

If the minimum sphere of the second antenna does not contain the sources of the first

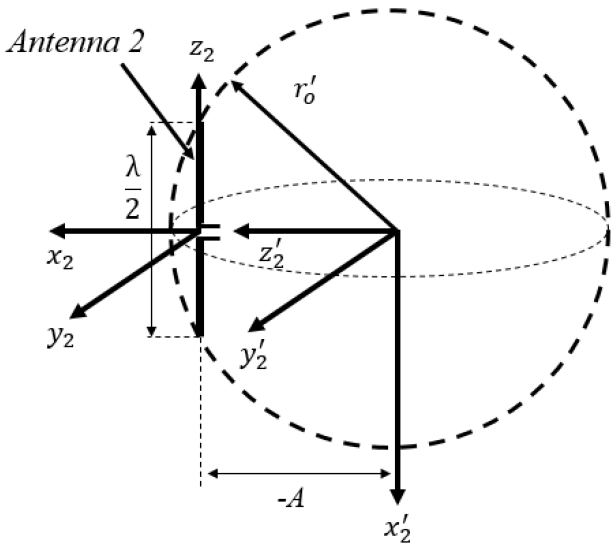

Figure 3.3: Translation of coordinate system for antenna 2.

antenna, translation of single antenna would be sufficient to find a "proper" reaction surface as in the case shown in Figure 3.1. However, if we move the expansion centers of both antennas away from each other, the required translation distance will be smaller. This approach offers two advantages:

- The radii of the minimum spheres are reduced, resulting in a smaller value of N'.
- It becomes easier to find a suitable reaction surface that is sufficiently distant from the minimum spheres of both antennas.

Nevertheless, it is important to note that the number of SWE (spherical wave expansion) coefficients is higher in the primed coordinate system. This implies a higher computational load, which is the price we pay in solving the problem.

3.3 Numerical method for computation of mutual impedance between two half-wave dipoles

The main objective of this section is to apply the proposed method to numerically compute the mutual impedance between two infinitely thin half-wave dipoles. To

achieve this, it is necessary to calculate the spherical harmonic coefficients of these dipoles either analytically or numerically. Since the literature provides well-defined analytical expressions for the near fields of an infinitely thin dipole, the spherical harmonic coefficients can be obtained using these near field expressions and the orthogonality relation. The subsequent section provides a concise overview of the derivation process for the near field expressions of an infinitely thin dipole.

3.3.1 Near-field expressions of infinitely thin half-wave dipole

To compute the mutual impedance between two antennas, the near fields of the elements must be known. The near fields of an antenna can be calculated either analytically or numerically using an EM solver. In the literature, there are well-known near-field expressions for an infinitely thin dipole of arbitrary length, which can be found in references [26] and [36]. This section provides a brief overview of the derivation of these analytical expressions.

Consider an infinitely thin half-wave dipole antenna placed in a right handed rectangular coordinate system as illustrated in Figure 3.4. The feed point of the dipole is positioned at the origin, the arms of the dipole extend along z-axis. The near fields are derived based on the geometry in Figure 3.4. In the following derivation, we will utilize cylindrical coordinate system described in the usual manner with respect to the rectangular coordinate system.

For an infinitely thin half-wave dipole, the magnetic potential can be obtained by assuming a sinusoidal current distribution from which the magnetic field can be found as:

$$\bar{H} = \frac{1}{\mu}\nabla \times \bar{A} = -\hat{a}_\phi \frac{1}{\mu}\frac{\partial A_z}{\partial \rho} \tag{3.5}$$

It can be shown that the magnetic field radiated by the dipole is

$$\bar{H} = \hat{a}_\phi H_\phi = -\hat{a}_\phi \frac{I_o}{4\pi j}\frac{1}{\rho}\left[e^{-jkR_1} + e^{-jkR_2} - 2\cos\left(\frac{kl}{2}\right)e^{-jkr}\right] \tag{3.6}$$

where l represents the length of the dipole, and

$$r = \sqrt{x^2 + y^2 + z^2} = \sqrt{\rho^2 + z^2} \tag{3.7}$$

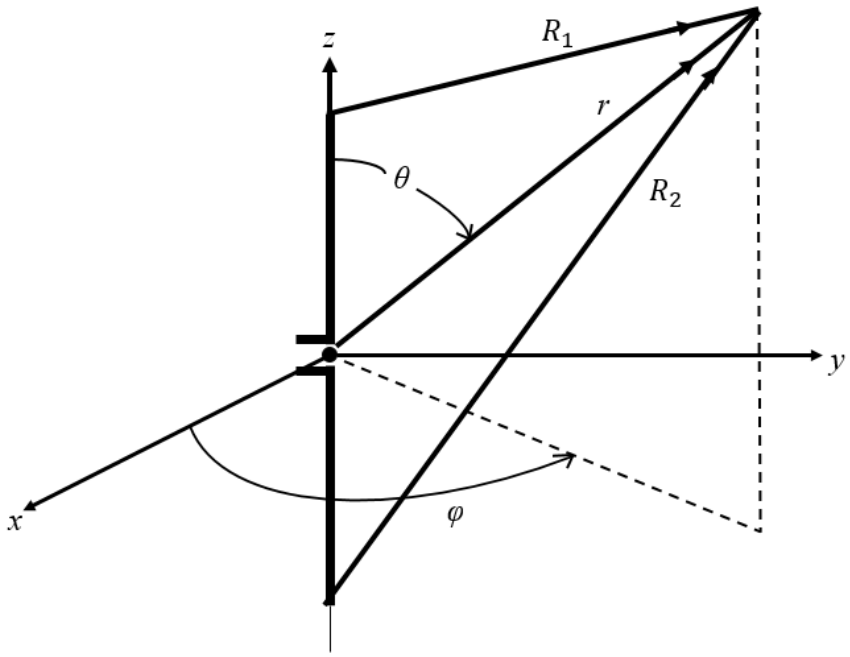

Figure 3.4: An infinitely thin dipole geometry for near-field analysis.

$$R_1 = \sqrt{x^2 + y^2 + \left(z - \frac{l}{2}\right)^2} = \sqrt{\rho^2 + \left(z - \frac{l}{2}\right)^2} \tag{3.8}$$

$$R_2 = \sqrt{x^2 + y^2 + \left(z + \frac{l}{2}\right)^2} = \sqrt{\rho^2 + \left(z + \frac{l}{2}\right)^2} \tag{3.9}$$

as shown in Figure 3.4. The corresponding $\bar{E}$-field can also be found using Maxwell equations as:

$$\bar{E} = \frac{1}{j\omega\epsilon} \nabla \times \bar{H} \tag{3.10}$$

The exact expression for the $\bar{E}$-field of an infinitely thin dipole of arbitrary length l is:

$$\bar{E} = \hat{a}_\rho E_\rho + \hat{a}_z E_z = -\hat{a}_\rho \frac{1}{j\omega\epsilon} \frac{\partial H_\phi}{\partial z} + \hat{a}_z \frac{1}{j\omega\epsilon} \frac{1}{\rho} \frac{\partial}{\partial \rho}(\rho H_\phi) \tag{3.11}$$

where

$$E_\rho = j\frac{\eta I_o}{4\pi\rho} \left[\left(z - \frac{l}{2}\right) \frac{e^{-jkR_1}}{R_1} + \left(z + \frac{l}{2}\right) \frac{e^{-jkR_2}}{R_2} - 2z\cos\left(\frac{kl}{2}\right) \frac{e^{-jkr}}{r} \right] \tag{3.12}$$

$$E_z = -j\frac{\eta I_o}{4\pi} \left[\frac{e^{-jkR_1}}{R_1} + \frac{e^{-jkR_2}}{R_2} - 2\cos\left(\frac{kl}{2}\right) \frac{e^{-jkr}}{r} \right] \tag{3.13}$$

The derivation of the $\bar{E}$ and $\bar{H}$ fields relies on the assumption of an infinitely thin wire. However, practical wire antennas have a thickness that is significantly smaller compared to the wavelength (typically considered as $\lambda/100$). Consequently, the fields obtained from the aforementioned derivation can be considered a reliable approximation for thin dipoles.

3.3.2 Computation of SWE coefficients of half-wave dipole

The spherical harmonic coefficients of an arbitrary antenna can be calculated using measured or computed fields with orthogonality relations as given in (3.14) and (3.15).

$$Q_{1mn} = \frac{\int_{\phi=0}^{2\pi}\int_{\theta=0}^{\pi}\bar{E}\cdot\bar{F}_{1mn}^{*}\sin\theta d\theta d\phi}{k\sqrt{\eta}\Delta_1(kr)}, \tag{3.14}$$

$$Q_{2mn} = \frac{\int_{\phi=0}^{2\pi}\int_{\theta=0}^{\pi}\bar{E}\cdot\bar{F}_{2mn}^{*}\sin\theta d\theta d\phi}{k\sqrt{\eta}\left[\frac{n(n+1)}{(kr)^2}\Delta_1(kr)+\Delta_2(kr)\right]} \tag{3.15}$$

where we have defined $\Delta_1(kr) = R_{1n}(kr)R_{1n}^{*}(kr)$, $\Delta_2(kr) = R_{2n}(kr)R_{2n}^{*}(kr)$, $R_{1n}(kr) = h_n^{(2)}(kr)$, and $R_{2n}(kr) = \frac{1}{kr}\frac{d(krh_n^{(2)}(kr))}{d(kr)}$. By substituting $\bar{E}$ field expressions given in (3.12) and (3.13) into (3.14), and (3.15), we can determine the spherical harmonic coefficients for an infinitely thin half-wave dipole antenna. The literature already provides analytical formulas for the SWE coefficients of an infinitely thin dipole [37]. However, since the proposed technique is applicable to all types of antennas, we provide the computation of SWE coefficients here in a general context.

3.3.3 Mutual impedance between two infinitely thin half-wave dipoles

The fields associated with antenna 1 can be expressed using spherical wave expansion associated with (x_1', y_1', z_1') coordinate system as:

$$\bar{E}_1 = k\sqrt{\eta}\sum_{s=1}^{2}\sum_{n=1}^{N_f}\sum_{m=-n}^{n} {}_1Q_{smn}^{(4)}\bar{F}_{smn}^{(4)}(r_1', \theta_1', \phi_1') \tag{3.16}$$

$$\bar{H}_1 = \frac{jk}{\sqrt{\eta}}\sum_{s=1}^{2}\sum_{n=1}^{N_f}\sum_{m=-n}^{n} {}_1Q_{smn}^{(4)}\bar{F}_{3-smn}^{(4)}(r_1', \theta_1', \phi_1') \tag{3.17}$$

where ${}_1Q^{(4)}_{smn}$ denotes the spherical harmonic coefficients referenced to (x'_1, y'_1, z'_1) coordinate system as depicted in Figure 3.2. The pre-subscript is utilized to indicate that the coefficients belong to the field expansion of antenna 1. $\bar{F}^{(4)}_{smn}(r'_1, \theta'_1, \phi'_1)$ represents the spherical harmonic functions in the primed (x'_1, y'_1, z'_1) coordinate system.

Considering that the outgoing waves are expanded using spherical harmonics within the region outside the minimum sphere that encloses the infinitely thin half-wave dipoles, hence, the upper superscript (c) equals to 4, as specified in (3.16) and (3.17). The spherical wave coefficients ${}_1Q^{(4)}_{smn}$ are obtained from known coefficients (Q_{1mn}, Q_{2mn}) referenced to unprimed coordinate frame in two steps: the first step is to rotate the unprimed coordinate frame about its y_1 axis by 90 degree, and the second step is to translate the rotated coordinate frame along its z_1 axis by a distance A as illustrated in Figure 3.2. The radius of the new minimum sphere r'_0 in the new (primed) coordinate system is given by (3.1). The truncation number N_f in the new (primed) coordinate frame is $kr'_0 + 3\sqrt[3]{kr'_0}$. The convergence analysis in the subsequent chapter will demonstrate that this expression for the truncation number is also valid in the translated frame. Note that the upper index (c) in the spherical harmonic functions is invariant under rotation operation as given in (3.2). In the translation step, since r'_o is greater than A, the expansion given in (3.3) indicates that the upper index (c) in spherical harmonic functions remain unchanged under translation.

The fields radiated by antenna 2 are also expanded in terms of spherical waves in the (x'_2, y'_2, z'_2) coordinate system as:

$$\bar{E}_2 = k\sqrt{\eta}\sum_{s=1}^{2}\sum_{n=1}^{N_f}\sum_{m=-n}^{n} {}_2Q^{(4)}_{smn}\bar{F}^{(4)}_{smn}(r'_2, \theta'_2, \phi'_2) \tag{3.18}$$

$$\bar{H}_2 = \frac{jk}{\sqrt{\eta}}\sum_{s=1}^{2}\sum_{n=1}^{N_f}\sum_{m=-n}^{n} {}_2Q^{(4)}_{smn}\bar{F}^{(4)}_{3-smn}(r'_2, \theta'_2, \phi'_2) \tag{3.19}$$

where ${}_2Q^{(4)}_{smn}$ represent the spherical harmonic coefficients in the (x'_2, y'_2, z'_2) coordinate system. The spherical wave functions, denoted as $\bar{F}^{(4)}_{smn}(r'_2, \theta'_2, \phi'_2)$, are referenced to the (x'_2, y'_2, z'_2) primed coordinate system. However, the computation of the spherical wave coefficients ${}_2Q^{(4)}_{smn}$ differs slightly from what was done for antenna 1. The first step remains the same as that of antenna 1. However, for antenna 2, the rotated frame is translated along the z_2-axis by a distance of $-A$, as depicted in Figure

3.3. By redefining convergence regions of spherical harmonic expansions representing outward propagating $\bar{E}$ and $\bar{H}$ fields of both antennas, a "proper" reaction surface can be defined as shown in Figure 3.5. The portion of the reaction surface located

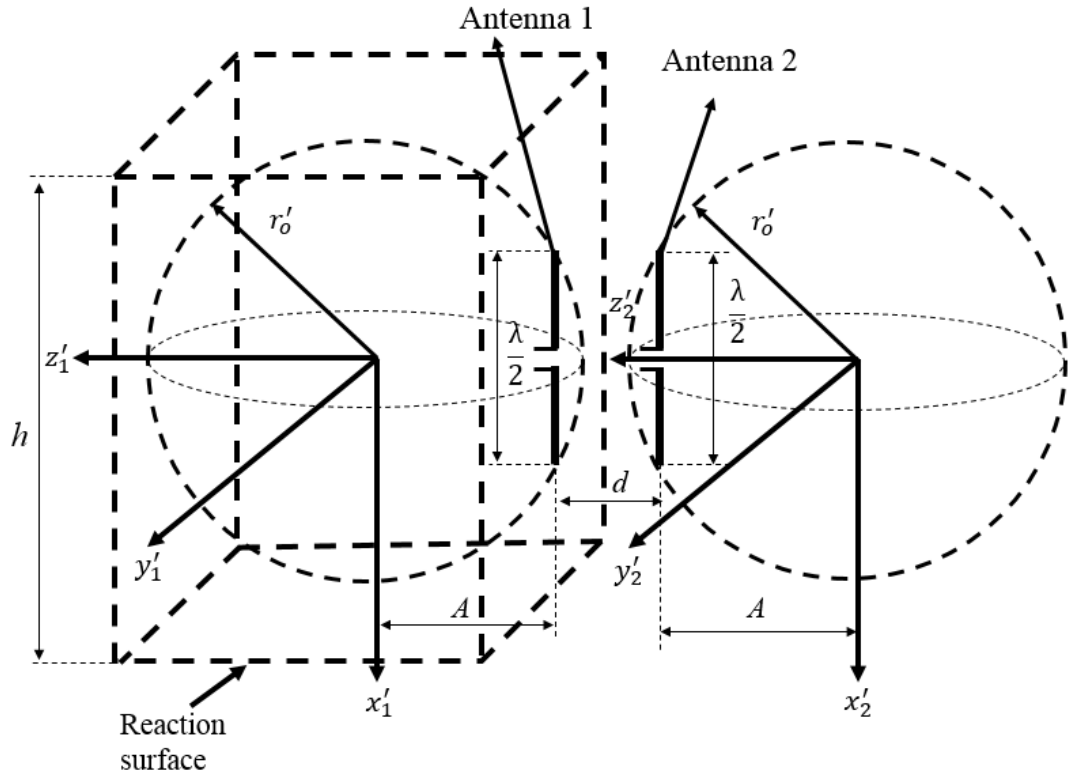

Figure 3.5: A "proper" reaction surface for mutual impedance computation after rotation and translation of coordinate frames of the antennas.

on the xy plane is chosen to have sufficiently large dimensions ($20\lambda \times 20\lambda$) in order to make the contribution from other surfaces negligible. It is important to note that the fields of the dipoles in free space are used, as it is assumed that the presence of the second antenna does not significantly affect the fields of the first antenna. By computing the outgoing fields provided in equations (3.16), (3.17), (3.18), and (3.19) on the reaction surface using (3.20), the mutual impedance between two closely spaced antennas is found by numerical integration.

$$z_{12} = -\frac{1}{I_1 I_2} \oint_{S_1} (\bar{E}_1 \times \bar{H}_2 - \bar{E}_2 \times \bar{H}_1) \cdot d\bar{S} \tag{3.20}$$

3.4 Computation of mutual impedance between two infinitely thin half-wave dipoles

The fields associated with antenna 1 are given in terms of spherical wave expansion in the (x_1', y_1', z_1') coordinate frame as:

$$\bar{E}_1 = k\sqrt{\eta}\sum_{s=1}^{2}\sum_{n=1}^{N_1'}\sum_{m=-n}^{n} {}_1Q_{smn}^{(4)}\bar{F}_{smn}^{(4)}(r_1', \theta_1', \phi_1') \tag{3.21}$$

$$\bar{H}_1 = \frac{jk}{\sqrt{\eta}}\sum_{s=1}^{2}\sum_{n=1}^{N_1'}\sum_{m=-n}^{n} {}_1Q_{smn}^{(4)}\bar{F}_{3-smn}^{(4)}(r_1', \theta_1', \phi_1') \tag{3.22}$$

where $\bar{F}_{smn}^{(4)}(r_1', \theta_1', \phi_1')$ represents the spherical harmonic functions referenced to (x_1', y_1', z_1') coordinate frame as illustrated in Figure 3.6. The upper index (c) is 4 as discussed in the previous section.

In order to obtain an analytical expression, the field expansions for antenna 2 given in (3.18), (3.19) must be translated to the coordinate system referenced to (x_1', y_1', z_1'). This translation is illustrated in Figure 3.6. The fields radiated by antenna 2 are

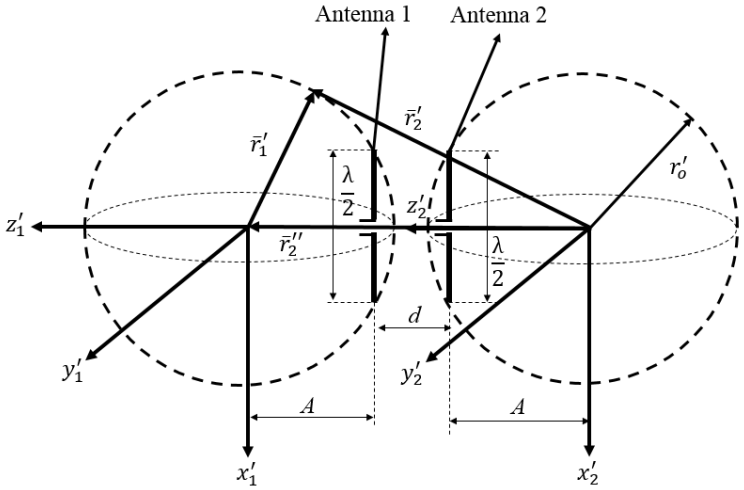

Figure 3.6: Translation of spherical harmonic coefficients of second antenna.

expressed in terms of spherical harmonics referenced to (x_1', y_1', z_1') coordinate system as:

$$\bar{E}_2 = k\sqrt{\eta}\sum_{\sigma=1}^{2}\sum_{v=1}^{N_2'}\sum_{\mu=-v}^{v} {}_2Q_{\sigma\mu v}^{(1)}\bar{F}_{\sigma\mu v}^{(1)}(r_1', \theta_1', \phi_1') \tag{3.23}$$

$$\bar{H}_2 = \frac{jk}{\sqrt{\eta}} \sum_{\sigma=1}^{2} \sum_{v=1}^{N_2'} \sum_{\mu=-v}^{v} {}_2Q_{\sigma\mu v}^{(1)} \bar{F}_{3-\sigma\mu v}^{(1)}(r_1', \theta_1', \phi_1') \tag{3.24}$$

where ${}_2Q_{\sigma\mu v}^{(1)}$ denotes the spherical harmonic coefficients of antenna 2 after translation along z_2' direction by a distance $2A + d$. $\bar{F}_{\sigma\mu v}^{(1)}(r_1', \theta_1', \phi_1')$ represents the spherical harmonics corresponding to those coefficients. Since the translation distance $2A + d$ is always greater than $r_1' = \sqrt{A^2 + (\frac{\lambda}{4})^2}$, the translation formula given in (3.25) is used to express the fields of antenna 2 in terms of spherical harmonics referenced to (x_1', y_1', z_1') coordinate frame.

$$\bar{F}_{s\mu n}^{(c)}(r_2', \theta_2', \phi_2') = \sum_{\sigma=1}^{2} \sum_{\substack{\nu=|\mu| \\ \nu\neq 0}}^{N_2'} C_{\sigma\mu\nu}^{sn(c)}(k(2A+d)) \bar{F}_{\sigma\mu\nu}^{(1)}(r_1', \theta_1', \phi_1') \quad r_1' < |2A + d| \tag{3.25}$$

where truncation number for this translation is chosen as $N_2' \simeq kr_1' + 3\sqrt[3]{kr_1'}$. The truncation number used in equations (3.23) and (3.24) may not have the same value provided in equation (3.25). Nevertheless, it is satisfactory to employ the same truncation value, denoted as $N_2' \simeq kr_1' + 3\sqrt[3]{kr_1'}$, in (3.23),(3.24), and (3.25) for our calculations. Note that after this translation the upper index (c) changes to 1 for the spherical harmonics referenced to (x_1', y_1', z_1').

The mutual impedance expression based on the reaction theorem is given as:

$$z_{12} = -\frac{1}{I_1 I_2} \oint_{S_1} (\bar{E}_1 \times \bar{H}_2 - \bar{E}_2 \times \bar{H}_1) \cdot d\bar{S}_1 \tag{3.26}$$

The reaction surface is chosen as the minimum sphere that encloses antenna 1 as depicted in Figure 3.6. The center point of this sphere is the origin of (x_1', y_1', z_1') coordinate frame. By substituting the fields (3.21), (3.22), (3.23), and (3.24) into (3.26), the surface integrals of $\bar{E}_1 \times \bar{H}_2$, and $\bar{E}_2 \times \bar{H}_1$ on reaction surface S_1 are given as:

$$\oint_{S_1} (\bar{E}_1 \times \bar{H}_2) \cdot d\bar{S}_1 = jk^2 \sum_{s=1}^{2} \sum_{n=1}^{N_1'} \sum_{m=-n}^{n} \sum_{\sigma=1}^{2} \sum_{v=1}^{N_2'} \sum_{\mu=-v}^{v} {}_1Q_{smn}^{(c)} \, {}_2Q_{\sigma\mu v}^{(\gamma)} \int_0^{2\pi} \int_0^{\pi} \left\{ \bar{F}_{smn}^{(c)} \times \bar{F}_{3-\sigma\mu v}^{(\gamma)} \right\} \cdot \hat{r}_1' r_1'^{\,2} \sin\theta_1' d\theta_1' d\phi_1' \tag{3.27}$$

Table 3.1: The constant $A^{(c,\gamma)}$.

$A^{(c,\gamma)}$	$\gamma=1$	$\gamma=2$	$\gamma=3$	$\gamma=4$
$c=1$	0	1	j	$-j$
$c=2$	-1	0	-1	-1
$c=3$	$-j$	1	0	$-2j$
$c=4$	j	1	$2j$	0

$$\oint_{S_1}(\bar{E}_2\times\bar{H}_1)\cdot d\bar{S}_1 = jk^2\sum_{\sigma=1}^{2}\sum_{v=1}^{N_2'}\sum_{\mu=-v}^{v}\sum_{s=1}^{2}\sum_{n=1}^{N_1'}\sum_{m=-n}^{n} {}_2Q_{\sigma\mu v}^{(\gamma)}\,{}_1Q_{smn}^{(c)} \int_0^{2\pi}\int_0^{\pi}\left\{\bar{F}_{\sigma\mu v}^{(\gamma)}\times\bar{F}_{3-smn}^{(c)}\right\}\cdot\hat{r}_1' r_1'^{\,2}\sin\theta_1' d\theta_1' d\phi_1' \quad (3.28)$$

The orthogonality relations of the spherical harmonics are given in [10] as:

$$\int_{\phi=0}^{2\pi}\int_{\theta=0}^{\pi}\left\{\bar{F}_{smn}^{(c)}(r_1',\theta_1',\phi_1')\times\bar{F}_{\sigma\mu v}^{(\gamma)}(r_1',\theta_1',\phi_1')\right\}\cdot\hat{r}_1' r_1'^{\,2}\sin\theta_1' d\theta_1' d\phi_1' = -\delta_{s,3-\sigma}\delta_{m,-\mu}\delta_{n,v}(-1)^{m+s}R_{sn}^{(c)}(kr_1')R_{3-s,n}^{(\gamma)}(kr_1')r_1'^{\,2} \quad (3.29)$$

By inserting lefthand side of (3.29) into (3.27), (3.28) and using Wronksian given in (3.30)

$$R_{sn}^{(c)}(kr_1')R_{3-s,n}^{(\gamma)}(kr_1') - R_{sn}^{(\gamma)}(kr_1')R_{3-s,n}^{(c)}(kr_1') = -(-1)^s\frac{A^{(c,\gamma)}}{(kr_1')^2} \quad (3.30)$$

where the constant $A^{(c,\gamma)}$ is given in Table 3.1, the surface integral can be simplified as:

$$\oint_{S_1}(\bar{E}_1\times\bar{H}_2-\bar{E}_2\times\bar{H}_1)\cdot d\bar{S}_1 = j\sum_{n=1}^{N_1'}\sum_{m=-n}^{n}\left[{}_1Q_{1,m,n}^{(c)}\,{}_2Q_{1,-m,n}^{(\gamma)}(-1)^m A^{(c,\gamma)} + {}_1Q_{2,m,n}^{(c)}\,{}_2Q_{2,-m,n}^{(\gamma)}(-1)^m A^{(c,\gamma)}\right] \quad (3.31)$$

For $c=4$ and $\gamma=1$, $A^{(c,\gamma)}$ is determined as j as given in Table 3.1, the mutual impedance is expressed as a sum of the products of the spherical harmonic coefficients

for two closely spaced antennas as:

$$\begin{aligned} z_{12} &= -\frac{1}{I_1 I_2} \oint_{S_1} (\bar{E}_1 \times \bar{H}_2 - \bar{E}_2 \times \bar{H}_1) \cdot d\bar{S}_1 \\ &= \frac{1}{I_1 I_2} \sum_{n=1}^{N_1'} \sum_{m=-n}^{n} (-1)^m \left[{}_1Q^{(4)}_{1,m,n} \, {}_2Q^{(1)}_{1,-m,n} + {}_1Q^{(4)}_{2,m,n} \, {}_2Q^{(1)}_{2,-m,n} \right] \end{aligned} \tag{3.32}$$

While the mutual impedance z_{12} defined in (3.32) may initially appear to be influenced by the port currents I_1 and I_2, it is important to note that the products of the spherical harmonics within the summation inherently includes these currents. Consequently, the mutual impedance remains invariant with respect to the variations in port currents, establishing its independence from their effects.

CHAPTER 4

RESULTS

4.1 Computational results

This chapter focuses on the computational results of the mutual impedance between antennas using proposed technique.

4.1.1 Numerical computation results for mutual impedance between two infinitely thin half-wave dipoles

The reaction theorem states that if the port currents and the fields radiated by the antennas are known, then the mutual impedance between antennas can be calculated as follows [4]:

$$Z_{12} = -\frac{1}{I_1 I_2} \oint_{S_1} (\bar{E}_1 \times \bar{H}_2 - \bar{E}_2 \times \bar{H}_1) \cdot d\bar{S}_1 \tag{4.1}$$

If the reaction surface S_1 lies completely in the convergence region of the spherical harmonic functions representing outgoing waves of both antennas, it is possible to directly calculate the fields on S_1 and numerically evaluate (4.1). In this subsection, we present the computational results of the mutual impedance between two infinitely thin half-wave dipoles by numerically evaluating (4.1). The operating frequency is set to 300 MHz for infinitely thin half-wave dipoles.

Since the spherical harmonic coefficients of antenna 1 and antenna 2 in the modified coordinate systems are known, the $\bar{E}$ and $\bar{H}$ fields of both antennas on the reaction surface S_1 can be determined by using (3.16)-(3.19). Then, by numerically evaluating (4.1), the mutual impedance between two infinitely thin half-wave dipoles positioned

side-by-side can be calculated for small element spacing as illustrated in Figure 4.1. Figure 4.2 shows the real and imaginary parts of the mutual impedance as a function

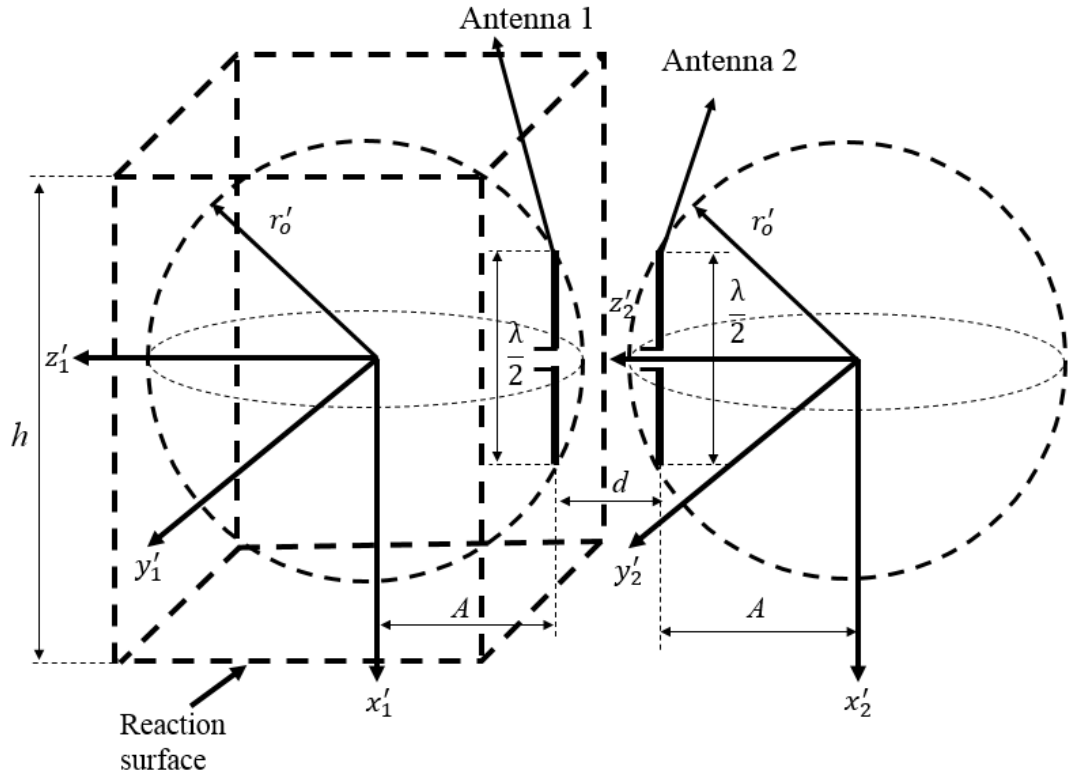

Figure 4.1: A "proper" reaction surface for mutual impedance computation after rotation and translation of coordinate frames of the antennas.

of antenna separation, along with those obtained by induced EMF method. The results are expected to be the same (except for numerical errors) since the induced EMF method also uses the free space fields. The results clearly demonstrate that mutual impedance between radiators can be accurately calculated even for small separation distances for which overlapping minimum sphere problem can occur.

4.1.2 Analytical computation results for mutual impedance between two infinitely thin half-wave dipoles

The primary aim of this section is to present the computational results of the mutual impedance between two infinitely thin half-wave dipoles using the analytical expression derived in the preceding chapter. The mutual impedance is expressed as a sum

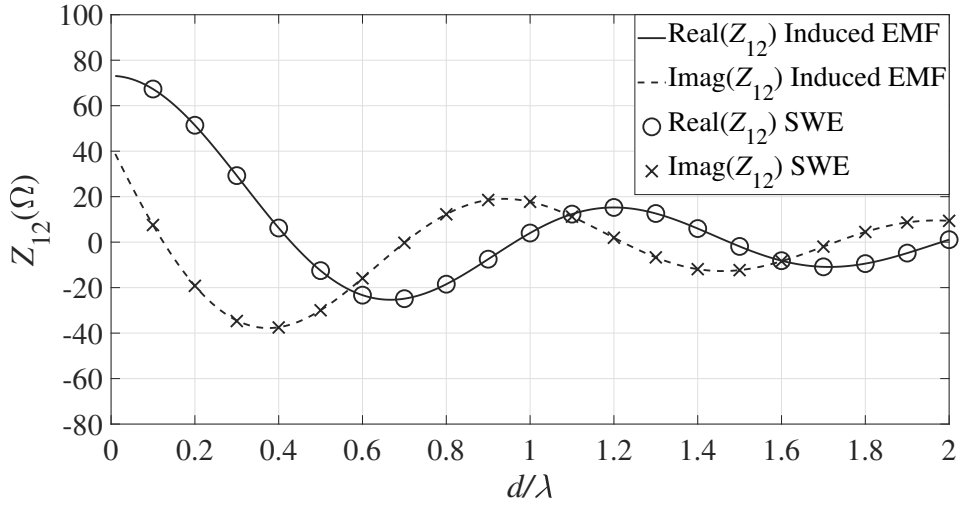

Figure 4.2: Comparison of mutual impedances of two infinitely thin half-wave dipoles computed using proposed method and induced EMF method.

of the products of the spherical harmonic coefficients for two closely spaced antennas as:

$$\begin{aligned} z_{12} &= -\frac{1}{I_1 I_2} \oint_{S_1} (\bar{E}_1 \times \bar{H}_2 - \bar{E}_2 \times \bar{H}_1) \cdot d\bar{S}_1 \\ &= \frac{1}{I_1 I_2} \sum_{n=1}^{N_1'} \sum_{m=-n}^{n} (-1)^m \left[{}_1Q^{(4)}_{1,m,n} \, {}_2Q^{(1)}_{1,-m,n} + {}_1Q^{(4)}_{2,m,n} \, {}_2Q^{(1)}_{2,-m,n} \right] \end{aligned} \tag{4.2}$$

With known coefficients in the translated coordinate frames, the mutual impedance is found using (4.2). Figure 4.3 shows the comparison of the real and imaginary parts of the mutual impedance as a function of antenna separation, along with those obtained by induced EMF method.

4.1.3 Convergence analysis

This subsection primarily emphasizes the convergence analysis of the spherical wave expansion (SWE) when the spherical harmonics are translated from the unprimed to the primed coordinate frame. This analysis plays crutial role in determining the appropriate range for selection of the truncation number in the translated coordinate frame.

The infinite sum in SWE must be truncated for numerical calculations. Different

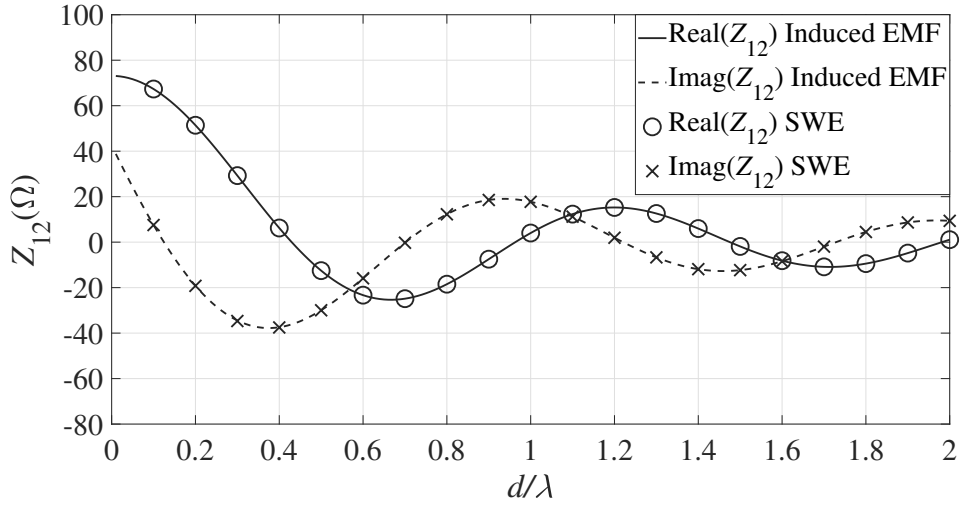

Figure 4.3: Comparison of mutual impedances of two infinitely thin half-wave dipoles computed using proposed method and induced EMF method.

expressions for the truncation value have been proposed in the literature. The choice of the truncation value affects the accuracy of the calculation: if it is too small, the series will not converge, while if it is too high, the singularity of wave functions will result in numerical errors. To address this issue, a convergence analysis based on the conservation of radiated power is performed.

The radiated power of an infinitely thin half-wave dipole can be calculated using radiation resistance and input current as:

$$P_{rad} = \frac{1}{2} R_{rad} |I_o|^2 \tag{4.3}$$

or by summing the spherical harmonic coefficients in the translated coordinate frame as:

$$\hat{P}_{rad} = \frac{1}{2} \sum_{s=1}^{2} \sum_{n=1}^{N'} \sum_{m=-n}^{n} |Q_{smn}^{T}|^2 \tag{4.4}$$

where Q_{smn}^{T} represents the spherical harmonic coefficients in the translated coordinate frame. The relative error between these two methods is defined as:

$$\epsilon_{rel} = |P_{rad} - \hat{P}_{rad}| / P_{rad} \tag{4.5}$$

Figure 4.4 shows the relative error (in dB) as a function of truncation value in the translated coordinate frame as a function of N'. In this work, N' is chosen as $kr_0 +$

$3\sqrt[3]{kr_0}$ as suggested in [10] and Figure 4.4 shows this choice to be appropriate. The wide range of N' for which the error remains low allows for flexibility in choosing a suitable expression from the various proposals in the literature. In fact, different expressions suggested in the literature fall within this low-error range.

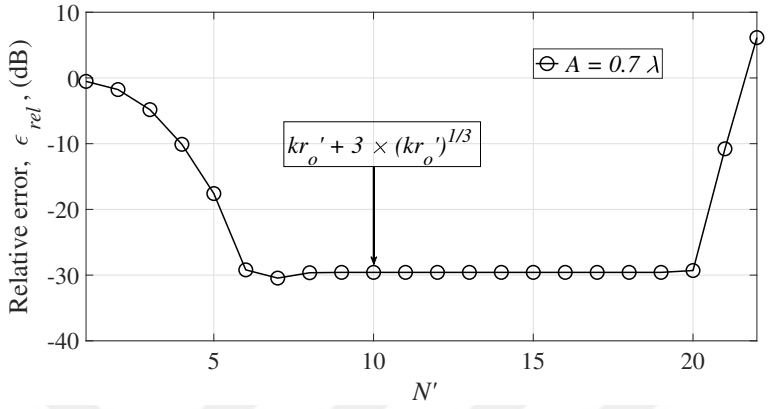

Figure 4.4: Relative error in radiated power with respect to truncation value, N'.

The convergence of SWE becomes challenging as it approaches the boundary of the region of convergence. To obtain accurate calculations on the reaction surface, the translation distance A must be carefully selected. Larger values of A allow for more accurate results, but they also require a higher value of N', leading to increased computation. Additionally, larger values of A can result in increased numerical errors. Therefore, choosing the correct value of A is crucial. Figure 4.5 illustrates the error as a function of translation distance A for different antenna separations. The error in this scenario is defined as the difference between the mutual impedances calculated by the proposed method and the induced EMF method.

The optimal value of A for the given antenna separations is found to be 0.9λ, which places the reaction surface at a distance slightly greater than 0.01λ from the edge of the region of convergence in the numerical evaluation of reaction integral. Beyond this point, the error remains low, and the selection of A becomes less critical, as shown in Figure 4.5. It must be noted that the horizontal axis of Figure 4.5 starts from $A = 0.6\lambda$ so that for all antenna separations considered, a "proper" reaction surface can be found.

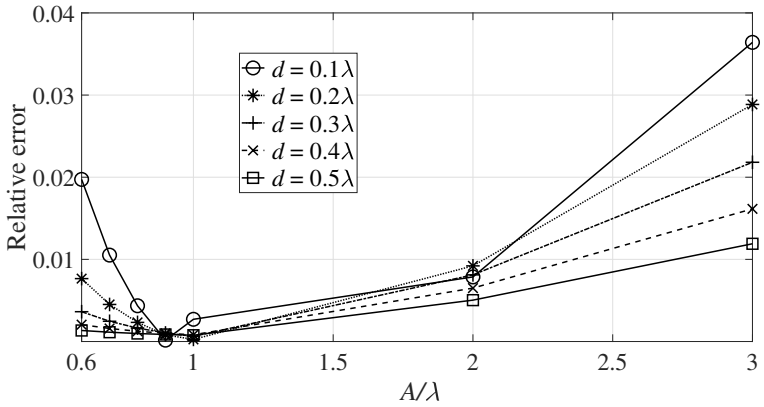

Figure 4.5: Relative error in mutual impedance with respect to translation distance A.

4.2 Experimental results

4.2.1 Printed dipole antenna

A printed dipole antenna is a suitable choice for testing the proposed method, primarily due to relatively high level of coupling and ease of fabrication. Therefore, the printed dipole antenna described in [38], which incorporates a balun, is selected as the antenna to test the proposed method and to conduct mutual coupling measurements. The printed dipole has two layers and its front and back side views are illustrated in Figure 4.6, along with the design parameters. The antenna is simulated using HFSS Electromagnetic analysis tool, and its resonance frequency is tuned to 3 GHz which resulted in the dimensions listed in Table 4.1. The antenna is manufactured using ROGERS 4003 material ($\epsilon_r = 3.55$, and a loss tangent of 0.002) with 0.813 mm substrate thickness. The mutual impedance computations and the measurements are conducted at 3 GHz frequency.

4.2.2 Spherical near-field measurement of the printed dipole

This section primarily focuses on conducting spherical near-field measurements of the manufactured printed dipole antenna to determine its spherical harmonic coefficients Q_{1mn} and Q_{2mn}. These coefficients are obtained from measurements using the MVG SATIMO spherical near-field measurement device, as shown in Figure 4.7. The

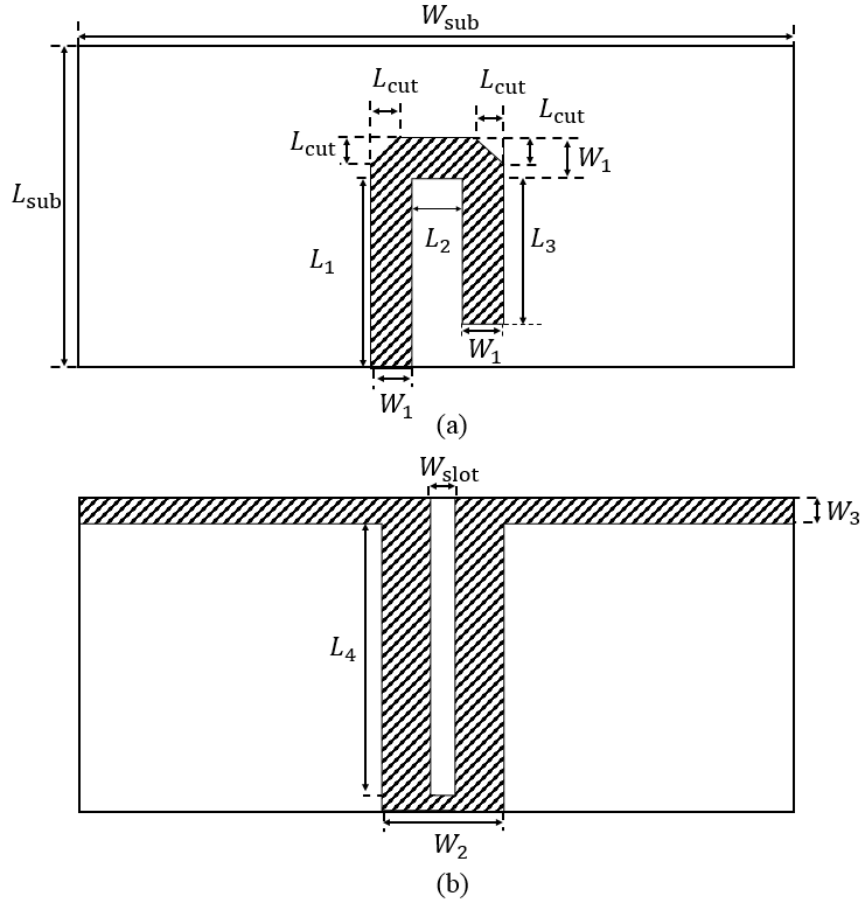

Figure 4.6: Printed dipole antenna, (a) front and (b) back view.

Table 4.1: The dimensions of manufactured printed dipole antenna.

L_{sub} = 19.9265 mm	W_{sub} = 44.34 mm
W_1 = 1.818 mm	W_{slot} = 1mm
W_2 = 7.548 mm	L_1 = 11.793mm
L_2 = 2.956 mm	L_3 = 9.0322 mm
L_{cut} = 1.09 mm	L_4 = 17.92 mm
W_3 = 1 mm	

device provides the SWE (Spherical Wave Expansion) coefficients of the measured antenna, using the same notation for spherical harmonic functions and expansion coefficients as outlined in [10].

Once the SWE coefficients are obtained, the proposed technique is implemented to

calculate the mutual impedances between two such dipole antennas positioned side-by-side at different distances, as depicted in Figure 4.8.

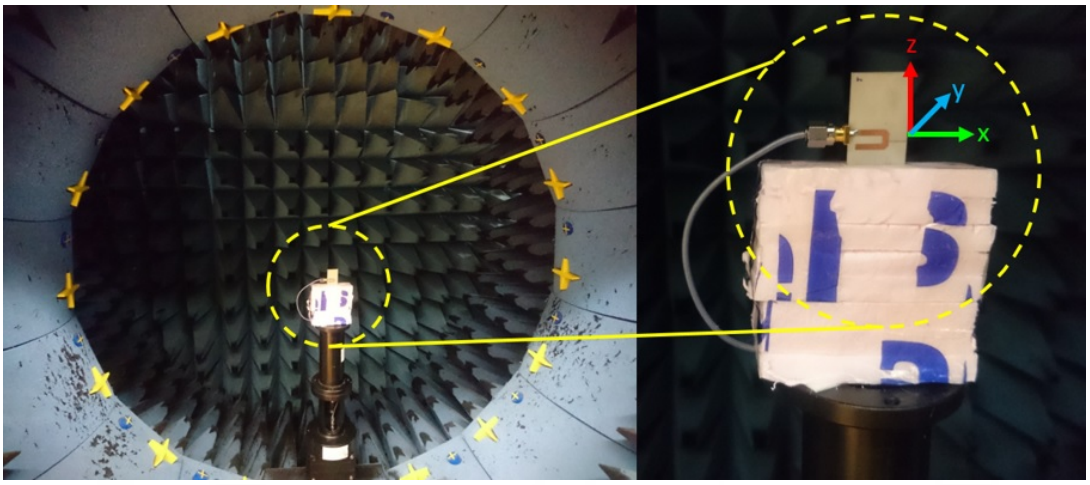

Figure 4.7: Printed dipole antenna measurement using SATIMO spherical near-field measurement device.

4.2.3 Numerical computation of mutual impedance between two printed dipoles

The primary focus of this subsection is to compute the mutual impedance between two side-by-side printed dipoles using the proposed method. This is achieved by numerically evaluating the reaction integral specified in (4.6).

$$Z_{12} = -\frac{1}{I_1 I_2} \oint_{S_1} (\bar{E}_1 \times \bar{H}_2 - \bar{E}_2 \times \bar{H}_1) \cdot d\bar{S}_1 \tag{4.6}$$

To apply the proposed technique, we utilize the measured coefficients obtained from a single antenna to determine the fields of both antennas on the reaction surface directly. This allows us to evaluate the reaction integral numerically. Figure 4.9 illustrates the placement of the printed dipoles in the primed coordinate systems.

The fields radiated from printed dipole 1 can be expressed using spherical wave expansion associated with the (x'_1, y'_1, z'_1) coordinate system as:

$$\bar{E}_1 = k\sqrt{\eta} \sum_{s=1}^{2} \sum_{n=1}^{N_{fp}} \sum_{m=-n}^{n} {}_1Q^{(3)}_{smn} \bar{F}^{(3)}_{smn}(r'_1, \theta'_1, \phi'_1) \tag{4.7}$$

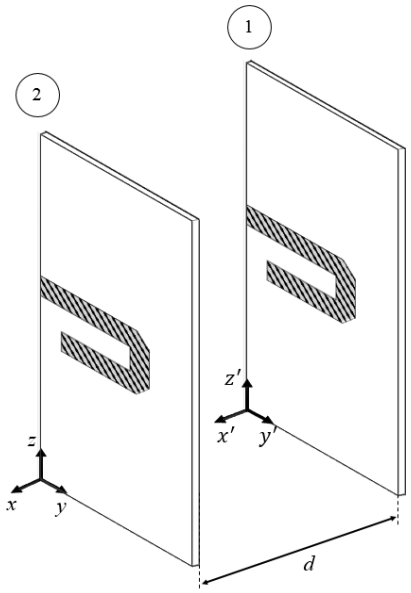

Figure 4.8: Two printed dipole antennas in a side-by-side configuration.

$$\bar{H}_1 = -\frac{jk}{\sqrt{\eta}} \sum_{s=1}^{2} \sum_{n=1}^{N_{fp}} \sum_{m=-n}^{n} {}_1Q_{smn}^{(3)} \bar{F}_{3-s,m,n}^{(3)}(r_1', \theta_1', \phi_1') \tag{4.8}$$

where ${}_1Q_{smn}^{(3)}$ denotes the spherical harmonic coefficients for the printed dipole in the (x_1', y_1', z_1') coordinate system, as depicted in Figure 4.9. The pre-subscript is utilized to indicate that the coefficients belong to the field expansion of the printed dipole 1. $\bar{F}_{smn}^{(3)}(r_1', \theta_1', \phi_1')$ represents the spherical harmonic functions in the primed (x_1', y_1', z_1') coordinate system. The SATIMO near-field measurement device uses the $e^{-j\omega t}$ time convention, and the radial variation of the outgoing waves in the outside region of the minimum sphere encompassing the printed dipole antenna is represented by the first kind Hankel functions (upper superscript equal to 3, in (4.7) and (4.8)).

Similarly, the fields generated by printed dipole 2 can be expressed using spherical wave expansion associated with the (x_2', y_2', z_2') coordinate system as:

$$\bar{E}_2 = k\sqrt{\eta} \sum_{s=1}^{2} \sum_{n=1}^{N_{fp}} \sum_{m=-n}^{n} {}_2Q_{smn}^{(3)} \bar{F}_{smn}^{(3)}(r_2', \theta_2', \phi_2') \tag{4.9}$$

$$\bar{H}_2 = -\frac{jk}{\sqrt{\eta}} \sum_{s=1}^{2} \sum_{n=1}^{N_{fp}} \sum_{m=-n}^{n} {}_2Q_{smn}^{(3)} \bar{F}_{3-s,m,n}^{(3)}(r_2', \theta_2', \phi_2') \tag{4.10}$$

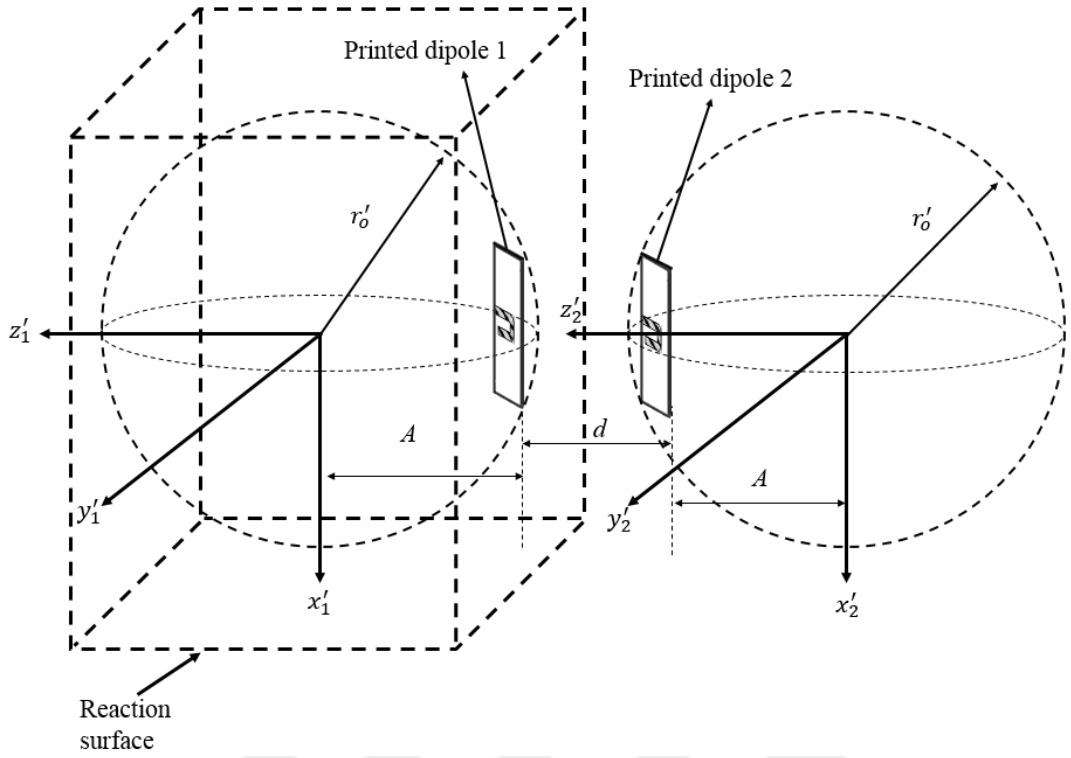

Figure 4.9: Numerical computation of mutual impedance between two closely spaced printed dipoles.

To use the reaction integral provided in (4.6), it is essential to have knowledge of the input port currents of the printed dipoles. To determine the input port current, we need to know both the radiated power and the radiation resistance of the printed dipole

$$P_{rad} = \frac{1}{2}|I|^2 R_{rad} \tag{4.11}$$

The radiated power can be obtained by using the measured spherical harmonic coefficients Q_{1mn} and Q_{2mn} through (4.12).

$$P_{rad} = \frac{1}{2}\sum_{n=1}^{\infty}\sum_{m=-n}^{n} |Q_{1mn}|^2 + |Q_{2mn}|^2 \tag{4.12}$$

Furthermore, the efficiency formula given in (4.13) establishes a relationship between the radiation resistance and the real part of the antenna input impedance.

$$\eta_{eff} = \frac{R_{rad}}{R_{in}} \tag{4.13}$$

The real part of the input impedance is obtained by measuring the return loss of a single printed dipole antenna. Additionally, MVG SATIMO provides the efficiency

of the measured antenna. By utilizing the measured input impedance and efficiency, we can calculate the radiation resistance of the printed dipole using (4.13). With the radiated power known from the measured spherical harmonic coefficients via (4.12), we can determine the input port current of the printed dipole using (4.11).

Once the spherical harmonic coefficients are known in the translated coordinate systems, we determine the fields radiated by printed dipoles in the modified coordinate frames. Subsequently, utilizing these fields, we numerically evaluate the reaction integral provided in (4.6) to find the mutual impedance. We also perform a full-wave analysis using HFSS to determine the mutual impedance between two printed dipoles arranged side-by-side.

4.2.4 s-parameter measurement of two-element printed dipole array

Consider two manufactured printed dipoles arranged side-by-side to form a two-element array, as depicted in Figure 4.8. The s-parameters of the two-element array are measured for separation distances ranging from $d = 0.1\lambda$ to $d = 2\lambda$. Based on these measured s-parameters, the mutual impedance between the elements is determined.

4.2.5 Comparison of proposed method with s-parameter measurements and full-wave analysis

Figure 4.10 displays the mutual impedances that were determined using three different methods: reaction theorem, s-parameter measurements, and full-wave analysis using HFSS. It is worth mentioning that we calculate the mutual impedances without translating SWE coefficients when d/λ exceeds 0.6. Overall, the results obtained from these methods exhibit a high level of agreement, with the exception of the value for $d/\lambda = 0.1$. Figure 4.2 reveals that the proposed method does not encounter any convergence issues for this distance. The mutual impedances computed using both the measurement and full-wave analysis methods are consistent with each other, but our solution differs, suggesting that the discrepancy at $d/\lambda = 0.1$ is due to the presence of multiple reflections that were not accounted for in our approach. To better visu-

alize this error, we present Figure 4.11, which shows the difference between mutual impedances calculated by SWE and full-wave analysis. When the antenna separation is large, the overlapping spheres problem is not a concern, and for very small distances, multiple reflections cannot be ignored. However, this example indicates that there is a range of antenna separations where the minimum spheres overlap, and multiple reflections can be disregarded, and our method provides accurate results. This range is significant in practice since most antenna arrays employ such distances.

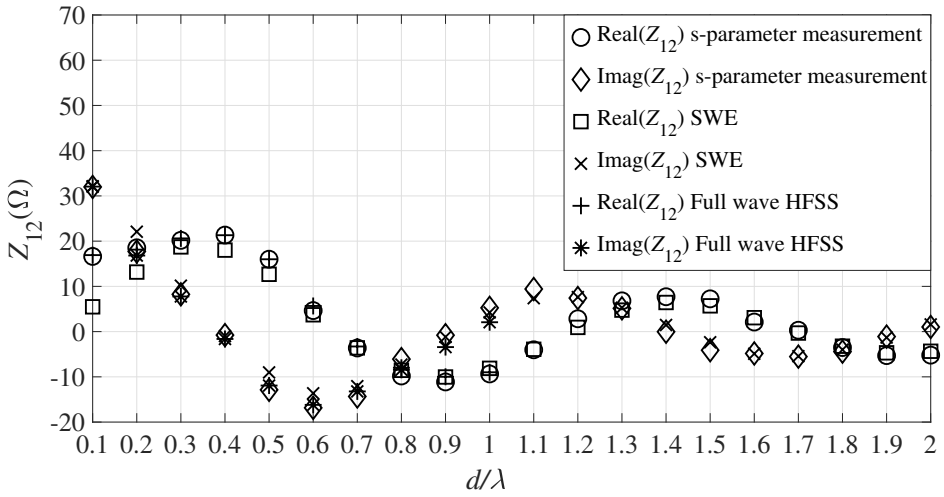

Figure 4.10: Comparison of mutual impedances of two printed dipoles computed using the proposed method by numerically evaluating the integral in (4.6) , s-parameter measurements, and full-wave analysis.

4.2.6 Mutual impedance in terms of SWE coefficients

Consider two printed dipoles positioned side-by-side, as illustrated in Figure 4.12. The fields radiated from dipole 1 can be expressed in terms of spherical wave expansion referenced to the (x_1', y_1', z_1') coordinate frame as:

$$\bar{E}_1 = k\sqrt{\eta}\sum_{s=1}^{2}\sum_{n=1}^{N_1'}\sum_{m=-n}^{n} {}_1Q_{smn}^{(3)}\bar{F}_{smn}^{(3)}(r_1', \theta_1', \phi_1') \tag{4.14}$$

$$\bar{H}_1 = -\frac{jk}{\sqrt{\eta}}\sum_{s=1}^{2}\sum_{n=1}^{N_1'}\sum_{m=-n}^{n} {}_1Q_{smn}^{(3)}\bar{F}_{3-smn}^{(3)}(r_1', \theta_1', \phi_1') \tag{4.15}$$

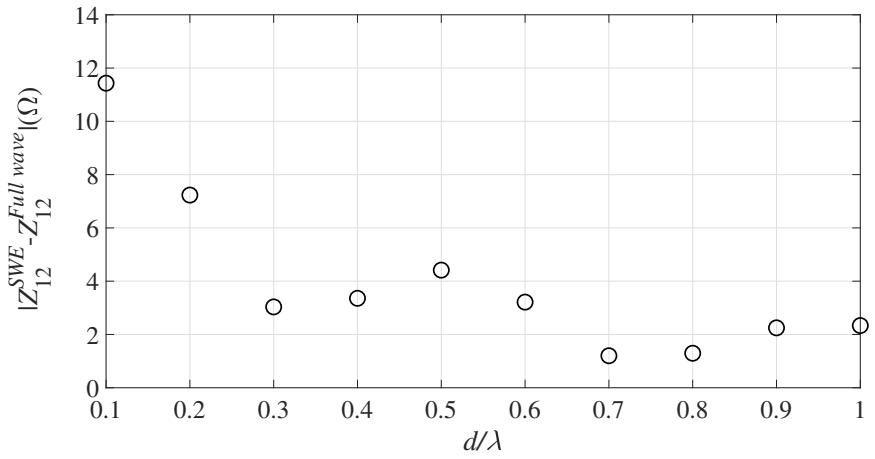

Figure 4.11: Absolute error between the proposed method and full-wave analysis.

where $\bar{F}^{(3)}_{smn}(r'_1, \theta'_1, \phi'_1)$ represents the spherical harmonic functions associated with the (x'_1, y'_1, z'_1) coordinate frame as illustrated in Figure 4.12.

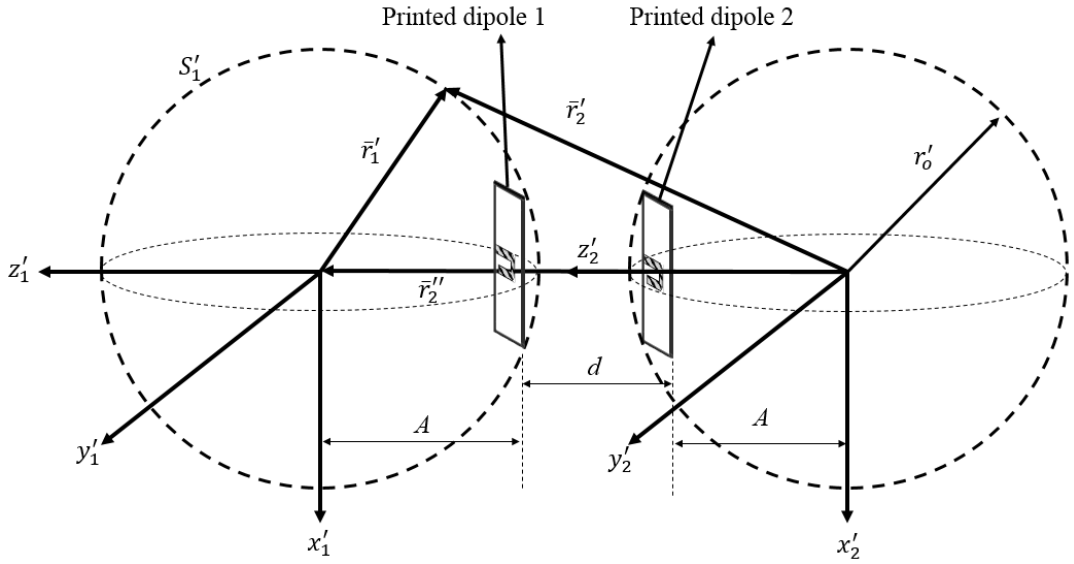

Figure 4.12: Analytical computation of mutual impedance between two closely spaced printed dipoles.

The fields of the second antenna can also be expanded in the coordinate frame of the first antenna by using translational addition theorems for spherical wave functions. If the reaction surface is chosen as a sphere centered at (x_1, y_1, z_1), the integral in (4.6) can be analytically evaluated. As a result, mutual impedance can be expressed as a

Table 4.2: The constant $A^{(c,\gamma)}$.

$A^{(c,\gamma)}$	$\gamma = 1$	$\gamma = 2$	$\gamma = 3$	$\gamma = 4$
$c = 1$	0	1	j	$-j$
$c = 2$	-1	0	-1	-1
$c = 3$	$-j$	1	0	$-2j$
$c = 4$	j	1	$2j$	0

sum of the product of the SWE coefficients.

To obtain an analytical expression, the field expansions for printed dipole 2 must be translated to the coordinate system referenced to (x_1', y_1', z_1'). This translation is illustrated in Figure 4.12. The fields radiated by printed dipole 2 are expressed in terms of spherical harmonics referenced to the (x_1', y_1', z_1') coordinate system as:

$$\bar{E}_2 = k\sqrt{\eta}\sum_{\sigma=1}^{2}\sum_{v=1}^{N_2'}\sum_{\mu=-v}^{v} {}_2Q_{\sigma\mu v}^{(1)}\bar{F}_{\sigma\mu v}^{(1)}(r_1', \theta_1', \phi_1') \tag{4.16}$$

$$\bar{H}_2 = -\frac{jk}{\sqrt{\eta}}\sum_{\sigma=1}^{2}\sum_{v=1}^{N_2'}\sum_{\mu=-v}^{v} {}_2Q_{\sigma\mu v}^{(1)}\bar{F}_{3-\sigma\mu v}^{(1)}(r_1', \theta_1', \phi_1') \tag{4.17}$$

where ${}_2Q_{\sigma\mu v}^{(1)}$ denotes the spherical harmonic coefficients of printed dipole 2 after translation along the z_2' direction by a distance of $2A + d$. $\bar{F}_{\sigma\mu v}^{(1)}(r_1', \theta_1', \phi_1')$ represents the spherical harmonics corresponding to those coefficients. For $c = 3$ and $\gamma = 1$, $A^{(c,\gamma)}$ is determined as $-j$ as given in Table 4.2, and the mutual impedance is expressed as a sum of the products of the spherical harmonic coefficients for two closely spaced printed dipoles as:

$$\begin{aligned} z_{12} &= -\frac{1}{I_1 I_2}\oint_{S_1}(\bar{E}_1 \times \bar{H}_2 - \bar{E}_2 \times \bar{H}_1)\cdot d\bar{S}_1 \\ &= \frac{1}{I_1 I_2}\sum_{n=1}^{N_1'}\sum_{m=-n}^{n}(-1)^m\left[{}_1Q_{1,m,n}^{(3)}\,{}_2Q_{1,-m,n}^{(1)} + {}_1Q_{2,m,n}^{(3)}\,{}_2Q_{2,-m,n}^{(1)}\right] \end{aligned} \tag{4.18}$$

The mutual impedance between the printed dipoles positioned as shown in Figure 4.12 is calculated using (4.18). Figure 4.13 illustrates the mutual impedances that were determined using (4.18), s-parameter measurements, and full-wave analysis using HFSS. Note that the two approaches give the same result as can be seen from (4.10) and (4.13).

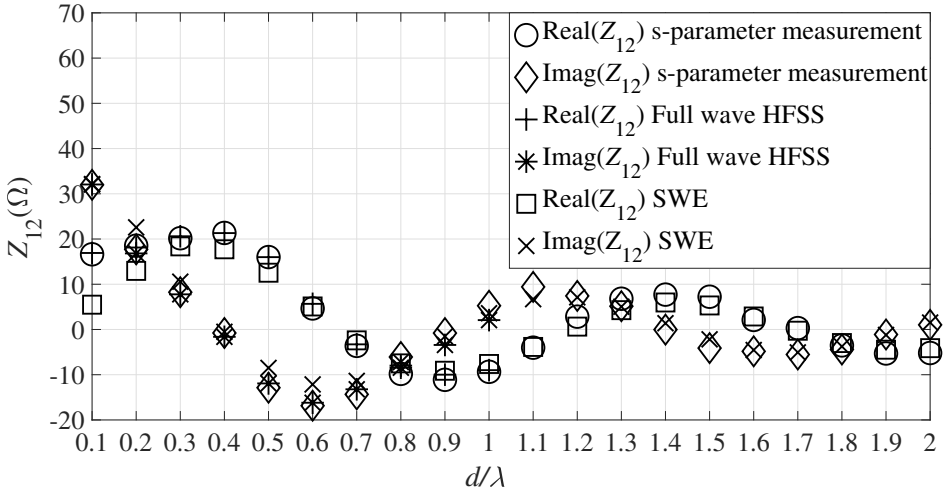

Figure 4.13: Comparison of mutual impedances of two printed dipoles computed using the proposed method by evaluating the sum in (4.18), s-parameter measurements, and full-wave analysis.

4.2.7 s-parameter measurement of four-element printed dipole array

Consider a uniformly spaced four-element array constructed using manufactured printed dipoles, where the elements of the array are positioned side-by-side, as shown in Figure 4.14. The s-parameters of the constructed array are measured for three different element spacings: $d = 0.1\lambda$, $d = 0.3\lambda$, and $d = 0.5\lambda$. Based on these measured s-parameters, we calculate the input impedance of each dipole and the mutual impedance between the elements for various separation distances.

The mutual impedance values obtained from s-parameter measurements for a separation distance of 0.1λ are presented in Table 4.3. Similarly, for separation distances of 0.3λ and 0.5λ, the corresponding mutual impedance values between the elements can be found in Table 4.4 and Table 4.5, respectively.

4.3 Active return loss computation for four-element printed dipole array

Consider a four-element array constructed using manufactured printed dipoles, where the elements are positioned side-by-side, as shown in Figure 4.14. To investigate the

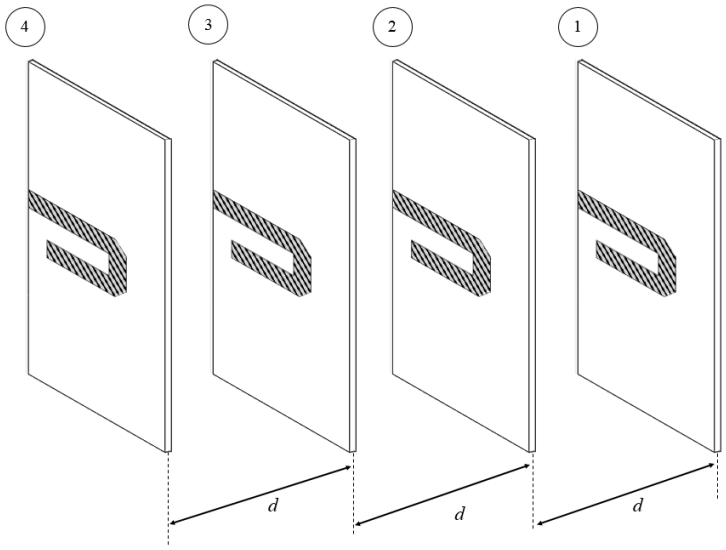

Figure 4.14: Four element printed dipole array in a side-by-side configuration.

Table 4.3: The mutual impedance values of the four-element printed dipole array determined based on s-parameter measurement for $d = 0.1\lambda$.

$Z_{12} = 13.60 + j27.12\ \Omega$	$Z_{21} = 13.40 + j27.21\ \Omega$
$Z_{13} = 22.30 + j0.81\ \Omega$	$Z_{31} = 22.28 + j0.87\ \Omega$
$Z_{14} = 6.07 - j13.96\ \Omega$	$Z_{41} = 6.14 - j14.07\ \Omega$
$Z_{23} = 12.15 + j27.75\ \Omega$	$Z_{32} = 12.07 + j27.79\ \Omega$
$Z_{24} = 22.82 + j0.83\ \Omega$	$Z_{42} = 22.71 + j0.96\ \Omega$
$Z_{34} = 14.56 + j28.54\ \Omega$	$Z_{43} = 14.41 + j28.61\ \Omega$

Table 4.4: The mutual impedance values of four-element printed dipole array determined based on s-parameter measurement for $d = 0.3\lambda$.

$Z_{12} = 23.49 + j8.53\ \Omega$	$Z_{21} = 23.37 + j8.75\ \Omega$
$Z_{13} = -5.91 - j11.3\ \Omega$	$Z_{31} = -5.80 - j11.20\ \Omega$
$Z_{14} = -2.14 + j6.33\ \Omega$	$Z_{41} = -2.11 + j6.36\ \Omega$
$Z_{23} = 23.65 + j8.96\ \Omega$	$Z_{32} = 23.61 + j9.11\ \Omega$
$Z_{24} = -5.71 - j12.78\ \Omega$	$Z_{42} = -5.65 - j12.76\ \Omega$
$Z_{34} = 26.17 + j14.87\ \Omega$	$Z_{43} = 26.19 + j15.09\ \Omega$

Table 4.5: The mutual impedance values of four-element printed dipole array determined based on s-parameter measurement for $d = 0.5\lambda$.

$Z_{12} = 20.77 - j5.62\ \Omega$	$Z_{21} = 20.77 - j5.25\ \Omega$
$Z_{13} = -11.66 + j1.35\ \Omega$	$Z_{31} = -11.57 + j1.19\ \Omega$
$Z_{14} = 4.46 + j2.89\ \Omega$	$Z_{41} = 4.36 + j2.87\ \Omega$
$Z_{23} = 24.01 - j3.07\ \Omega$	$Z_{32} = 24.14 - j2.66\ \Omega$
$Z_{24} = -8.65 - j0.48\ \Omega$	$Z_{42} = -8.51 - j0.75\ \Omega$
$Z_{34} = 22.45 - j2.58\ \Omega$	$Z_{43} = 22.39 - j2.28\ \Omega$

effects of mutual impedance in the array, we determine the input impedance of each dipole and the mutual impedance between the elements based on the measured s-parameters. In this arrangement, we assume that all the elements are excited with a uniform current, but each subsequent element has a progressive phase lead of ϕ compared to the previous one.

The input impedance of each element can be determined using the mutual impedances between the elements, as expressed in the following equation:

$$Z_{in,1} = Z_{11} + Z_{12}\frac{I_2}{I_1} + Z_{13}\frac{I_3}{I_1} + Z_{14}\frac{I_4}{I_1} \tag{4.19}$$

$$Z_{in,2} = Z_{21}\frac{I_1}{I_2} + Z_{22} + Z_{23}\frac{I_3}{I_2} + Z_{24}\frac{I_4}{I_2} \tag{4.20}$$

$$Z_{in,3} = Z_{31}\frac{I_1}{I_3} + Z_{32}\frac{I_2}{I_3} + Z_{33} + Z_{34}\frac{I_4}{I_3} \tag{4.21}$$

$$Z_{in,4} = Z_{41}\frac{I_1}{I_4} + Z_{42}\frac{I_2}{I_4} + Z_{43}\frac{I_3}{I_4} + Z_{44} \tag{4.22}$$

The antennas are excited with a uniform current, while the phase difference between the elements is set to ϕ as indicated below:

$$I_1 = I_0 e^{j\phi} \tag{4.23}$$

$$I_2 = I_0 e^{j2\phi} \tag{4.24}$$

$$I_3 = I_0 e^{j3\phi} \tag{4.25}$$

$$I_4 = I_0 e^{j4\phi} \tag{4.26}$$

The active return loss for each element can be computed as:

$$\Gamma_{in,n} = \frac{Z_{in,n} - Z_0}{Z_{in,n} + Z_0} \tag{4.27}$$

where Z_0 is 50Ω.

The proposed method also provides mutual impedance values for various separation distances when two printed dipoles are positioned side-by-side. For example, consider the mutual impedance Z_{12} between two such dipoles, determined using the proposed method for separation distances of $d = 0.3\lambda$, $d = 0.6\lambda$, and $d = 0.9\lambda$. In the context of a four-element printed dipole array arranged side-by-side, adjusting the separation distance to 0.3λ results in the mutual impedance between the first and third elements being equivalent to the Z_{12} value obtained from the proposed method at a separation distance of $d = 0.6\lambda$, assuming the absence of multiple reflections between the elements. Under this assumption, the mutual impedance between the first and the fourth elements in the four-element printed dipole array corresponds to the Z_{12} value calculated using the proposed method with a separation distance of 0.9λ.

Thus we can estimate the mutual impedance values between individual elements in this four-element array by utilizing computed mutual impedances with the proposed method at separation distances of 0.3λ, 0.6λ, and 0.9λ.

4.3.1 Active return loss comparison using s-parameter measurement and the proposed method

By utilizing the proposed method to compute mutual impedances for a four-element printed dipole array, we determine the active return loss of each port within the array at separation distances of $d = 0.3\lambda$, and $d = 0.5\lambda$. For a separation distance of $d = 0.3\lambda$, Figure 4.15 shows a comparison between active return loss variation with ϕ calculated using the proposed method and the value obtained from s-parameter measurements for port 1. Similarly, for the same separation distance, Figure 4.16, Figure 4.17, and Figure 4.18 illustrate the comparisons of the active return loss variations obtained from the proposed method and s-parameter measurements for port 2, port 3, and port 4, respectively.

The differences between the results of the proposed method and s-parameter measurement are attributed to the multiple reflections between printed dipoles, which are neglected in the computation of the mutual impedance using the proposed method. We

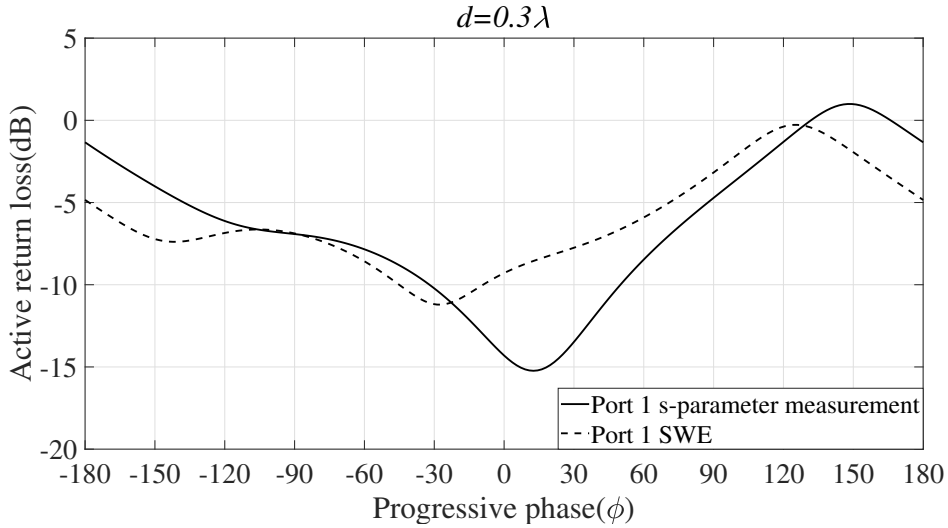

Figure 4.15: Comparison of the active return loss variations with progressive phase computed using the proposed method and s-parameter measurement for port 1 ($d = 0.3\lambda$).

also perform an active return loss comparison for a separation distance of $d = 0.5\lambda$, and the results for all the ports are given in Figure 4.19, 4.20, 4.21, and 4.22, respectively.

As the separation distance between elements increases, the active return loss variation with ϕ computed using the proposed method approaches the results that obtained from s-parameter measurements.

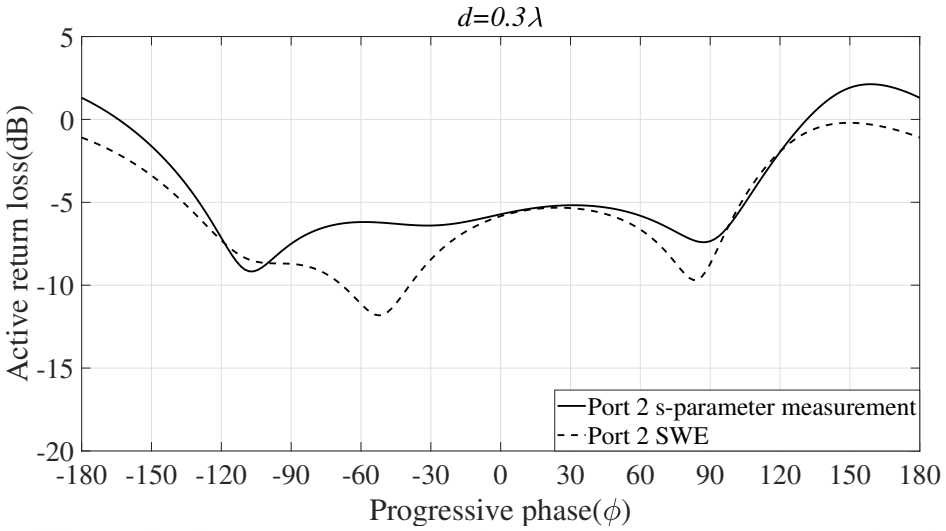

Figure 4.16: Comparison of the active return loss variations with progressive phase computed using the proposed method and s-parameter measurement for port 2 ($d = 0.3\lambda$).

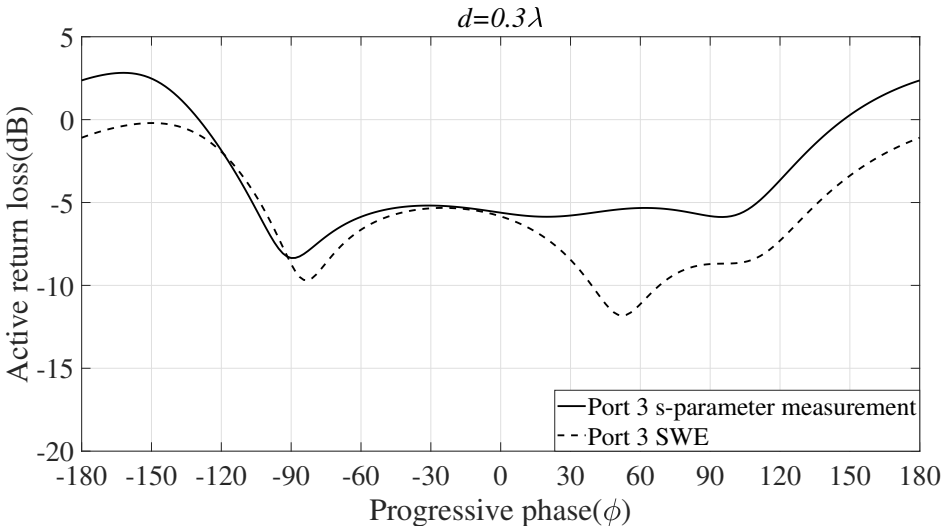

Figure 4.17: Comparison of the active return loss variations with progressive phase computed using the proposed method and s-parameter measurement for port 3 ($d = 0.3\lambda$).

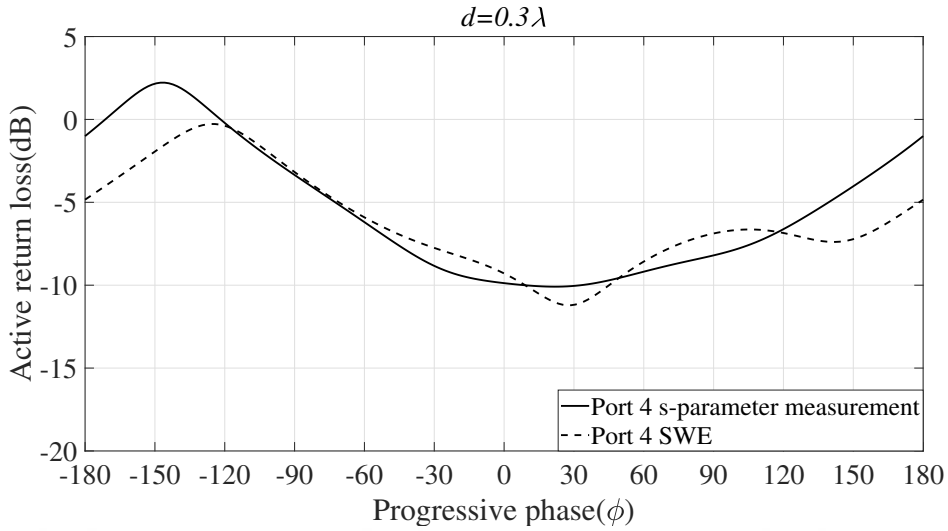

Figure 4.18: Comparison of the active return loss variations with progressive phase computed using the proposed method and s-parameter measurement for port 4 ($d = 0.3\lambda$).

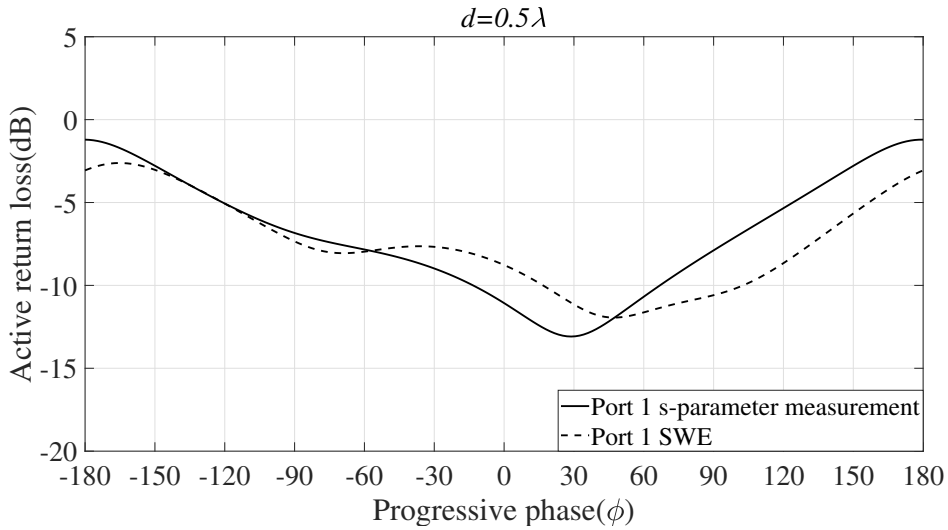

Figure 4.19: Comparison of the active return loss variations with progressive phase computed using the proposed method and s-parameter measurement for port 1 ($d = 0.5\lambda$).

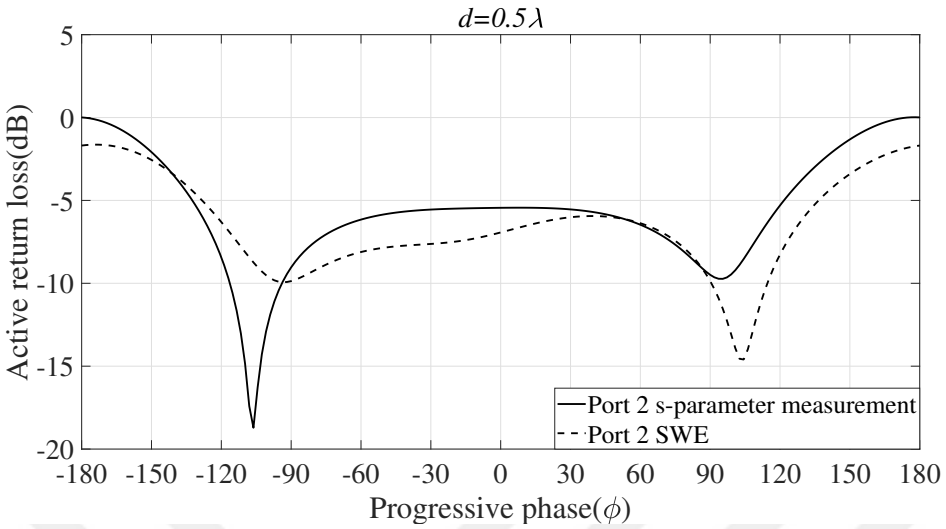

Figure 4.20: The active return loss variation with progressive phase computed using the proposed method and s-parameter measurement for port 2 ($d = 0.5\lambda$).

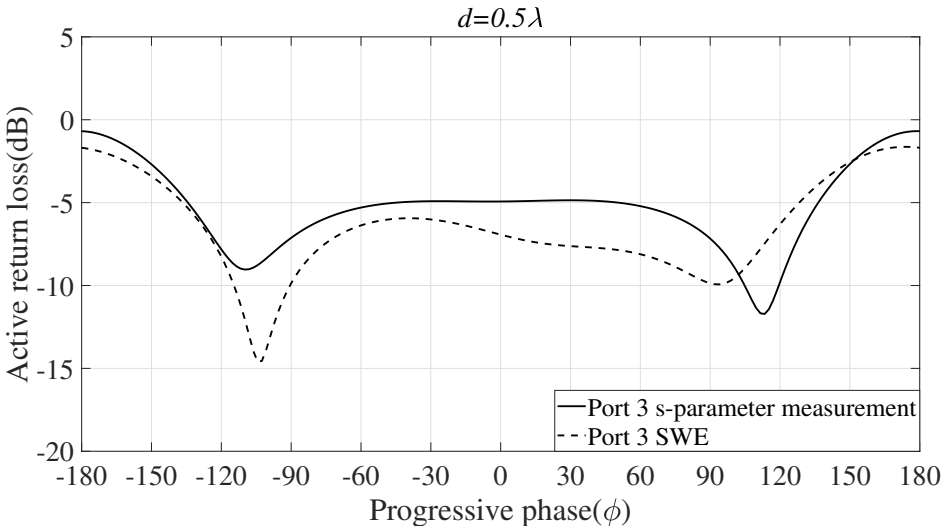

Figure 4.21: The active return loss variation with progressive phase computed using the proposed method and s-parameter measurement for port 3 ($d = 0.5\lambda$).

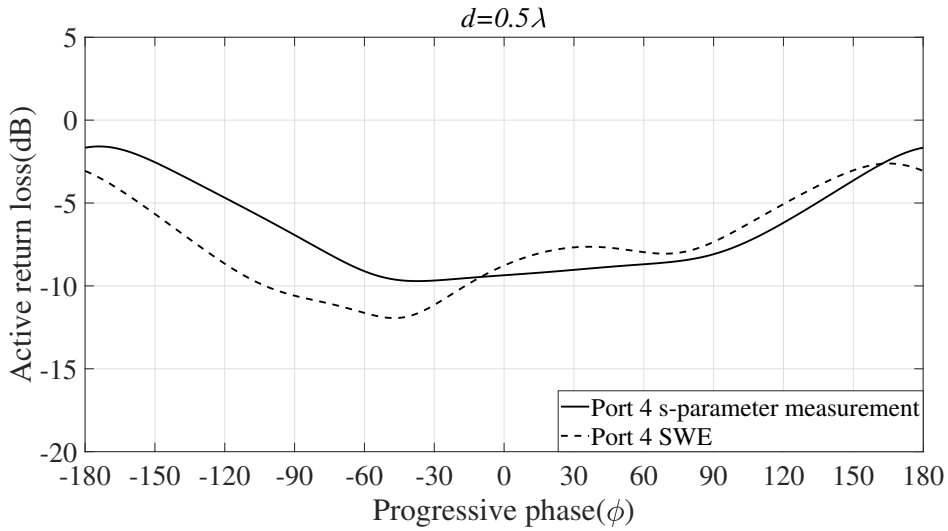

Figure 4.22: The active return loss variation with progressive phase computed using the proposed method and s-parameter measurement for port 4 ($d = 0.5\lambda$).

CHAPTER 5

MUTUAL IMPEDANCE COMPUTATION USING PLANE WAVE SPECTRUM AND REACTION THEOREM

5.1 Plane wave spectrum

An arbitrary monochromatic EM wave can be expanded as a superposition of plane waves travelling in different directions with different amplitudes [26]. The plane wave spectrum is a function that defines the complex amplitudes of the plane waves propagating in all directions. Using the Fourier theory, an electric field, $\bar{E}$ can be expressed as[26]:

$$\bar{E}(x,y,z) = \frac{1}{4\pi^2}\int_{-\infty}^{\infty}\int_{-\infty}^{\infty}\bar{f}(k_x,k_z)e^{-j\bar{k}\cdot\bar{r}}dk_x dk_z \tag{5.1}$$

where $\bar{r} = x\hat{a}_x + y\hat{a}_y + z\hat{a}_z$ is the position vector, and $\bar{k} = k_x\hat{a}_x + k_y\hat{a}_y + k_z\hat{a}_z$ is the wavenumber vector. k_y is defined in terms of k_x and k_z as given in (5.2) and (5.3)

$$k_y = \sqrt{k^2 - k_x^2 - k_z^2} \quad k^2 > k_x^2 + k_z^2 \tag{5.2}$$

$$k_y = -j\sqrt{k_x^2 + k_z^2 - k^2} \quad k^2 < k_x^2 + k_z^2 \tag{5.3}$$

$\bar{f}(k_x,k_z)$ represents the plane wave spectrum of the field as:

$$\bar{f}(k_x,k_z) = f_x(k_x,k_z)\hat{a}_x + f_y(k_x,k_z)\hat{a}_y + f_z(k_x,k_z)\hat{a}_z \tag{5.4}$$

The $\bar{H}$ field can also be written as:

$$\bar{H}(x,y,z) = -\frac{1}{4\pi^2 k\eta}\int_{-\infty}^{\infty}\int_{-\infty}^{\infty}\left(\bar{f}\times\bar{k}\right)e^{-j\bar{k}\cdot\bar{r}}dk_x dk_z \tag{5.5}$$

The next section briefly summarizes the material given in [39] to express the analyticiy of the spectrum and far-field pattern functions. These definitions will be used in the following sections to compute the near fields of an infinitely thin half-wave dipole from its far-field pattern function.

5.2 Analiticity of spectrum, far-field pattern functions

To show that the spectrum and the far-field pattern function are analytical functions with respect to their arguments in a certain complex domain, we will need the following theorem.

Theorem 5-1: Let S be a smooth surface enclosing a finite volume. Suppose that the complex function $g(\bar{r}, w)$ is analytic with respect to complex variable w for all $\bar{r} \in S$, and for all $w \in A$ where A is a region in the complex plane. Then,

$$G(w) = \int_S g(\bar{r}, w) dS \tag{5.6}$$

is also an analytical function of $w \in A$.

Let $w = u + jv$ where u and v are two real variables. If the function $g(\bar{r}, w)$ is sufficiently smooth on S, it can be shown that [39], [40].

$$\frac{\partial}{\partial u} \int_S g(r', u + jv) dS' = \int_S \frac{\partial}{\partial u} g(r', u + jv) dS' \tag{5.7}$$

$$\frac{\partial}{\partial v} \int_S g(r', u + jv) dS' = \int_S \frac{\partial}{\partial v} g(r', u + jv) dS' \tag{5.8}$$

Since the analytical function $g(\bar{r}, w)$ satisfies the Cauchy-Riemann conditions, its integral ($\int_S g(\bar{r}, w) dS'$) also satisfies the Cauchy-Riemann conditions which shows that $G(w)$ is analytic for $w \in A$.

5.2.1 Analyticity of the spectrum

Suppose $\bar{E}(\bar{r})$ and $\bar{H}(\bar{r})$ are known on a closed smooth surface S that encloses all the sources contained in the volume V, and the surface lies entirely outside of V as shown in Figure 5.1. The expressions for the electromagnetic spectra using these surface fields (Huygens' sources) are given as:

$$\begin{aligned} \bar{f}(k_x, k_z) = & \frac{1}{2kk_y} \sqrt{\frac{\mu}{\epsilon}} \bar{k} \times \left(\bar{k} \times \int_S \hat{n} \times \bar{H}(\bar{r}) e^{j(k_x x + k_y y + k_z z)} dS \right) \\ & - \frac{1}{2k_y} \bar{k} \times \int_S \hat{n} \times \bar{E}(\bar{r}) e^{j(k_x x + k_y y + k_z z)} dS \end{aligned} \tag{5.9}$$

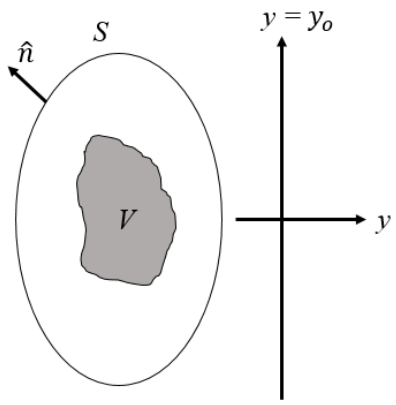

Figure 5.1: The source region V, the surrounding surface S and the plane $y = y_o$.

where $\bar{f}(k_x, k_z)$ is the spectrum function for electric field. Since the surface S is smooth, and located outside the source region V as illustrated in Figure 5.1, $\hat{n} \times \bar{E}(\bar{r})$ and $\hat{n} \times \bar{H}(\bar{r})$ are continuous on S. The spectrum function $\bar{f}(k_x, k_z)$ has an integral expression that satisfy the conditions of Theorem 5-1 where k_x and k_z are the complex variables. Note that the function $e^{j(k_x x + k_y y + k_z z)}/k_y$ determines the analyticity of the spectrum function on the complex variables k_x and k_z.

In order to determine the analyticity region of the spectrum functions in the complex k_x and k_z plane, the branch cut of the square root function describing k_y must be specified. This branch cut can be chosen such that it does not go through the real k_x and k_z axis, so that the spectrum functions are analytic around the real k_x and k_z axis, except the singular point at $k_y = 0$.

5.2.2 Analyticity of the far-field pattern

The far-field pattern is defined as:

$$\bar{F}^E(\theta, \phi) = \lim_{r \to \infty} r e^{jkr} \bar{E}(\bar{r}) \tag{5.10}$$

The far-field pattern function of the $\bar{E}$ field is expressed in terms of Huygens' sources as:

$$\bar{F}^E(\theta, \phi) = \frac{jk}{4\pi} \hat{r} \times \int_S \left[-\hat{n}' \times \bar{E}(\bar{r}') + \sqrt{\frac{\mu}{\epsilon}} \hat{r} \times (\hat{n}' \times \bar{H}(\bar{r}')) \right] e^{jk\hat{r} \cdot \bar{r}'} dS' \tag{5.11}$$

where $\hat{r}$ is unit vector, and $\hat{n}'$ is the outward normal vector to the surface S'. It is important to note that the vector $\bar{r} = \hat{x}\sin\theta\cos\phi + \hat{y}\sin\theta\sin\phi + \hat{z}\cos\theta$ is an analytic function that remains valid for all complex values of θ and ϕ. Consequently, $\bar{r}$ represents an entire function of complex θ and ϕ. Since the fields and the normal vector $\hat{n}'$ are continuous on S', utilizing equation (5.11) along with Theorem 5-1, it can be deduced that the far-field pattern function of the $\bar{E}$ field is also an entire function of complex θ and ϕ.

The far-field pattern function is related to spectrum through following expression:

$$\bar{F}^E(\theta,\phi) = jk\sin\theta\sin\phi\bar{f}(k_x,k_z) \quad 0<\theta<\pi, \quad 0<\phi<\pi \tag{5.12}$$

where $k_x = k\sin\theta\cos\phi$, and $k_z = k\cos\theta$. $\bar{f}(k_x,k_z)$ is given in (5.13)

$$\bar{f}(k_x,k_z) = \int_{-\infty}^{\infty}\int_{-\infty}^{\infty}\bar{E}(\bar{r})e^{-j(k_x x+k_y y+k_z z)}dxdz \quad y \geq y_o \tag{5.13}$$

Given the existing connections between trigonometric and hyperbolic sine and cosine functions, it becomes evident that the spectrum within the invisible region $k_x^2 + k_z^2 > k^2$ can be determined by analyzing the far-field patterns within the complex region.

5.2.3 Analytic continuation

Analytical continuation allows for the extension of the domain of a complex function, which is initially defined only in a limited region of the complex plane [41]. Suppose that $f_1(z)$ is a complex function which is expanded in terms of Taylor series as:

$$f_1(z) = \sum_{n=0}^{\infty}(-z)^n \tag{5.14}$$

Such a series expansion is generally valid within a convergence region. For this case, this expansion converges for $|z| < 1$ in the complex plane, and $|z| < 1$ corresponds to a region inside the circle C_1 with radius r_1 as illustrated in Figure 5.2.

Consider that $f_2(z)$ is a complex function which can be written in terms of Taylor series as:

$$f_2(z) = \frac{1}{1+j}\sum_{n=0}^{\infty}(-\frac{z-j}{1+j})^n \tag{5.15}$$

This series converges for $|z-j| < |j+1| = \sqrt{2}$. The center of the convergence circle is at $z_2 = j$ point on the imaginary axis as depicted in Figure 5.2. f_1 and f_2

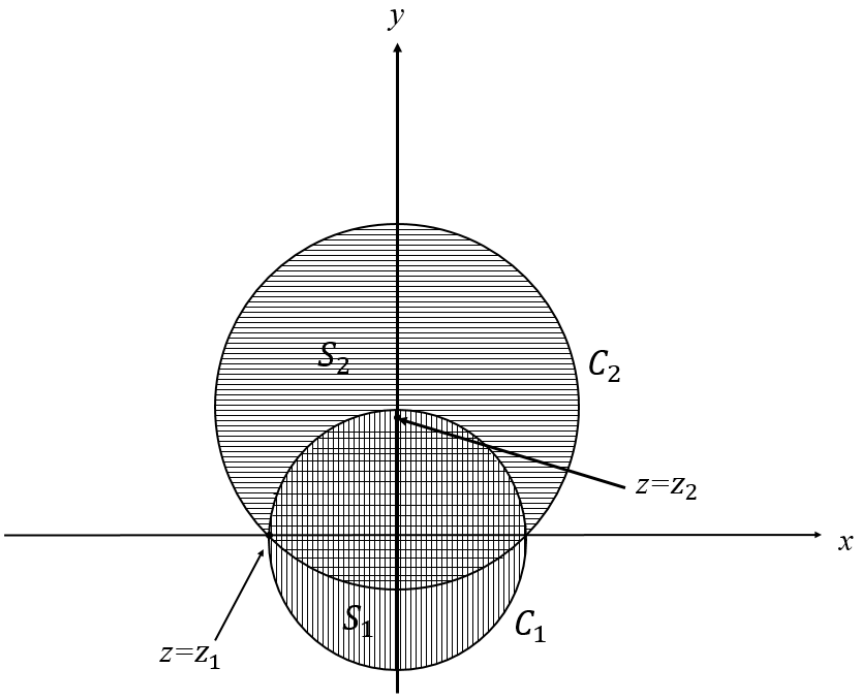

Figure 5.2: Analytic continuation.

represent analytic functions defined on domains S_1 and S_2, respectively. S_1 and S_2 overlaps in the intersection region $S_1 \cap S_2$, and it is known that f_1 equals f_2 within this common region. In such cases, f_2 is referred to as an analytical continuation of f_1 to S_2, and vice versa, as stated in [42]. Additionally, if an analytical continuation of f_1 to S_2 exists, it is guaranteed to be unique.

(5.14), and (5.15) give two different representation of the same function ($f(z) = 1/(1+z)$). Each representation has its own convergence region in the complex plane. Using analytical continuity, it can be said that $f(z) = 1/(1+z)$ is analytical continuation of either of the series given by (5.14) and (5.15).

5.3 Mutual impedance between two infinitely thin half-wave dipoles

The reaction theorem states that if the port currents, and the fields associated with the antennas are known on an arbitrary surface enclosing one of the antennas, then the

mutual impedance between antennas can be calculated as:

$$Z_{12} = -\frac{1}{I_1 I_2} \oint_{S_1} (\bar{E}_1 \times \bar{H}_2 - \bar{E}_2 \times \bar{H}_1) \cdot d\bar{S} \tag{5.16}$$

An infinitely large plane that separates two antennas, and closed by a hemisphere on one side is introduced as the reaction surface as illustrated in Figure 5.3. The closed

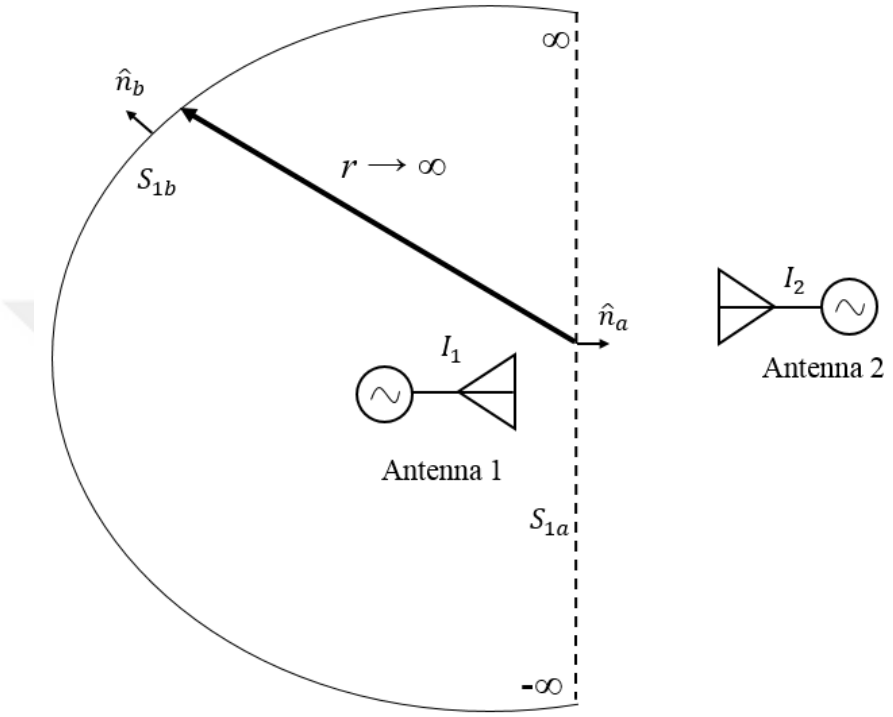

Figure 5.3: The modified reaction surface.

surface integral given in (5.16) can be decomposed into two different surface integrals as:

$$\oint_{S_1} (\bar{E}_1 \times \bar{H}_2 - \bar{E}_2 \times \bar{H}_1) \cdot d\bar{S} = \int_{S_{1a}} (\bar{E}_1 \times \bar{H}_2 - \bar{E}_2 \times \bar{H}_1) \cdot d\bar{S} + \int_{S_{1b}} (\bar{E}_1 \times \bar{H}_2 - \bar{E}_2 \times \bar{H}_1) \cdot d\bar{S} \tag{5.17}$$

where S_{1a} denotes the infinite plane, while S_{1b} represents the hemisphere which closes S_{1a} on one side. When S_{1b} surface extends to infinity, the integrand of the surface integral $\bar{E}_1 \times \bar{H}_2 - \bar{E}_2 \times \bar{H}_1$ becomes zero on S_{1b} as derived in Appendix F. In this case, the reaction surface can be defined as a plane at $y = d/2$ which extends from $-\infty$ to ∞ as shown in Figure 5.4. Since the unit normal vector on the reaction

plane is along y direction and $H_z = 0$ for both antennas, E_z and H_x near-field components of both antennas will be sufficient for mutual impedance computation using reaction theorem as given in (5.18).

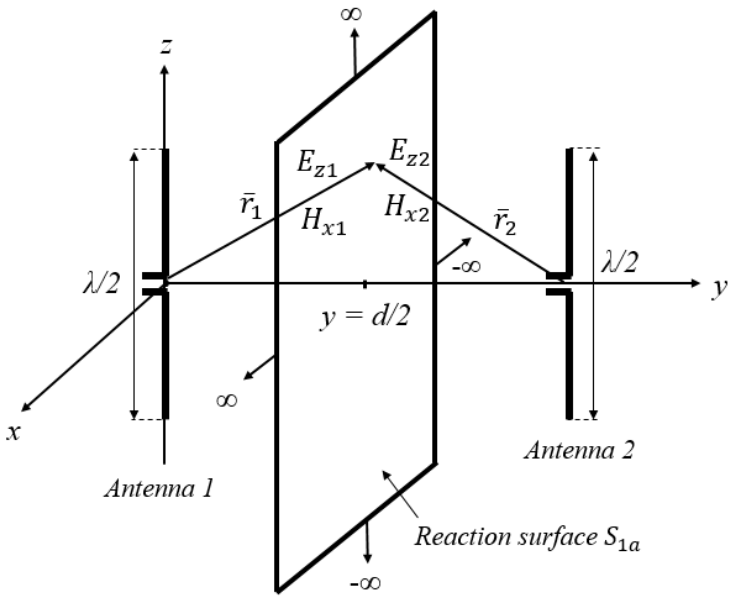

Figure 5.4: Two infinitely thin half-wave dipole antennas are separated by a reaction plane which extends to infinity.

$$Z_{12} = -\frac{1}{I_1 I_2} \int_{S_{1a}} (E_{z1} H_{x2} - E_{z2} H_{x1}) dS_{1a} \tag{5.18}$$

5.3.1 Asymptotic evaluation of plane wave spectrum integral

Asymptotic evaluation of the plane wave spectrum integral is presented to establish a relationship between the spectrum and the far-field pattern function of an infinitely thin half-wave dipole. By utilizing this relationship, the spectrum and its analyticity allow for the determination of the near-field components E_z and H_x, from the known far-field pattern function of an infinitely thin half-wave dipole antenna.

Consider an infinitely thin half-wave dipole is placed on the right-handed rectangular coordinate system as shown in Figure 5.5. The feed point of the dipole is positioned at the origin, and its arms extend along z-axis. The plane located at $y = y_o$ denotes the specific region where the near-fields of the dipole will be computed. The $\bar{E}$ field of an infinitely thin half-wave dipole can be expressed in terms of plane wave

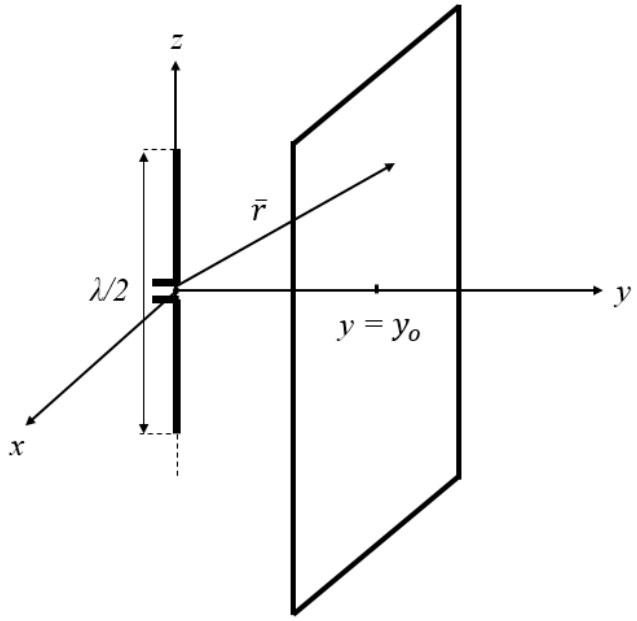

Figure 5.5: The placement of an infinitely thin half-wave dipole in the right-handed rectangular coordinate system.

spectrum of the field as:

$$\bar{E}(x,y,z) = \frac{1}{4\pi^2}\int_{-\infty}^{\infty}\int_{-\infty}^{\infty}\bar{f}(k_x,k_z)e^{-j\bar{k}\cdot\bar{r}}dk_x dk_z \tag{5.19}$$

where $\bar{r} = x\hat{a}_x + y\hat{a}_y + z\hat{a}_z$ is the position vector, and $\bar{k} = k_x\hat{a}_x + k_y\hat{a}_y + k_z\hat{a}_z$ is the wavenumber vector. $\bar{f}(k_x,k_z)$ represents the plane wave spectrum of the field as:

$$\bar{f}(k_x,k_z) = f_x(k_x,k_z)\hat{a}_x + f_y(k_x,k_z)\hat{a}_y + f_z(k_x,k_z)\hat{a}_z \tag{5.20}$$

The $\bar{H}$ field can also be written as:

$$\bar{H}(x,y,z) = -\frac{1}{4\pi^2 k\eta}\int_{-\infty}^{\infty}\int_{-\infty}^{\infty}\left(\bar{f}\times\bar{k}\right)e^{-j\bar{k}\cdot\bar{r}}dk_x dk_z \tag{5.21}$$

By using asymptotic evaluation of the plane wave spectrum integral, the expression given in (5.19) can be simplified as:

$$\bar{E}(r,\theta,\phi) \cong \frac{jke^{-jkr}}{2\pi r}\left[\sin\theta\sin\phi\bar{f}(k_1 = k\sin\theta\cos\phi, k_2 = k\cos\theta)\right] \tag{5.22}$$

The detailed derivation of the asymptotic evaluation of the plane wave spectrum integral is given in Appendix G. In order to find $\bar{f}(k_1,k_2)$ in terms of θ and ϕ in far-zone, the $\bar{E}(r,\theta,\phi)$ field expression need to be known in the far-field region. In the literature [26], the electric field of an infinitely thin half-wave dipole in the far-zone is

clearly described as:

$$E_\theta \cong \frac{j\eta I_o e^{-jkr}}{2\pi r}\left[\frac{\cos(\frac{\pi}{2}\cos\theta)}{\sin\theta}\right] \tag{5.23}$$

By setting the expression on the right hand side of (5.22) equal to the right hand side of (5.23), f_θ can be written as:

$$f_\theta = \frac{\eta I_o}{k}\frac{\cos(\frac{\pi}{2}\cos\theta)}{\sin^2\theta\sin\phi} \tag{5.24}$$

Using the vector transformation from spherical to cartesian given in (5.25),

$$\hat{a}_\theta = \hat{a}_x\cos\theta\cos\phi + \hat{a}_y\cos\theta\sin\phi - \hat{a}_z\sin\theta \tag{5.25}$$

we can readily determine the components of plane wave spectrum function f_x, f_y, and f_z in terms of θ and ϕ for an infinitely thin half-wave dipole, as indicated in (5.26), (5.27), and (5.28), respectively.

$$f_x = \frac{\eta I_o}{k}\left[\frac{\cos(\frac{\pi}{2}\cos\theta)}{\sin\theta}\right]\left[\frac{\cos\theta\cos\phi}{\sin\theta\sin\phi}\right] \tag{5.26}$$

$$f_y = \frac{\eta I_o}{k}\left[\frac{\cos(\frac{\pi}{2}\cos\theta)}{\sin\theta}\right]\left[\frac{\cos\theta}{\sin\theta}\right] \tag{5.27}$$

$$f_z = -\frac{\eta I_o}{k}\left[\frac{\cos(\frac{\pi}{2}\cos\theta)}{\sin\theta}\right]\left[\frac{1}{\sin\phi}\right] \tag{5.28}$$

where the θ and ϕ are described in terms of the components of the wavenumber vector as:

$$\cos\theta = \tfrac{k_z}{k} \tag{5.29}$$

$$\sin\theta = \sqrt{1-\left(\tfrac{k_z}{k}\right)^2} = \tfrac{1}{k}\sqrt{k_x^2+k_y^2} \tag{5.30}$$

$$\sin\phi = \tfrac{k_y}{\sqrt{k_x^2+k_y^2}} \tag{5.31}$$

$$\cos\phi = \tfrac{k_x}{\sqrt{k_x^2+k_y^2}} \tag{5.32}$$

In order to calculate the fields using (5.19) and (5.21), the vector components of the plane wave spectrum function f_x, f_y, and f_z need to be expressed in terms of k_x, k_y, and k_z. This can be accomplished by utilizing the relationships provided in (5.29)-(5.32). Specifically, by inserting (5.29), (5.30), (5.31) into (5.28), the expression for f_z can be obtained as:

$$f_z(k_x,k_z) = -\eta I_o\frac{\cos(\frac{\pi}{2}\frac{k_z}{k})}{k_y} \tag{5.33}$$

By substituting $f_z(k_x, k_z)$ into (5.19), the z component of the $\bar{E}$ field can be found as:

$$E_z(x,y,z) = -\frac{\eta I_0}{4\pi^2}\int_{-\infty}^{\infty}\int_{-\infty}^{\infty}\left[\frac{\cos(\frac{\pi}{2}\frac{k_z}{k})}{k_y}\right]e^{-j(k_x x+k_y y+k_z z)}dk_x dk_z \tag{5.34}$$

Furthermore, the x component of the magnetic field can be written as:

$$H_x(x,y,z) = -\frac{I_o}{4\pi^2 k}\int_{-\infty}^{\infty}\int_{-\infty}^{\infty}\left(\left[\frac{\cos(\frac{\pi}{2}\frac{k_z}{k})}{k_x^2+k_y^2}\right]k_z^2 + \cos(\frac{\pi}{2}\frac{k_z}{k})\right) e^{-j(k_x x+k_y y+k_z z)}dk_x dk_z \tag{5.35}$$

$f_z(k_x, k_z)$ is an analytical function, except at the point where k_y equals to zero. By employing analytical contiunity and utilizing the plane wave spectrum integral provided in (5.34), the E_z can be determined in the near-field region based on the far-field pattern function of an infinitely thin half-wave dipole. To consider propagating and evanescent waves, the integrals in (5.34) and (5.35) need to be evaluated in the visible and invisible regions. The visible and invisible regions in the k domain are depicted in Figure 5.6.

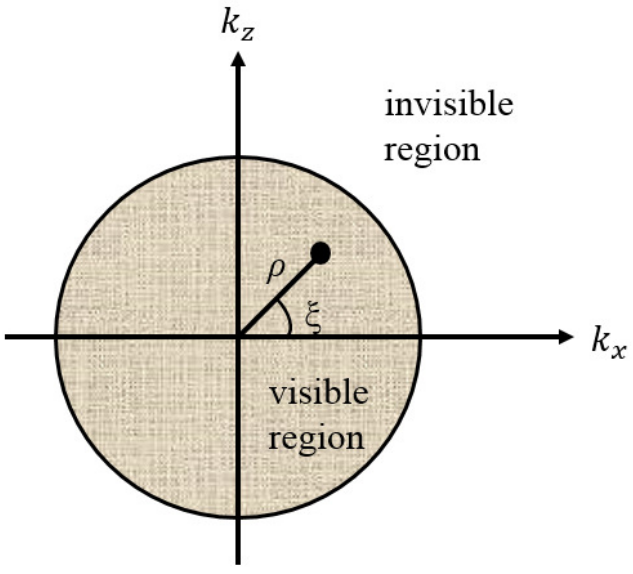

Figure 5.6: Representation of the visible (inside circle), and invisible (outside circle) regions in k-domain.

k_x and k_z can be described in terms of ρ and ξ as:

$$k_x = \rho\cos\xi \tag{5.36}$$

$$k_z = \rho\sin\xi \tag{5.37}$$

$$dk_x dk_z = \rho d\rho d\xi \tag{5.38}$$

Using the definitions of k_x and k_z in terms of ρ and ξ, E_z and H_x can be written as:

$$\begin{aligned} E_z = &-\frac{\eta I_o}{4\pi^2}\int_0^{2\pi}\int_0^{k}\left[\frac{\cos(\frac{\pi\rho\sin\xi}{2k})}{\sqrt{k^2-\rho^2}}\right]e^{-j(\rho\cos(\xi)x+\sqrt{k^2-\rho^2}y+\rho\sin(\xi)z)}\rho d\rho d\xi + \\ &-\frac{\eta I_o}{4\pi^2}\int_0^{2\pi}\int_k^{\infty}\left[\frac{\cos(\frac{\pi\rho\sin\xi}{2k})}{-j\sqrt{\rho^2-k^2}}\right]e^{-j(\rho\cos(\xi)x-j\sqrt{\rho^2-k^2}y+\rho\sin(\xi)z)}\rho d\rho d\xi \end{aligned} \tag{5.39}$$

$$\begin{aligned} H_x = &-\frac{I_o}{4\pi^2 k}\int_0^{2\pi}\int_0^{k}\left[\frac{\cos(\frac{\pi\rho\sin\xi}{2k})(\rho\sin\xi)^2}{\sqrt{k^2-(\rho\sin\xi)^2}}+\cos(\frac{\pi\rho\sin\xi}{2k})\right] \\ &e^{-j(\rho\cos(\xi)x+\sqrt{k^2-\rho^2}y+\rho\sin(\xi)z)}\rho d\rho d\xi + \\ &-\frac{I_o}{4\pi^2 k}\int_0^{2\pi}\int_k^{\infty}\left[\frac{\cos(\frac{\pi\rho\sin\xi}{2k})(\rho\sin\xi)^2}{\sqrt{k^2-(\rho\sin\xi)^2}}+\cos(\frac{\pi\rho\sin\xi}{2k})\right] \\ &e^{-j(\rho\cos(\xi)x+\sqrt{k^2-\rho^2}y+\rho\sin(\xi)z)}\rho d\rho d\xi \end{aligned} \tag{5.40}$$

5.3.2 Results

The primary emphasis of this section lies in presenting the results of the mutual impedance between two infinitely thin half-wave dipoles computed using PWS-Reaction theorem. The fields E_z, H_x are computed using (5.39), and (5.40) for both antennas, and these fields are inserted into (5.41) to determine the mutual impedance between two infinitely thin half-wave dipoles arranged side by side.

$$Z_{12} = -\frac{1}{I_1 I_2}\int_{S_{1a}}(E_{z1}H_{x2} - E_{z2}H_{x1})dS_{1a} \tag{5.41}$$

However, it should be noted that the reaction surface mentioned in (5.41) is defined as an infinitely large plane that separates the two antennas. To investigate the limits of this plane, the behaviour of the integrand of the reaction integral, specifically $E_{z1}H_{x2} - E_{z2}H_{x1}$, is examined on a $4\lambda \times 4\lambda$ planar reaction surface as illustrated in Figure 5.7. This analysis takes into account the magnitude and phase variations of

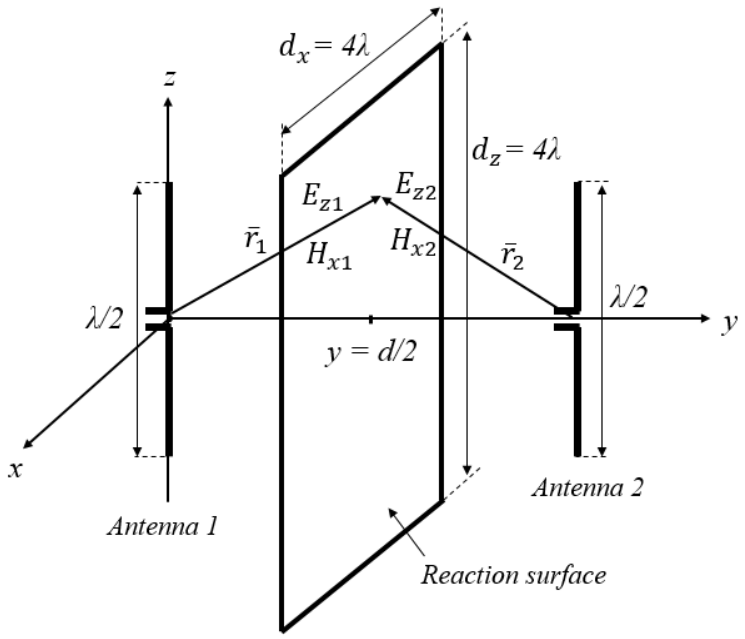

Figure 5.7: $4\lambda \times 4\lambda$ reaction plane separates two half-wave dipoles.

the integrand, which represent the distribution of the coupling on the planar reaction surface.

Figure 5.8 illustrates the magnitude variation of the integrand of the reaction integral on a $4\lambda \times 4\lambda$ plane for a separation distance of 0.5λ. Additionally, Figure 5.9 displays the phase variation of the integrand of the reaction integral for the same separation distance. Furthermore, Figure 5.10 and Figure 5.11 provide the magnitude and phase distributions of the integrand of the reaction integral, respectively, for a separation distance of $d = 1\lambda$.

By utilizing the plane wave spectrum (PWS) and the reaction theorem, the mutual impedance between two half-wave dipoles positioned side-by-side is determined using a $4\lambda \times 4\lambda$ reaction plane at various separation distances. Figure 5.12 depicts a comparison between the mutual impedance values computed by using PWS-Reaction theorem and the values obtained from the induced EMF method.

The phase distribution on the planar reaction surface reveals that the phase of the reaction integrand oscillates between -π and π, as the observation point approaches the far-field region. Moreover, it is evident that the magnitude of the integrand changes slowly. The phase of the reaction integrand oscillates rapidly outside the region where

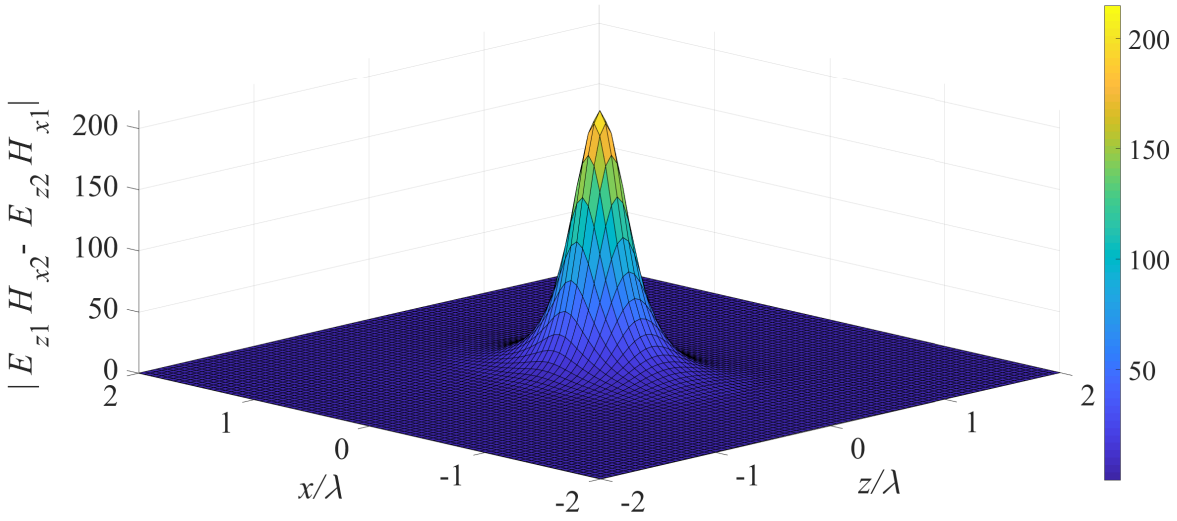

Figure 5.8: The magnitude variation of the integrand of the reaction integral on $4\lambda \times 4\lambda$ reaction plane for $d = 0.5\lambda$.

stationary points are positioned, but the contribution to mutual impedance from this region is negligible. Therefore, it is unnecessary to evaluate the reaction integral across the entire planar reaction surface. The restricted region which involves the stationary points on planar reaction surface will be sufficient for mutual impedance computation with very small error. The results clearly show that the reaction integral evaluated in the region which is positioned outside $4\lambda \times 4\lambda$ reaction plane does not make a major contribution to mutual coupling.

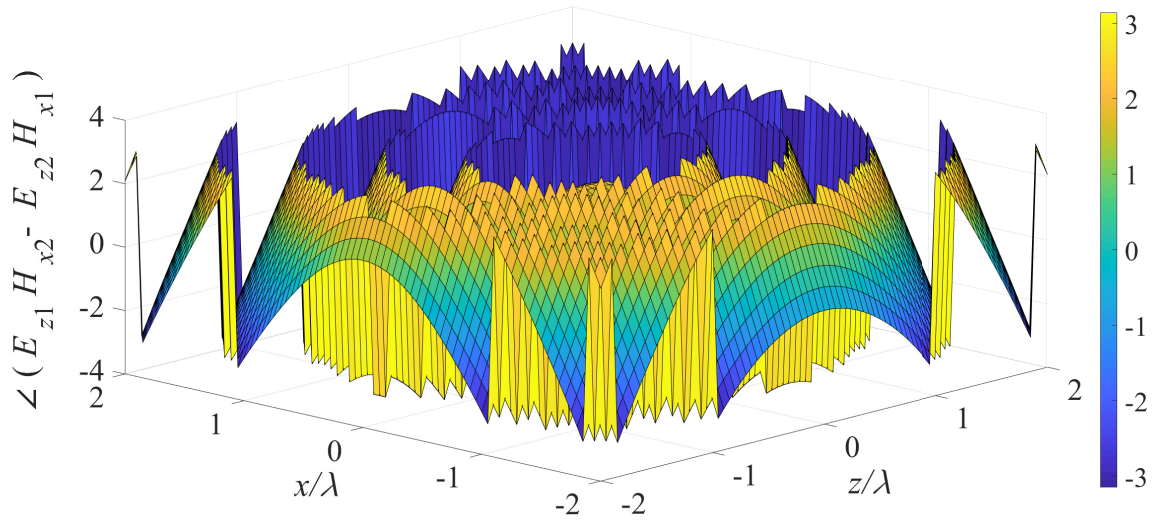

Figure 5.9: The phase variation of the integrand of the reaction integral on $4\lambda \times 4\lambda$ reaction plane for $d = 0.5\lambda$.

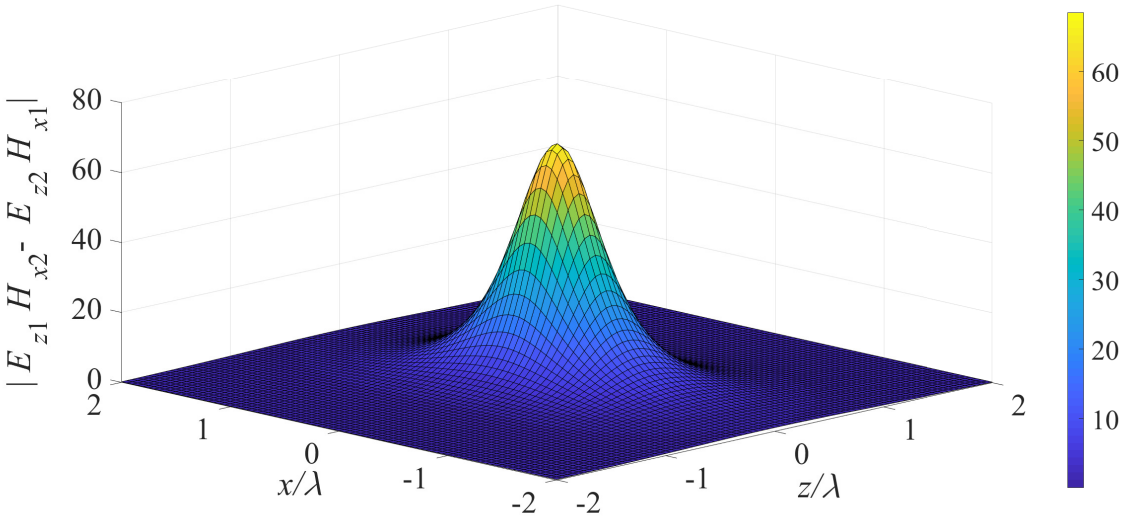

Figure 5.10: The magnitude variation of the integrand of the reaction integral on $4\lambda \times 4\lambda$ reaction plane for $d = 1\lambda$.

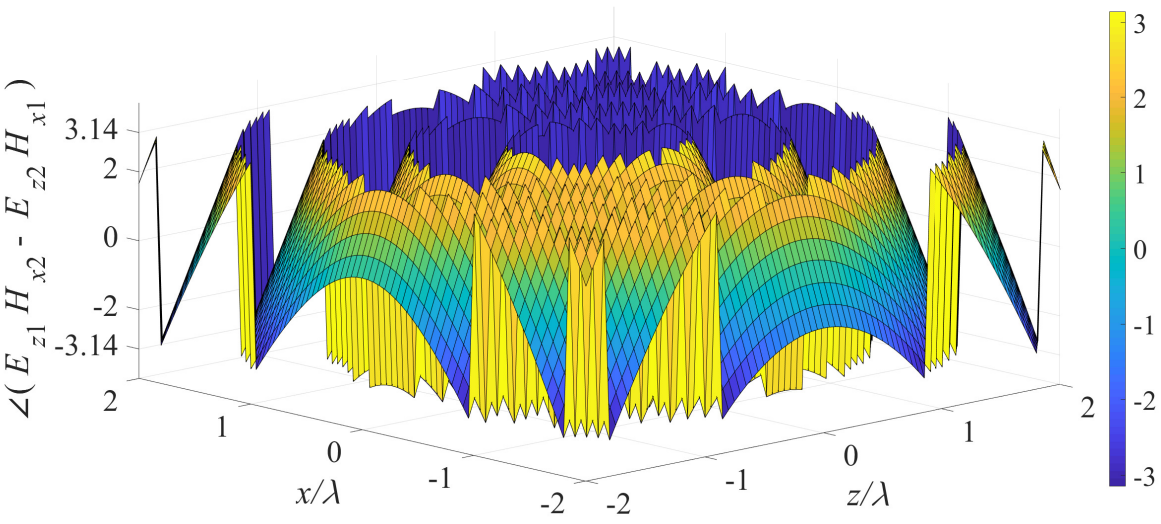

Figure 5.11: The phase variation of the integrand of the reaction integral on $4\lambda \times 4\lambda$ reaction plane for $d = 1\lambda$.

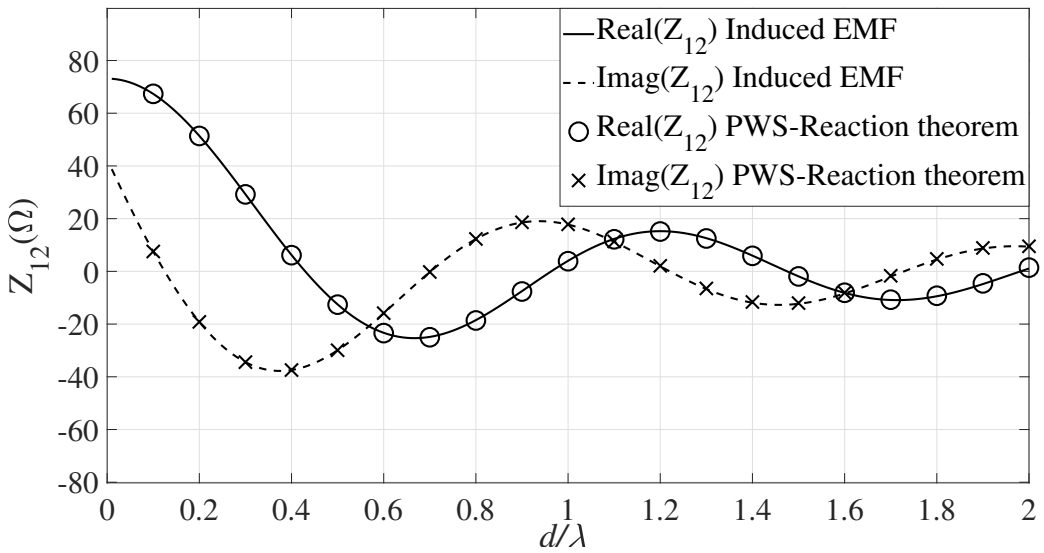

Figure 5.12: The comparison of the mutual impedance values computed using PWS-Reaction theorem and the values obtained from induced EMF method.

CHAPTER 6

CONCLUSION AND FUTURE WORK

The primary goal of this thesis is to determine the mutual impedance between antennas by utilizing either measured or computed fields of a single antenna. Spherical harmonic expansion is employed to express the fields of an antenna, however this expansion representing the outgoing fields converges within the external region of the minimum sphere surrounding the antenna. When two antennas are closely spaced, the minimum spheres of the antennas overlap, it becomes impossible to define a "proper" reaction surface to compute the mutual impedance using reaction theorem.

This study extends the method proposed in [8] to include scenarios where the minimum spheres of the antennas overlap. The idea is to translate the origin of SWEs so that the minimum spheres do not overlap in the new coordinate frame. After this translation, a proper reaction surface is defined in the region where spherical harmonics representing the outgoing waves of both antennas converge. By utilizing spherical harmonics with reaction theorem, the proposed technique allows for the numerical computation of mutual impedance between two closely spaced antennas. Additionally, an analytical expression for the mutual impedance is derived using proposed technique. The resulting analytical formula expresses the mutual impedance as a sum of products involving the spherical harmonic coefficients of both antennas in the same coordinate frame. The proposed method is validated by calculating the mutual impedance between two infinitely thin half-wave dipoles using analytical field expressions and orthogonality relations. The computed values show excellent agreement with the values that obtained from the induced EMF method. The disadvantage of the proposed method is the increase in the number of harmonics required to describe the fields outside the new minimum spheres enclosing the antennas after translation. In

order to perform numerical calculations in the translated coordinate frame, the infinite sum in SWE is truncated. The choice of the truncation value affects the accuracy of the calculation: if it is too small, the series will not converge, while it is too high, numerical errors due to the singularity of wave functions may arise. To adress this issue, a convergence analysis is conducted based on the conservation of radiated power. The radiated power of an infinitely thin half-wave dipole is calculated using two different approaches: by utilizing radiation resistance and input current, or by summing the magnitude squares of the spherical harmonic coefficients in the translated coordinate frame. The relative error in radiated power is investigated to determine the limits of the truncation value, denoted as N' values where the error remains low, providing flexibility in selecting an appropriate expression from the various proposals available in the literature. In fact, different expressions suggested in the literature fall within this low-error range.

The convergence of SWE becomes challenging as it approaches the boundary of the region of convergence. On one hand, larger values of A allow for more accurate results, but on the other hand, it requires a higher value of N', leading to increased computation. Additionally larger values of A can result in increased numerical errors. Thus, the value of the translation distance is investigated to obtain accurate calculations on the reaction surface. The mutual impedance between two infinitely thin half-wave dipoles are computed as a function of translation distance A values from 0.6λ to 3λ for different antenna separations. The error in this scenario is defined as the difference between the mutual impedances calculated by proposed method and the induced EMF method. The optimal value of A for the given antenna separations is found to be 0.9λ, which places the reaction surface at a distance greater than 0.01λ from the edge of the region of convergence. Beyond this point, the error remains low, and the selection of A becomes less critical.

The proposed method is also validated by calculating the mutual impedance between two printed dipoles using near field measurement data. A single printed dipole antenna is measured using MVG SATIMO spherical near field measurement device. SATIMO near field measurement device gives the SWE coefficients of the measured antenna. With the available SWE coefficients, the proposed numerical and analytical techniques are employed to compute the mutual impedances between two such

dipoles in a side-by-side configuration at different distances. The mutual impedances are also determined from measured s-parameters, and the full-wave simulation using HFSS for the same configuration. The results obtained from these methods are consistent with each other, but our solution differs, suggesting that discrepancy is due to presence of multiple reflections that were not accounted for in our approach. For large antenna separations ($d > d_{\text{max}}$) the minimum spheres of antennas do not overlap. For very small distances ($d > d_{\text{min}}$) multiple reflections cannot be ignored. Hence, there is a range of antenna separations ($d_{\text{min}} < d < d_{\text{max}}$) where the minimum spheres overlap, and multiple reflections can be disregarded. This range is significant in practice since most antenna arrays employ such distances and the proposed method provides accurate results in this range.

A uniform array is constructed by arranging four printed dipoles side by side. The input impedance of each dipole and the mutual impedance between them are determined based on the measured s-parameters. It is assumed that all the elements are excited with uniform current, but each subsequent element has a progressive phase lead of ϕ compared to the previous one. For this arrangement, the active return loss variation with progressive phase lead is investigated to explore the effects of the mutual impedance in the constructed array. Using proposed method, the active return loss of each port is computed for four-element printed dipole array. The results of the proposed method are compared to that obtained from s-parameter measurements. As the distance between elements increases, the active return loss values from the proposed method converges towards the results that obtained from s-parameter measurements for specific progressive phase angles.

In chapter 5, by using analyticity of spectrum and asymptotic evaluation of radiated fields, the near fields of an infinitely thin half-wave dipole is found from far-field pattern function for mutual impedance computation. The magnitude and phase distribution of the integrand of the reaction integral is investigated to explore the effective size of the reaction surface. The mutual impedance between two infinitely thin half-wave dipoles is computed for various separation distances on a limited reaction surface, and the results show excellent agreement with that obtained from the induced EMF method.

The proposed method is currently employed to compute the mutual impedance between two antennas using the data of the single antenna. This means that the multiple reflections between these elements are not taken into account. As a potential avenue for future research, the computation of mutual impedance can be further enhanced by utilizing the proposed method, which incorporates the consideration of multiple reflections between elements.

Appendix A

To explain this analytical technique in detail, let's consider antenna 1 positioned at the origin of the unprimed coordinate system, while antenna 2 is placed at the origin of the primed coordinate system as shown in Figure A.1. The position vector, $\bar{\mathbf{r}}$, is measured from the origin of the unprimed coordinate system. The origin of the primed coordinate system is aligned with the unprimed coordinate system by the position vector $\bar{\mathbf{r}}''$. The position vector $\bar{\mathbf{r}}'$ is measured from the origin of the primed coordinate system, and $\hat{\mathbf{r}}'$ represents the unit vector for this coordinate frame. These position vectors are related by the addition equation:

$$\bar{\mathbf{r}} = \bar{\mathbf{r}}' + \bar{\mathbf{r}}'' \tag{A.1}$$

The fields of antenna 1 are expanded in terms of vector spherical harmonics associated with the unprimed coordinate system as given in (A.2) and (A.3). However, in order to compute surface integration on the surface of antenna 2, $\bar{\mathbf{E}}_\mathbf{1}$ and $\bar{\mathbf{H}}_\mathbf{1}$ should be expressed in terms of vector spherical harmonics associated with the primed coordinate system. For this purpose, the addition theorem can be used to translate fields from the unprimed to the primed coordinate system.

$$\bar{\mathbf{E}}_\mathbf{1} = \sum_{n=1}^{\infty} \sum_{m=-n}^{n} [b_{n,m}^{TE} \bar{\mathbf{M}}_{n,m}^{(2)}(\bar{\mathbf{r}}) + b_{n,m}^{TM} \bar{\mathbf{N}}_{n,m}^{(2)}(\bar{\mathbf{r}})] \tag{A.2}$$

$$\bar{\mathbf{H}}_\mathbf{1} = \frac{jk}{\omega\mu} \sum_{n=1}^{\infty} \sum_{m=-n}^{n} [b_{n,m}^{TE} \bar{\mathbf{N}}_{n,m}^{(2)}(\bar{\mathbf{r}}) + b_{n,m}^{TM} \bar{\mathbf{M}}_{n,m}^{(2)}(\bar{\mathbf{r}})] \tag{A.3}$$

The normalized vector spherical harmonic functions $\bar{\mathbf{M}}_{n,m}^{(i)}(\bar{\mathbf{r}})$ and $\bar{\mathbf{N}}_{n,m}^{(i)}(\bar{\mathbf{r}})$ are defined as given in (A.4),(A.5). The coefficients $b_{n,m}^{TE}$ and $b_{n,m}^{TM}$ represent the spherical harmonic coefficients for the TE and TM modes, respectively. The function $P_n^m(x)$

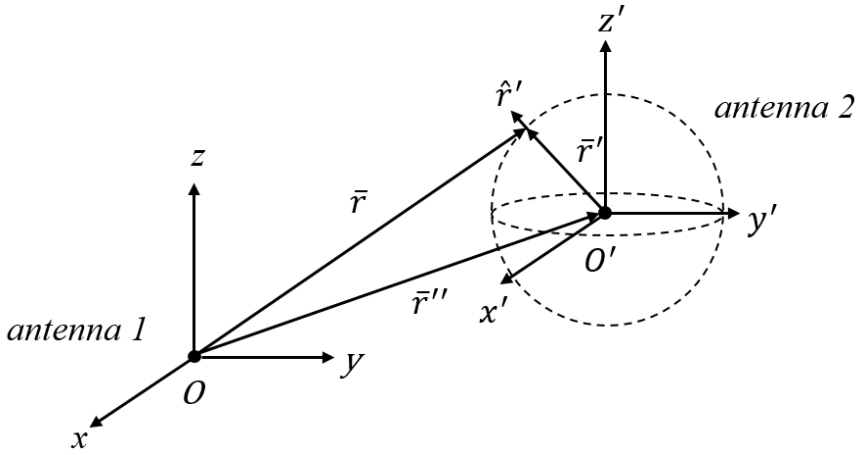

Figure A.1: The placement of two antennas in the right hand coordinate systems.

represents the associated Legendre function. The vector spherical expansions provided in (A.4), and (A.5) are also known as the multipole expansion in the literature [9].

$$\bar{\mathbf{M}}_{n,m}^{(i)}(\bar{\mathbf{r}}) = jC_{n,m}\frac{e^{jm\phi}}{2\sqrt{\pi}}[\frac{jm}{\sin\theta}z_n^{(i)}(kr)P_n^m(\cos\theta)\hat{\theta} + \sin\theta z_n^{(i)}(kr)\frac{d}{dx}P_n^m(x)\mid_{x=\cos\theta}\hat{\phi}] \quad \text{(A.4)}$$

$$\bar{\mathbf{N}}_{n,m}^{(i)}(\bar{\mathbf{r}}) = jC_{n,m}\frac{e^{jm\phi}}{2\sqrt{\pi}}[\frac{z_n^{(i)}(kr)}{kr}n(n+1)P_n^m(\cos\theta)\hat{r} + \frac{1}{kr}\frac{\partial}{\partial r}(rz_n^{(i)}(kr))(-\sin\theta\frac{d}{dx}P_n^m(x)\mid_{x=\cos\theta}\hat{\theta} + \frac{jm}{\sin\theta}P_n^m(\cos\theta)\hat{\phi}\,)\,] \quad \text{(A.5)}$$

where $C_{n,m}$ is determined based on n and m as shown in (A.6)

$$C_{n,m} = \sqrt{\frac{(2n+1)(n-m)!}{n(n+1)(n+m)!}} \quad \text{(A.6)}$$

The spherical Hankel functions, $z_n^i(kr)$, represent different cases as described in (A.7). The upper index (i) specifies the radial dependencies of the spherical wave functions, and the time dependence $e^{j\omega t}$ is assumed in [8]. When $i = 1$, the expansion uses the spherical Hankel functions of the first kind, indicating an incoming wave. On the other hand, when $i = 2$, the expansion employs the spherical Hankel functions of the second kind, representing an outwardly propagating wave. If the antenna is enclosed by the minimum sphere with a radius of a, the expansion is

truncated at $n = ka + 3\sqrt[3]{ka}$ as described in [10],[11].

$$z_n^{(i)}(kr) = \begin{cases} h_n^{(1)}(kr); i = 1 \\ h_n^{(2)}(kr); i = 2 \\ j_n(kr); i = 3 \\ y_n(kr); i = 4 \end{cases} \tag{A.7}$$

Using the addition theorem, $\bar{\mathbf{M}}_{n,m}^{(2)}(\bar{\mathbf{r}})$ and $\bar{\mathbf{N}}_{n,m}^{(2)}(\bar{\mathbf{r}})$ can be expressed as a sum of $\bar{\mathbf{M}}_{n,m}^{(2)}(\bar{\mathbf{r}}')$, and $\bar{\mathbf{N}}_{n,m}^{(2)}(\bar{\mathbf{r}}')$ with coefficients $A_{n',m';n,m}$ and $B_{n',m';n,m}$. For the translation $\bar{\mathbf{r}} = \bar{\mathbf{r}}' + \bar{\mathbf{r}}''$, the general addition theorem states that $\bar{\mathbf{M}}_{n,m}^{(2)}(\bar{\mathbf{r}})$ and $\bar{\mathbf{N}}_{n,m}^{(2)}(\bar{\mathbf{r}})$ can be expressed as shown in (A.8), and (A.9) where $A_{n',m';n,m}$ is determined by (A.10) and $B_{n',m';n,m}$ is determined by (A.11).

$$\bar{\mathbf{M}}_{n,m}^{(2)}(\bar{\mathbf{r}}) = \sum_{n',m'} A_{n',m';n,m}\bar{\mathbf{M}}_{n',m'}^{(i)}(\bar{\mathbf{r}}') + B_{n',m';n,m}\bar{\mathbf{N}}_{n',m'}^{(i)}(\bar{\mathbf{r}}') \tag{A.8}$$

$$\bar{\mathbf{N}}_{n,m}^{(2)}(\bar{\mathbf{r}}) = \sum_{n',m'} A_{n',m';n,m}\bar{\mathbf{N}}_{n',m'}^{(i)}(\bar{\mathbf{r}}') + B_{n',m';n,m}\bar{\mathbf{M}}_{n',m'}^{(i)}(\bar{\mathbf{r}}') \tag{A.9}$$

where

$$A_{n',m';n,m} = \frac{2\pi j^{n'-n}}{\sqrt{n(n+1)n'(n'+1)}} \sum_{n''}(j^{n''}[n(n+1) + n'(n'+1) - n''(n''+1)] A(m,n,-m',n',n'')z_{n''}^{(i')}(kr_w'')Y_{n'',m-m'}(\theta_w'',\phi_w'')) \tag{A.10}$$

and

$$B_{n',m';n,m} = \frac{2\pi j^{n'-n}}{\sqrt{n(n+1)n'(n'+1)}} \sum_{n''}\left(j^{n''}B(m,n,-m',n',n'')z_{n''}^{(i')}(kr_w'')Y_{n'',m-m'}(\theta_w'',\phi_w'')\right) \tag{A.11}$$

In (A.10) and (A.11), $Y_{n,m}(\theta,\phi)$ represents the scalar spherical harmonic.

$$Y_{n,m}(\theta,\phi) = \sqrt{\frac{(2n+1)}{4\pi}\frac{(n-m)!}{(n+m)!}}P_n^m(\cos\theta)e^{jm\phi} \tag{A.12}$$

The choice of the spherical Bessel function $z_{n'}^{(i)}(kr')$ within $\bar{\mathbf{M}}_{n',m'}^{(i)}(\bar{\mathbf{r}}')$ and $\bar{\mathbf{N}}_{n',m'}^{(i)}(\bar{\mathbf{r}}')$ in equations (A.8) and (A.9) depends on the relative sizes of r' and r'' as given in (A.13).

$$z_{n'}^{(i)}(kr') = \begin{cases} j_{n'}(kr'), & r' < r'' \\ \\ h_{n'}^{(2)}(kr'), & r' > r'' \end{cases} \tag{A.13}$$

The selection rule for the coefficients $A_{n',m';n,m}$ and $B_{n',m';n,m}$ is provided in (A.14).

Since $\bar{\mathbf{r}}'$ and $\bar{\mathbf{r}}''$ are constant on the reaction surface, the spherical Bessel functions are also constant. The expressions for $A(m,n,m',n',n'')$ and $B(m,n,m',n',n'')$ are given in [8].

$$z_{n''}^{(i')}(kr'') = \begin{cases} h_{n''}^{(2)}(kr''), & r' < r'' \\ \\ j_{n''}(kr''), & r' > r'' \end{cases} \tag{A.14}$$

By inserting (A.8) and (A.9) into (A.2) and (A.3), we obtain the expressions for the fields of antenna 1 referenced to the primed coordinate system as shown in (A.15), (A.16).

$$\bar{\mathbf{E}}_1 = \sum_{n=1}^{\infty}\sum_{m=-n}^{n}[b_{n,m}^{TE}\sum_{n',m'}(A_{n',m';n,m}\bar{\mathbf{M}}_{n',m'}^{(i)}(\bar{\mathbf{r}}') + B_{n',m';n,m}\bar{\mathbf{N}}_{n',m'}^{(i)}(\bar{\mathbf{r}}')) + b_{n,m}^{TM}\sum_{n',m'}(A_{n',m';n,m}\bar{\mathbf{N}}_{n',m'}^{(i)}(\bar{\mathbf{r}}') + B_{n',m';n,m}\bar{\mathbf{M}}_{n',m'}^{(i)}(\bar{\mathbf{r}}'))] \tag{A.15}$$

and

$$\bar{\mathbf{H}}_1 = j\frac{k}{\omega\mu}\sum_{n=1}^{\infty}\sum_{m=-n}^{n}[b_{n,m}^{TE}\sum_{n',m'}(A_{n',m';n,m}\bar{\mathbf{N}}_{n',m'}^{(i)}(\bar{\mathbf{r}}') + B_{n',m';n,m}\bar{\mathbf{M}}_{n',m'}^{(i)}(\bar{\mathbf{r}}')) + b_{n,m}^{TM}\sum_{n',m'}(A_{n',m';n,m}\bar{\mathbf{M}}_{n',m'}^{(i)}(\bar{\mathbf{r}}') + B_{n',m';n,m}\bar{\mathbf{N}}_{n',m'}^{(i)}(\bar{\mathbf{r}}'))] \tag{A.16}$$

Then, $\bar{\mathbf{E}}_1$ and $\bar{\mathbf{H}}_1$ are expressed as:

$$\bar{\mathbf{E}}_1 = \sum_{n=1}^{\infty}\sum_{m=-n}^{n}\sum_{n',m'}[(b_{n,m}^{TE}A_{n',m';n,m} + b_{n,m}^{TM}B_{n',m';n,m})\bar{\mathbf{M}}_{n',m'}^{(i)}(\bar{\mathbf{r}}') + (b_{n,m}^{TE}B_{n',m';n,m} + b_{n,m}^{TM}A_{n',m';n,m})\bar{\mathbf{N}}_{n',m'}^{(i)}(\bar{\mathbf{r}}')] \tag{A.17}$$

and

$$\bar{\mathbf{H}}_1 = j\frac{k}{\omega\mu}\sum_{n=1}^{\infty}\sum_{m=-n}^{n}\sum_{n',m'}[(b_{n,m}^{TE}A_{n',m';n,m} + b_{n,m}^{TM}B_{n',m';n,m})\bar{\mathbf{N}}_{n',m'}^{(i)}(\bar{\mathbf{r}}') + (b_{n,m}^{TE}B_{n',m';n,m} + b_{n,m}^{TM}A_{n',m';n,m})\bar{\mathbf{M}}_{n',m'}^{(i)}(\bar{\mathbf{r}}')] \tag{A.18}$$

The order of the summation is changed as:

$$\bar{\mathbf{E}}_1 = \sum_{n'=1}^{\infty} \sum_{m'=-n'}^{n'} ({}_1b^{TE}_{n',m'} \bar{\mathbf{M}}^{(i)}_{n',m'}(\bar{\mathbf{r}}') + {}_1b^{TM}_{n',m'} \bar{\mathbf{N}}^{(i)}_{n',m'}(\bar{\mathbf{r}}')) \tag{A.19}$$

and

$$\bar{\mathbf{H}}_1 = j\frac{k}{\omega\mu} \sum_{n'=1}^{\infty} \sum_{m'=-n'}^{n'} ({}_1b^{TE}_{n',m'} \bar{\mathbf{N}}^{(i)}_{n',m'}(\bar{\mathbf{r}}') + {}_1b^{TM}_{n',m'} \bar{\mathbf{M}}^{(i)}_{n',m'}(\bar{\mathbf{r}}')) \tag{A.20}$$

where

$${}_1b^{TE}_{n',m'} = \sum_{n=1}^{\infty} \sum_{m=-n}^{n} (b^{TE}_{n,m} A_{n',m';n,m} + b^{TM}_{n,m} B_{n',m';n,m}) \tag{A.21}$$

and

$${}_1b^{TM}_{n',m'} = \sum_{n=1}^{\infty} \sum_{m=-n}^{n} (b^{TE}_{n,m} B_{n',m';n,m} + b^{TM}_{n,m} A_{n',m';n,m}) \tag{A.22}$$

The pre-subscripts are utilized to denote the coefficients correspond to the expansion of the fields associated with antenna 1. The fields of antenna 2 are expanded as follows:

$$\bar{\mathbf{E}}_2 = \sum_{n'=1}^{\infty} \sum_{m'=-n'}^{n'} ({}_2b^{TE}_{n',m'} \bar{\mathbf{M}}^{(2)}_{n',m'}(\bar{\mathbf{r}}') + {}_2b^{TM}_{n',m'} \bar{\mathbf{N}}^{(2)}_{n',m'}(\bar{\mathbf{r}}')) \tag{A.23}$$

and

$$\bar{\mathbf{H}}_2 = j\frac{k}{\omega\mu} \sum_{n'=1}^{\infty} \sum_{m'=-n'}^{n'} ({}_2b^{TE}_{n',m'} \bar{\mathbf{N}}^{(2)}_{n',m'}(\bar{\mathbf{r}}') + {}_2b^{TM}_{n',m'} \bar{\mathbf{M}}^{(2)}_{n',m'}(\bar{\mathbf{r}}')) \tag{A.24}$$

where

$${}_2b^{TE}_{n,m} = b^{TE}_{n,m} \tag{A.25}$$

$${}_2b^{TM}_{n,m} = b^{TM}_{n,m} \tag{A.26}$$

- Mutual impedance computation using reaction theorem

  The fields radiated by each antenna are expanded in terms of vector spherical harmonics in the primed coordinate system as:

$$\bar{\mathbf{E}}_1 = \sum_{n'=1}^{\infty} \sum_{m'=-n'}^{n'} ({}_1b^{TE}_{n',m'} \bar{\mathbf{M}}^{(i)}_{n',m'}(\bar{\mathbf{r}}') + {}_1b^{TM}_{n',m'} \bar{\mathbf{N}}^{(i)}_{n',m'}(\bar{\mathbf{r}}')) \tag{A.27}$$

$$\bar{\mathbf{H}}_1 = j\frac{k}{\omega\mu} \sum_{n'=1}^{\infty} \sum_{m'=-n'}^{n'} ({}_1b^{TE}_{n',m'} \bar{\mathbf{N}}^{(i)}_{n',m'}(\bar{\mathbf{r}}') + {}_1b^{TM}_{n',m'} \bar{\mathbf{M}}^{(i)}_{n',m'}(\bar{\mathbf{r}}')) \tag{A.28}$$

$$\bar{\mathbf{E}}_2 = \sum_{n'=1}^{\infty} \sum_{m'=-n'}^{n'} \left({}_2b^{TE}_{n',m'} \bar{\mathbf{M}}^{(2)}_{n',m'}(\bar{\mathbf{r}}') + {}_2b^{TM}_{n',m'} \bar{\mathbf{N}}^{(2)}_{n',m'}(\bar{\mathbf{r}}') \right) \tag{A.29}$$

$$\bar{\mathbf{H}}_2 = j\frac{k}{\omega\mu} \sum_{n'=1}^{\infty} \sum_{m'=-n'}^{n'} \left({}_2b^{TE}_{n',m'} \bar{\mathbf{N}}^{(2)}_{n',m'}(\bar{\mathbf{r}}') + {}_2b^{TM}_{n',m'} \bar{\mathbf{M}}^{(2)}_{n',m'}(\bar{\mathbf{r}}') \right) \tag{A.30}$$

The superscript (i) on the spherical harmonic functions designate the type of spherical Bessel functions utilized in the expansion of the fields antenna 1. Since the fields of antenna 1 have already translated by using addition theorem, ${}_1b^{TE}_{n',m'}$ and ${}_1b^{TM}_{n',m'}$ denote translated coefficients in the primed coordinate frame. The relative sizes of the distance from unprimed coordinate origin to primed origin, $\bar{\mathbf{r}}''$, and the distance from primed origin to the field point $\bar{\mathbf{r}}'$ specify the type of the spherical Bessel functions in (A.27), and (A.28).

The mutual impedance between antennas is computed using reaction theorem as:

$$z_{12} = z_{21} = -\frac{1}{i_1 i_2} \int_0^{2\pi} \int_0^{\pi} (\bar{\mathbf{E}}_1 \times \bar{\mathbf{H}}_2 - \bar{\mathbf{E}}_2 \times \bar{\mathbf{H}}_1) \cdot \hat{\mathbf{r}}' r'^2 \sin\theta' d\theta' d\phi' \tag{A.31}$$

where the integral (reaction) surface is defined on the spherical surface with radius $|r'|$ =constant, and this surface encloses the antenna 2. The reaction theorem dictates that the reaction surface must enclose one of the antennas to compute the mutual impedance exactly. Since the reaction sphere includes only antenna 2, the following relation must hold:

$$|\bar{\mathbf{r}}'| < |\bar{\mathbf{r}}''| \tag{A.32}$$

By inserting fields into (A.31) yields:

$$z_{12} = z_{21} = \frac{1}{i_1 i_2} \frac{1}{k^2} \sqrt{\frac{\epsilon}{\mu}} \sum_{n=1}^{\infty} \sum_{m=-n}^{n} (-1)^m ({}_1b^{TE}_{n,-m}\, {}_2b^{TE}_{n,m} + {}_2b^{TM}_{n,m}\, {}_1b^{TM}_{n,-m}) \tag{A.33}$$

Appendix B

SPHERICAL HARMONIC FUNCTIONS

B.1 General expressions

The general expressions for vector spherical wave functions are given as:

$$\bar{F}^{(c)}_{1mn}(r,\theta,\phi) = \frac{1}{\sqrt{2\pi}}\frac{1}{\sqrt{n(n+1)}}\left(-\frac{m}{|m|}\right)^m \left\{ z^{(c)}_n(kr)\frac{jm\bar{P}^{|m|}_n(\cos\theta)}{\sin\theta}e^{jm\phi}\hat{a}_\theta - z^{(c)}_n(kr)\frac{d\bar{P}^{|m|}_n(\cos\theta)}{d\theta}e^{jm\phi}\hat{a}_\phi \right\} \tag{B.1}$$

$$\begin{aligned}\bar{F}^{(c)}_{2mn}(r,\theta,\phi) = {} & \frac{1}{\sqrt{2\pi}}\frac{1}{\sqrt{n(n+1)}}\left(-\frac{m}{|m|}\right)^m \\ & \Big(\frac{n(n+1)}{kr}z^{(c)}_n(kr)\bar{P}^{|m|}_n(\cos\theta)e^{jm\phi}\hat{a}_r \\ & + \frac{1}{kr}\frac{d(krz^{(c)}_n(kr))}{d(kr)}\frac{d\bar{P}^{|m|}_n(\cos\theta)}{d\theta}e^{jm\phi}\hat{a}_\theta \\ & + \frac{1}{kr}\frac{d(krz^{(c)}_n(kr))}{d(kr)}\frac{jm\bar{P}^{|m|}_n(\cos\theta)}{\sin\theta}e^{jm\phi}\hat{a}_\phi\Big)\end{aligned} \tag{B.2}$$

where spherical hankel functions are defined as follows:

$$z^{(1)}_n(kr) = j_n(kr) \tag{B.3}$$

$$z^{(2)}_n(kr) = n_n(kr) \tag{B.4}$$

$$z^{(3)}_n(kr) = h^{(1)}_n(kr) = j_n(kr) + jn_n(kr) \tag{B.5}$$

$$z^{(4)}_n(kr) = h^{(2)}_n(kr) = j_n(kr) - jn_n(kr) \tag{B.6}$$

The upper index (c) indicates the particular function in the radial dependencies of spherical wave functions.

$c = 1$ Spherical Bessel function representing a radial standing wave, finite at the origin.

$c = 2$ Spherical Neumann function representing a radial standing wave, infinite at the origin.

$c = 3$ Spherical Hankel function of the first kind, representing a radial incoming wave, infinite at the origin.

$c = 4$ Spherical Hankel function of the second kind, representing a radial outgoing wave, infinite at the origin.

The normalized associated Legendre function is defined as follows:

$$\bar{P}_n^{|m|}(\cos\theta) = (-1)^m \sqrt{\frac{2n+1}{2}\frac{(n-|m|)!}{(n+|m|)!}} P_n^{|m|}(\cos\theta) \tag{B.7}$$

where

$$P_n^{|m|}(\cos\theta) = (\sin\theta)^{|m|} \frac{d^{|m|} P_n(\cos\theta)}{d(\cos\theta)^{|m|}} \tag{B.8}$$

and the Legendre function is

$$P_n(\cos\theta) = \frac{1}{2^n n!} \frac{d^n}{d(\cos\theta)^n} (\cos^2\theta - 1)^n \tag{B.9}$$

Appendix C

ADDITION THEOREM

$$\bar{\mathbf{M}}^{(2)}_{n,m}(\bar{\mathbf{r}}) = \sum_{n',m'} A_{n',m';n,m}\bar{\mathbf{M}}^{(i)}_{n',m'}(\bar{\mathbf{r}}') + B_{n',m';n,m}\bar{\mathbf{N}}^{(i)}_{n',m'}(\bar{\mathbf{r}}') \tag{C.1}$$

$$\bar{\mathbf{N}}^{(2)}_{n,m}(\bar{\mathbf{r}}) = \sum_{n',m'} A_{n',m';n,m}\bar{\mathbf{N}}^{(i)}_{n',m'}(\bar{\mathbf{r}}') + B_{n',m';n,m}\bar{\mathbf{M}}^{(i)}_{n',m'}(\bar{\mathbf{r}}') \tag{C.2}$$

$$\begin{aligned} A_{n',m';n,m} = {} & \frac{2\pi j^{n'-n}}{\sqrt{n(n+1)n'(n'+1)}} \\ & \sum_{n''}(j^{n''}[n(n+1)+n'(n'+1)-n''(n''+1)] \\ & A(m,n,-m',n',n'')z^{(i')}_{n''}(kr''_w)Y_{n'',m-m'}(\theta''_w,\phi''_w)) \end{aligned} \tag{C.3}$$

and

$$\begin{aligned} B_{n',m';n,m} = {} & \frac{2\pi j^{n'-n}}{\sqrt{n(n+1)n'(n'+1)}} \\ & \sum_{n''}\left(j^{n''}B(m,n,-m',n',n'')z^{(i')}_{n''}(kr''_w)Y_{n'',m-m'}(\theta''_w,\phi''_w)\right) \end{aligned} \tag{C.4}$$

In (C.3) (C.4), $Y_{n,m}(\theta,\phi)$ denotes the scalar spherical harmonic which is defined in (C.5).

$$Y_{n,m}(\theta,\phi) = \sqrt{\frac{(2n+1)}{4\pi}\frac{(n-m)!}{(n+m)!}}P^m_n(\cos\theta)e^{jm\phi} \tag{C.5}$$

The relative sizes of r' and r'' determine the choice of spherical Bessel function $z^{(i)}_{n'}(kr')$ as given in (C.6) and (C.7) in $\bar{\mathbf{M}}^{(i)}_{n',m'}(\bar{\mathbf{r}}')$ and $\bar{\mathbf{N}}^{(i)}_{n',m'}(\bar{\mathbf{r}}')$:

$$z^{(i)}_{n'}(kr') = \left\{ \begin{array}{l} j_{n'}(kr'), \quad r' < r'' \\ \\ h^{(2)}_{n'}(kr'), \quad r' > r'' \end{array} \right\} \tag{C.6}$$

and

in $A_{n',m';n,m}$ and $B_{n',m';n,m}$:

$$z_{n''}^{(i')}(kr'') = \begin{Bmatrix} h_{n''}^{(2)}(kr''),\ r' < r'' \\ \\ j_{n''}(kr''),\ r' > r'' \end{Bmatrix} \tag{C.7}$$

$A(m,n,m',n',n'')$ and $B(m,n,m',n',n'')$ are defined as follows:

$$A(m,n,m',n',n'') = (-1)^m \sqrt{\frac{(2n+1)(2n'+1)(2n''+1)}{4\pi}} \begin{pmatrix} n & n' & n'' \\ 0 & 0 & 0 \end{pmatrix} \begin{pmatrix} n & n' & n'' \\ -m & -m' & m+m' \end{pmatrix} \tag{C.8}$$

$$\begin{aligned} B(m,n,m',n',n'') &= \sqrt{\frac{2n''+1}{2n''-1}} \\ -\sqrt{(n'+m')(n'-m'+1)(n''+m+m')(n''+m+m'-1)}&A(m,n,m'-1,n',n''-1) \\ (+\sqrt{(n'-m')(n'+m'+1)(n''-m-m')(n''-m-m'-1)}&A(m,n,m'+1,n',n''-1)) \\ -2m'\sqrt{(n''-m-m')(n''+m+m')}&A(m,n,m',n',n''-1) \end{aligned} \tag{C.9}$$

and $\begin{pmatrix} n & n' & n'' \\ 0 & 0 & 0 \end{pmatrix}$ represents Wigner 3-j symbols. The notation used in [8] is slightly different from that given in [35] for the definition of $B(m,n,m',n',n'')$.

Appendix D

TRANSLATION AND ROTATION OF SPHERICAL WAVES

D.1 Rotation formulas for spherical waves

A spherical vector wave function referenced to unprimed coordinate system $\bar{F}^{(c)}_{smn}(r,\theta,\phi)$ may be expanded as a summation of spherical vector wave functions referenced to primed coordinate system (r',θ',ϕ') which is rotated with respect to the unprimed one. This expansion is given as follows:

$$\bar{F}^{(c)}_{smn}(r,\theta,\phi) = \sum_{\mu=-n}^{n} e^{jm\phi_o} d^n_{\mu m}(\theta_o) e^{j\mu\chi_o} \bar{F}^{(c)}_{s\mu n}(r',\theta',\phi') \tag{D.1}$$

The spherical coordinate system is placed in a conventional way with respect to rectangular coordinate system. It can be clearly seen that the index, s, remains unchanged under rotation operation. Also note that the spherical wave functions on the right and left hand-side have identical n values. The elementary rotations through ϕ_o and χ_o angles only lead to phase shifts in the general formula. However, the rotation through θ_o is represented by rotation coefficient $d^n_{\mu m}(\theta_o)$ whose mathematical formulation is much more complex than the other elementary rotations.

D.1.1 The rotation coefficient

$$d^n_{\mu m}(\theta) = \left\{ \frac{(n+\mu)!(n-\mu)!}{(n+m)!(n-m)!} \right\}^{1/2} \sum_{\sigma} \binom{n+m}{n-\mu-\sigma} \binom{n-m}{\sigma} (-1)^{n-\mu-\sigma} \left(\cos\frac{\theta}{2}\right)^{2\sigma+\mu+m} \left(\sin\frac{\theta}{2}\right)^{2n-2\sigma-\mu-m} \tag{D.2}$$

where the symbol

$$\binom{i}{j} = \frac{i!}{(i-j)!j!} \tag{D.3}$$

is binomial coefficient.

D.2 Translation formulas for spherical waves

A spherical vector wave function $\bar{F}^{(c)}_{smn}(r,\theta,\phi)$ referenced to unprimed coordinate system may be expressed as a summation of vector spherical wave functions referenced to primed coordinate system which is translated with respect to the unprimed one. Translation is performed in the z direction by a distance A. The expressions for two cases are given in (D.4) and (D.5).

$$\bar{F}^{(c)}_{s\mu n}(r,\theta,\phi) = \sum_{\sigma=1}^{2}\sum_{\substack{\nu=|\mu|\\ \nu\neq 0}}^{\infty} C^{sn(c)}_{\sigma\mu\nu}(kA)\bar{F}^{(1)}_{\sigma\mu\nu}(r',\theta',\phi') \qquad r' < |A| \tag{D.4}$$

$$\bar{F}^{(c)}_{s\mu n}(r,\theta,\phi) = \sum_{\sigma=1}^{2}\sum_{\substack{\nu=|\mu|\\ \nu\neq 0}}^{\infty} C^{sn(1)}_{\sigma\mu\nu}(kA)\bar{F}^{(c)}_{\sigma\mu\nu}(r',\theta',\phi') \qquad r' > |A| \tag{D.5}$$

where translation coefficient $C^{sn(c)}_{\sigma\mu\nu}(kA)$ takes the product of wave number k and translation distance A as the input argument. It is evident that the spherical wave functions on the right hand side include the same azimuthal index μ as the left-hand side. This means that translation in the z direction does not affect the ϕ dependence of spherical wave functions. These formulas describing z-translation should be considered as a special form of general translation in arbitrary direction. However, the translation in arbitrary direction may be achieved by consecutive application of three operations: rotation,axial translation, and inverse rotation.

Translation coefficients in the z direction for positive arguments $(kA > 0)$ may be calculated as follows:

$$\begin{aligned} C^{sn(c)}_{\sigma\mu\nu}(kA) &= \sqrt{\frac{(2n+1)(2\nu+1)}{n(n+1)\nu(\nu+1)}}\sqrt{\frac{(\nu+\mu)!(n-\mu)!}{(\nu-\mu)!(n+\mu)!}}(-1)^{\mu}\frac{1}{2}(j)^{n-\nu} \\ &\sum_{p=|n-\nu|}^{n+\nu}\Big[(j)^{-p}(\delta_{s,\sigma}\{n(n+1)+\nu(\nu+1)-p(p+1)\} \\ &+ \delta_{3-s,\sigma}\{2j\mu kA\})a(\mu,n,-\mu,\nu,p)z^{(c)}_{p}(kA)\Big] \end{aligned} \tag{D.6}$$

where $a(\mu,n,-\mu,\nu,p)$ is a linearization coefficient. The linearization coefficients

may be expressed using Wigner $3-j$ symbols as follows:

$$a(\mu,n,-\mu,\nu,p)=(2p+1)\left\{\frac{(n+\mu)!(\nu-\mu)!}{(n-\mu)!(\nu+\mu)!}\right\}^{\frac{1}{2}} \begin{pmatrix} n & \nu & p \\ 0 & 0 & 0 \end{pmatrix}\begin{pmatrix} n & \nu & p \\ \mu & -\mu & 0 \end{pmatrix} \tag{D.7}$$

It may be demonstrated that Wigner $3-j$ symbols are zero when $(n+\nu+p)$ is odd number [43].

$$\begin{pmatrix} n & \nu & p \\ 0 & 0 & 0 \end{pmatrix}=0,\ for\ (n+\nu+p)\ is\ odd\ number \tag{D.8}$$

The linearization coefficients for z translation can be easily generated by using recurrence relations given in [20]. Translation coefficients for negative arguments may be evaluated by using simple symmetry relation given below.

$$C^{sn(c)}_{\sigma\mu\nu}(-kA)=(-1)^{s+\sigma}(-1)^{n+\nu}C^{sn(c)}_{\sigma\mu\nu}(kA) \tag{D.9}$$

Appendix E

S AND Z MATRIX TRANSFORMATIONS

E.1 S to Z Transform

$$Z_{11} = \frac{(1+S_{11})(1-S_{22})+S_{12}S_{21}}{(1-S_{11})(1-S_{22})-S_{12}S_{21}}Z_{01} \tag{E.1}$$

$$Z_{12} = \frac{2S_{12}}{(1-S_{11})(1-S_{22})-S_{12}S_{21}}Z_{02} \tag{E.2}$$

$$Z_{21} = \frac{2S_{21}}{(1-S_{11})(1-S_{22})-S_{12}S_{21}}Z_{01} \tag{E.3}$$

$$Z_{22} = \frac{(1-S_{11})(1+S_{22})+S_{12}S_{21}}{(1-S_{11})(1-S_{22})-S_{12}S_{21}}Z_{02} \tag{E.4}$$

E.2 Z to S Transform

$$S_{11} = \frac{(Z_{11}-Z_{01})(Z_{22}+Z_{02})-Z_{12}Z_{21}}{(Z_{11}+Z_{01})(Z_{22}+Z_{02})-Z_{12}Z_{21}} \tag{E.5}$$

$$S_{12} = \frac{2Z_{12}Z_{01}}{(Z_{11}+Z_{01})(Z_{22}+Z_{02})-Z_{12}Z_{21}} \tag{E.6}$$

$$S_{21} = \frac{2Z_{21}Z_{02}}{(Z_{11}+Z_{01})(Z_{22}+Z_{02})-Z_{12}Z_{21}} \tag{E.7}$$

$$S_{22} = \frac{(Z_{11}+Z_{01})(Z_{22}-Z_{02})-Z_{12}Z_{21}}{(Z_{11}+Z_{01})(Z_{22}+Z_{02})-Z_{12}Z_{21}} \tag{E.8}$$

Appendix F

REACTION INTEGRAL ON MODIFIED REACTION SURFACE

If the surface S_{1b} extends to infinity, only θ and ϕ components of the electric and magnetic fields are dominant on this surface, the field components of antenna 1, and antenna 2 in the far-zone can be defined as:

$$\bar{E}_1 = \hat{a}_\theta E_{\theta 1} + \hat{a}_\phi E_{\phi 1} \tag{F.1}$$

$$\bar{H}_1 = \hat{a}_\theta H_{\theta 1} + \hat{a}_\phi H_{\phi 1} \tag{F.2}$$

$$\bar{E}_2 = \hat{a}_\theta E_{\theta 2} + \hat{a}_\phi E_{\phi 2} \tag{F.3}$$

$$\bar{H}_2 = \hat{a}_\theta H_{\theta 2} + \hat{a}_\phi H_{\phi 2} \tag{F.4}$$

Using $E_\theta = \eta H_\phi$, and $E_\phi = -\eta H_\theta$, $\bar{E}_1 \times \bar{H}_2$ and $\bar{E}_2 \times \bar{H}_1$ can be written in the far-field region as given in (F.5), and (F.6), respectively.

$$\bar{E}_1 \times \bar{H}_2 = \hat{a}_r \left(E_{\theta 1} H_{\phi 2} - E_{\phi 1} H_{\theta 2}\right) = \hat{a}_r \left(\eta H_{\phi 1} H_{\phi 2} + \eta H_{\theta 1} H_{\theta 2}\right) \tag{F.5}$$

$$\bar{E}_2 \times \bar{H}_1 = \hat{a}_r \left(E_{\theta 2} H_{\phi 1} - E_{\phi 2} H_{\theta 1}\right) = \hat{a}_r \left(\eta H_{\phi 2} H_{\phi 1} + \eta H_{\theta 2} H_{\theta 1}\right) \tag{F.6}$$

If $\bar{E}_2 \times \bar{H}_1$ is substracted from $\bar{E}_1 \times \bar{H}_2$ in the far-zone region, then the integrand of the surface integral will be zero as given in (F.7)

$$\bar{E}_1 \times \bar{H}_2 - \bar{E}_2 \times \bar{H}_1 = 0 \tag{F.7}$$

Then the surface integral will also be zero on S_{1b} as:

$$\int_{S_{1b}} (\bar{E}_1 \times \bar{H}_2 - \bar{E}_2 \times \bar{H}_1) \cdot d\bar{S}_{1b} = 0 \tag{F.8}$$

Appendix G

METHOD OF STATIONARY PHASE

The $\bar{E}$ field can be expressed in terms of plane wave spectrum of the field as:

$$\bar{E}(x,y,z) = \frac{1}{4\pi^2}\int_{-\infty}^{\infty}\int_{-\infty}^{\infty}\bar{f}(k_x,k_z)e^{-j\bar{k}\cdot\bar{r}}dk_x dk_z \tag{G.1}$$

The integral given in (G.1) is evaluated asymptotically for large values of kr using the method of stationary phase to find the $\bar{E}$ field in terms of $\bar{f}(k_x,k_z)$. The first step in the asymptotic evaluation of (G.1) is to find the stationary points of $\bar{k}\cdot\bar{r}$. In order to do that, $\bar{k}\cdot\bar{r}$ is written as:

$$\bar{k}\cdot\bar{r} = (k_x\hat{a}_x + k_y\hat{a}_y + k_z\hat{a}_z)\cdot\hat{a}_r r \tag{G.2}$$

where

$$\hat{a}_r = \sin\theta\cos\phi\hat{a}_x + \sin\theta\sin\phi\hat{a}_y + \cos\theta\hat{a}_z \tag{G.3}$$

which reduces

$$\bar{k}\cdot\bar{r} = r(k_x\sin\theta\cos\phi + k_y\sin\theta\sin\phi + k_z\cos\theta) \tag{G.4}$$

where k_y is defined in terms of k_x and k_z as given in (G.5) and (G.6)

$$k_y = \sqrt{k^2 - k_x^2 - k_z^2} \quad k^2 > k_x^2 + k_z^2 \tag{G.5}$$

$$k_y = -j\sqrt{k_x^2 + k_z^2 - k^2} \quad k^2 < k_x^2 + k_z^2 \tag{G.6}$$

By inserting (G.5) into (G.4), $\bar{k}\cdot\bar{r}$ can be defined as:

$$\bar{k}\cdot\bar{r} = r(k_x\sin\theta\cos\phi + \sqrt{k^2 - k_x^2 - k_z^2}\sin\theta\sin\phi + k_z\cos\theta) \tag{G.7}$$

The stationary points can be found by exploiting (G.8) and (G.9).

$$\frac{\partial(\bar{k}\cdot\bar{r})}{\partial k_x} = 0 \tag{G.8}$$

$$\frac{\partial(\bar{k}\cdot\bar{r})}{\partial k_z}=0 \tag{G.9}$$

Substitude (G.7) into (G.8) and (G.9), then the partial derivatives with respect to k_x and k_z can be obtained as:

$$\frac{\partial(\bar{k}\cdot\bar{r})}{\partial k_x}=r\left[\sin\theta\cos\phi+\frac{-k_x}{\sqrt{k^2-k_x^2-k_z^2}}\sin\theta\sin\phi\right]=0\rightarrow k_x\sin\phi=k_y\cos\phi \tag{G.10}$$

$$\frac{\partial(\bar{k}\cdot\bar{r})}{\partial k_z}=r\left[\frac{-k_z}{\sqrt{k^2-k_x^2-k_z^2}}\sin\theta\sin\phi+\cos\theta\right]=0\rightarrow k_z\sin\theta\sin\phi=k_y\cos\theta \tag{G.11}$$

Using (G.10) and (G.11), k_x and k_z can be defined in terms of k_y, ϕ, and θ as:

$$k_x=k_y\frac{\cos\phi}{\sin\phi} \tag{G.12}$$

$$k_z=k_y\frac{\cos\theta}{\sin\theta\sin\phi} \tag{G.13}$$

By using (G.14), k_x, k_y, and k_z are derived in terms of k, θ, ϕ as given in (G.15),(G.16) and (G.17), respectively.

$$k^2=k_x^2+k_y^2+k_z^2 \tag{G.14}$$

$$k_x=k\sin\theta\cos\phi=k_1 \tag{G.15}$$

$$k_y=k\sin\theta\sin\phi \tag{G.16}$$

$$k_z=k\cos\theta=k_2 \tag{G.17}$$

In the vicinity of k_1 and k_2, the function $\bar{k}\cdot\bar{r}$ can be approximated by utilizing a truncated Taylor series. This approximation considers the terms up to zeroth, first, and second order, as demonstrated in equation (G.18).

$$\bar{k}\cdot\bar{r}\cong\bar{k}\cdot\bar{r}|_{k_1,k_2}+\frac{\partial(\bar{k}\cdot\bar{r})}{\partial k_x}|_{k_1,k_2}(k_x-k_1)+\frac{\partial(\bar{k}\cdot\bar{r})}{\partial k_z}|_{k_1,k_2}(k_z-k_2)+$$
$$\frac{1}{2}\frac{\partial^2(\bar{k}\cdot\bar{r})}{\partial k_x^2}|_{k_1,k_2}(k_x-k_1)^2+\frac{1}{2}\frac{\partial^2(\bar{k}\cdot\bar{r})}{\partial k_z^2}|_{k_1,k_2}(k_z-k_2)^2+\frac{\partial^2(\bar{k}\cdot\bar{r})}{\partial k_x\partial k_z}|_{k_1,k_2}(k_x-k_1)(k_z-k_2) \tag{G.18}$$

The second and third terms vanish at the stationary points $k_x = k_1$ and $k_z = k_2$. The expression in (G.18) can be simplified as:

$$\bar{k} \cdot \bar{r} \cong \bar{k} \cdot \bar{r}|_{k_1,k_2} - A\zeta^2 - B\eta^2 - C\zeta\eta \tag{G.19}$$

where

$$\zeta = (k_x - k_1) \qquad \eta = (k_z - k_2) \tag{G.20}$$

and A, B and C can be written as:

$$A = -\frac{1}{2}\frac{\partial^2(\bar{k} \cdot \bar{r})}{\partial k_x^2}|_{k_1,k_2} \tag{G.21}$$

$$B = -\frac{1}{2}\frac{\partial^2(\bar{k} \cdot \bar{r})}{\partial k_z^2}|_{k_1,k_2} \tag{G.22}$$

$$C = -\frac{\partial^2(\bar{k} \cdot \bar{r})}{\partial k_x \partial k_z}|_{k_1,k_2} \tag{G.23}$$

After a few calculations, A, B, and C can be found as given in (G.24), (G.25), and (G.26).

$$A = \frac{r}{2k(\sin\phi)^2} \tag{G.24}$$

$$B = \frac{r}{2k}\left[1 + \left(\frac{\cos\theta}{\sin\theta\sin\phi}\right)^2\right] \tag{G.25}$$

$$C = \frac{r}{k}\left[\frac{\cos\phi\cos\theta}{\sin\theta(\sin\phi)^2}\right] \tag{G.26}$$

Since the startionary points $k_x = k_1$, $k_z = k_2$, and their neighbourhoods contribute mostly to the integral, the integral in (G.1) can be approximately found as:

$$\bar{E}(x,y,z) \cong \frac{1}{4\pi^2}\iint_{S_{1,2}} \bar{f}(k_x = k_1, k_z = k_2)e^{-j(kr - A\zeta^2 - B\eta^2 - C\zeta\eta)}d\zeta d\eta \tag{G.27}$$

The assumption is made that $\bar{f}(k_1, k_2)$ is a slowly varying function within the stationary region. As a result, it can be extracted from the integral, as shown in equation (G.28).

$$\bar{E}(x,y,z) \cong \frac{1}{4\pi^2}\bar{f}(k_1,k_2)e^{-jkr}\iint_{S_{1,2}} e^{j(A\zeta^2 + B\eta^2 + C\zeta\eta)}d\zeta d\eta \tag{G.28}$$

where $S_{1,2}$ is the surface which covers the region near the stationary point. The surface integral given in (G.29) can be defined as:

$$\iint_{S_{1,2}} e^{j(A\zeta^2+B\eta^2+C\zeta\eta)} d\zeta d\eta = j\frac{2\pi\delta}{\sqrt{|4AB-C^2|}} \tag{G.29}$$

where

$$\sqrt{4AB-C^2} = \frac{r}{k}\frac{1}{\sin\theta\sin\phi} \tag{G.30}$$

Three different conditions for δ are given in (G.31).

$$\delta = \begin{cases} +1 & if\ 4AB > C^2, A > 0 \\ -1 & if\ 4AB < C^2, A < 0 \\ -j & if\ 4AB < C^2 \end{cases} \tag{G.31}$$

Since $4AB > C^2$ and $A > 0$, the surface integral in (G.28) can be written as:

$$\iint_{S_{1,2}} e^{j(A\zeta^2+B\eta^2+C\zeta\eta)} d\zeta d\eta = j\frac{2\pi k}{r}\sin\theta\sin\phi \tag{G.32}$$

Substituting (G.32) into (G.28), $\bar{E}$ field can be defined in terms of plane wave functions as:

$$\bar{E}(r,\theta,\phi) \cong \frac{jke^{-jkr}}{2\pi r}\left[\sin\theta\sin\phi\bar{f}(k_1 = k\sin\theta\cos\phi, k_2 = k\cos\theta)\right] \tag{G.33}$$

REFERENCES

[1] Robert C Hansen. *Phased array antennas*. John Wiley & Sons, 2009.

[2] Robert Mark, Harsh Verdhan Singh, Kaushik Mandal, and Soma Das. Mutual coupling reduction using near-zero ε and μ metamaterial-based superstrate for an mimo application. *IET Microwaves, Antennas & Propagation*, 14(6):479–484, 2020.

[3] I Gupta and A Ksienski. Effect of mutual coupling on the performance of adaptive arrays. *IEEE Transactions on Antennas and Propagation*, 31(5):785–791, 1983.

[4] J Richmond. A reaction theorem and its application to antenna impedance calculations. *IRE Transactions on Antennas and Propagation*, 9(6):515–520, 1961.

[5] Arthur Yaghjian. Efficient computation of antenna coupling and fields within the near-field region. *IEEE Transactions on antennas and Propagation*, 30(1):113–128, 1982.

[6] G Borgiotti. A novel expression for the mutual admittance of planar radiating elements. *IEEE Transactions on Antennas and Propagation*, 16(3):329–333, 1968.

[7] Orest G Vendik and Dmitry S Kozlov. A novel method for the mutual coupling calculation between antenna array radiators: Analysis of the radiation pattern of a single radiator in the antenna array. *IEEE Antennas and Propagation Magazine*, 57(6):16–21, 2015.

[8] Billy C Brock. Using vector spherical harmonics to compute antenna mutual impedance from measured or computed fields. Technical report, Sandia National Labs., Albuquerque, NM, and Livermore, CA (US), 2000.

[9] John David Jackson. *Classical electrodynamics*. John Wiley & Sons, 2021.

[10] Jesper E Hansen. *Spherical near-field antenna measurements*, volume 26. Iet, 1988.

[11] J Bruning and Yuen Lo. Multiple scattering of em waves by spheres part ii–numerical and experimental results. *IEEE Transactions on Antennas and Propagation*, 19(3):391–400, 1971.

[12] Haobo Yuan, Hongguang Zhou, Hongwei Liu, Xiaojie Dang, and Xi Chen. Computing mutual impedance of antennas by spherical harmonic transform. *IEEE Transactions on Antennas and Propagation*, 67(7):4377–4384, 2019.

[13] Juan F Izquierdo, Jesús Rubio, and Juan Zapata. Spherical-waves-based analysis of arrays of volumetric antennas with overlapping minimum spheres. *IEEE Antennas and Wireless Propagation Letters*, 11:1296–1299, 2012.

[14] Jesús Rubio and Rafael Gómez-Alcalá. Mutual coupling of antennas with overlapping minimum spheres based on the transformation between spherical and plane vector waves. *IEEE Transactions on Antennas and Propagation*, 69(4):2103–2111, 2020.

[15] Torleif Martin. T-matrix method for closely adjacent obstacles. *Journal of Quantitative Spectroscopy and Radiative Transfer*, 234:40–46, 2019.

[16] Yinchao Chen and T Simpson. Radiation pattern analysis of arbitrary wire antennas using spherical mode expansions with vector coefficients. *IEEE Transactions on Antennas and Propagation*, 39(12):1716–1721, 1991.

[17] Jussi Rahola, Fabio Belloni, and Andreas Richter. Modelling of radiation patterns using scalar spherical harmonics with vector coefficients. In *2009 3rd European Conference on Antennas and Propagation*, pages 3361–3365. IEEE, 2009.

[18] Roxana Burghelea, Stephane Avrillon, and Bernard Uguen. Uwb antenna compact modeling using vector spherical harmonic theory. In *2009 IEEE Antennas and Propagation Society International Symposium*, pages 1–4. IEEE, 2009.

[19] Tomislav Marinovic. Vector spherical harmonic expansion.

[20] J Bruning and Yuen Lo. Multiple scattering of em waves by spheres part i–multipole expansion and ray-optical solutions. *IEEE Transactions on Antennas and Propagation*, 19(3):378–390, 1971.

[21] VH Rumsey. Reaction concept in electromagnetic theory. *Physical Review*, 94(6):1483, 1954.

[22] Robert E Collin. *Field theory of guided waves*, volume 5. John Wiley & Sons, 1990.

[23] Constantine A Balanis. *Advanced engineering electromagnetics*. John Wiley & Sons, 2012.

[24] Demetrius T Paris and Frank Kenneth Hurd. *Basic electromagnetic theory*. McGraw-Hill Companies, 1969.

[25] Roger F Harrington. *Time-harmonic electromagnetic fields*. McGraw-Hill College, 1961.

[26] Constantine A Balanis. *Antenna theory: analysis and design*. John wiley & sons, 2015.

[27] PS Carter. Circuit relations in radiating systems and applications to antenna problems. *Proceedings of the Institute of Radio Engineers*, 20(6):1004–1041, 1932.

[28] John Daniel Kraus and Ronald J Marhefka. Antennas for all applications. *Antennas for all applications*, 2002.

[29] Arthur Ludwig. Near-field far-field transformations using spherical-wave expansions. *IEEE Transactions on Antennas and Propagation*, 19(2):214–220, 1971.

[30] WW Hansen. A new type of expansion in radiation problems. *Physical review*, 47(2):139, 1935.

[31] Julius Adams Stratton. *Electromagnetic theory*, volume 33. John Wiley & Sons, 2007.

[32] Philip M Morse and Herman Feshbach. Methods of theoretical physics' mc graw-hill book company. *New York (1 953")*, 1953.

[33] Chen-To Tai. *Dyadic Green functions in electromagnetic theory*. IEEE, 1994.

[34] Robert E Collin and Francis J Zucker. *Antenna theory*. McGraw-Hill, 1969.

[35] Weng Cho Chew. *Waves and fields in inhomogenous media*, volume 16. John Wiley & Sons, 1999.

[36] Sophocles J Orfanidis. *Electromagnetic waves and antennas*. Rutgers University New Brunswick, NJ, 2002.

[37] Jeanne Rockway. *Electromagnetic field determination of antenna systems in complex structural environments by the spherical harmonic interface procedure*. The Ohio State University, 2005.

[38] RongLin Li, Terence Wu, Bo Pan, Kyutae Lim, Joy Laskar, and Manos M Tentzeris. Equivalent-circuit analysis of a broadband printed dipole with adjusted integrated balun and an array for base station applications. *IEEE Transactions on Antennas and Propagation*, 57(7):2180–2184, 2009.

[39] Thorkild B Hansen and Arthur D Yaghjian. *Plane-wave theory of time-domain fields: near-field scanning applications*, volume 10. John Wiley & Sons, 1999.

[40] EW Hobson. *The theory of functions of a real variable*, volume 1,2. New York, Dover, 1957.

[41] Hans-Jurgen Weber and George B Arfken. *Mathematical methods for physicists*. Elsevier Academic, 2005.

[42] Francis J Flanigan. *Complex variables: harmonic and analytic functions*. Courier Corporation, 1983.

[43] Alan Robert Edmonds. *Angular momentum in quantum mechanics*, volume 4. Princeton university press, 1996.

CURRICULUM VITAE

PERSONAL INFORMATION

Surname, Name: Öztürk, Mehmet Ali
Nationality:
Date and Place of Birth:
Marital Status:
Phone:
Fax:

EDUCATION

Degree	Institution	Year of Graduation
PhD.	METU Electric and Electronics Engineering	2023
M.S.	METU Electric and Electronics Engineering	2015
B.S.	Hacettepe University Electric and Electronics Engineering	2011
High School	Manisa Anadolu Öğretmen Lisesi	2006

PROFESSIONAL EXPERIENCE

Year	Place	Enrollment
5 year	Anketek Electronics	Engineer
3 year	ASELSAN	Engineer

PUBLICATIONS

Mutual impedance computation using spherical harmonics between two closely spaced antennas, AEU - International Journal of Electronics and Communications, Volume 168, 2023, 154711, ISSN 1434-8411, https://doi.org/10.1016/j.aeue.2023.154711.